UNIVERSITÉ DE MONTRÉAL

ORGANIC TRANSISTORS MAKING USE OF ROOM TEMPERATURE IONIC LIQUIDS AS GATING MEDIUM

JONATHAN JAVIER SAYAGO HOYOS

DÉPARTEMENT DE GÉNIE PHYSIQUE

ÉCOLE POLYTECHNIQUE DE MONTRÉAL

THÈSE PRÉSENTÉE EN VUE DE L'OBTENTION

DU DIPLÔME DE PHILOSOPHIÆ DOCTOR

(GÉNIE MÉTALLURGIQUE)

AOÛT 2015

UNIVERSITÉ DE MONTRÉAL

ÉCOLE POLYTECHNIQUE DE MONTRÉAL

Cette thèse intitulée :

ORGANIC TRANSISTORS MAKING USE OF ROOM TEMPERATURE IONIC LIQUIDS AS GATING MEDIUM

présentée par : SAYAGO HOYOS Jonathan Javier

en vue de l'obtention du diplôme de : Philosophiæ Doctor

a été dûment acceptée par le jury d'examen constitué de :

M. MARTINU Ludvik, Ph. D., président

Mme SANTATO Clara, Doctorat, membre et directrice de recherche

M. CICOIRA Fabio, Ph. D., membre et codirecteur de recherche

Mme SOAVI Francesca, Ph. D., membre et codirectrice de recherche

M. KÉNA-COHEN, Stéphane, Ph. D., membre

Mme TAVARES Ana, Ph. D., membre externe

ACKNOWLEDGEMENTS

I would like to thank my research director, Clara Santato, for your faith, leadership, support and dedication in our time together at Polytechnique Montréal. Thanks to my co-directors, Francesca Soavi and Fabio Cicoira, for your kind advice and for working side by side with me at many different stages of this work. To my dear colleagues, Julia Wuensche, Sareh Bayatpour, Dilek Isik, Farzaneh Mahvash, Mitesh Patel, Prajwal Kumar, Irina Valitova, Zhihui Yi, Shiming Zhang, Xiang Meng, Eduardo Di Mauro, Francis Quenneville, Frédéric Venne, Umar Shafique, Olga Berezhetska, Ri Xu and Tian Lan, thanks for your companionship, generosity and friendship, I learned many things from you.

Thanks to our visiting students Gaurav Nanda, Jonathan Borduas, Ahcene Bayou and Étienne Bourbeau for your contribution as summer students to the present thesis.

Many thanks to Patricia Moraille, for your help in AFM, to Christophe Clément and Xavier Perraton for your assistance in microfabrication, to Josianne Lefebvre for your support in XPS measurements. Thanks to Jean-Paul Lévesque, Joël Bouchard, Yves Drolet, Yves Leblanc and Francis Boutet for your sensible and always well-timed help in the laboratories.

Thanks to Polytechnique Montréal for your academic and administrative services and to CONACYT for the scholarship grant to let me pursue a Ph.D. in Canada.

To our father who art in heaven, family and friends, thanks for your love and blessings.

RÉSUMÉ

La capacité de transport ionique et électronique des couches minces organiques semiconductrices et conductrices est particulièrement intéressante dans le domaine de l'électronique imprimable et flexible.

L'incorporation d'un électrolyte en tant que milieu de grille dans les transistors organiques (Transistors EG), permet de moduler le courant en plusieurs ordres de grandeur à une tension relativement basse (<2 V) grâce à la capacitance exceptionnelle de l'interface du canal/électrolyte, déterminée par les faibles épaisseurs de la double couche électrique qui se forme à l'interface électrolyte/couche mince organique. Les liquides ioniques, soit des sels fondus à des températures inférieures à 100 °C, sont intéressants pour leur grande stabilité électrochimique (leur fenêtre de stabilité s'étend jusqu'à 5 V) et leur bonne conductivité ionique (1-15 mS cm^{-1}). La principale motivation derrière le présent travail est de démontrer un fonctionnement à faible tension des transistors organiques en faisant usage des liquides ioniques, en tant que milieu de grille.

Tout d'abord, nous avons établi l'importance de la nature et morphologie de l'électrode de grille sur la performance des transistors électrochimiques. L'utilisation de carbone actif à haute aire de surface comme électrode de grille limite des processus électrochimiques indésirables à l'interface électrolyte/grille et rend inutile la présence d'une électrode de référence pour contrôler le potentiel du canal. Ceci a été démontré en utilisant des électrodes de grille en carbone actif, le polymère semiconducteur MEH-PPV comme matériel du canal et le liquide ionique [EMIM][TFSI] en tant que milieu de grille. L'utilisation de carbone actif avec une aire de surface non-limitative en termes de sa capacité à fournir la charge nécessaire pour moduler la conductivité du canal du transistor, a entraîné un voltage d'opération en dessous de 1 V et une mobilité des porteurs charge de $(1,0 \pm 0,5) \times 10^{-2}$ $cm^2V^{-1}s^{-1}$.

Un défi dans le domaine des transistors électrochimiques est d'améliorer le temps de réponse, qui est une conséquence du temps nécessaire pour la redistribution des ions dans le canal du transistor à l'application d'un biais électrique. Nous avons systématiquement étudié des transistors employant différents liquides ioniques appartenant à une même famille, c'est à dire basées sur un anion commun et des différents cations. Une influence limitée des différents cations

pour établir le dopage type-*p* du polymère conducteur fut démontré par les caractéristiques électriques des transistors. Il est intéressant de noter que le temps de réponse du transistor dépend d'au moins deux processus: la redistribution des ions de l'électrolyte vers le canal du transistor, qui affecte le courant grille-source (I_{gs}), et la redistribution des charges dans le canal du transistor, qui affecte le courant drain-source (I_{ds}) en fonction du temps. Les deux processus ont des vitesses différentes, ce dernier étant le plus lent. L'incorporation du carbonate de propylène dans l'électrolyte a été bénéfique pour réduire le temps de réponse du transistor.

Les fonctions de transistor et supercondensateur (TransCap), i.e. la fonction logique des transistors et le stockage d'énergie, au sein de la structure des transistors EG sont simultanément possibles. L'empilement polymère/électrolyte/carbone du transistor électrochimique comporte la configuration de cellule d'un supercondensateur hybride dont le carbone actif est chargé par un processus électrostatique et le canal du transistor est chargé par un processus électrochimique. Les supercondensateurs sont des systèmes à puissance spécifique élevée que pour leur capacité à stocker et fournir charge dans des délais courts, pourraient surpasser la performance des batteries dans les applications où une puissance élevée est nécessaire. Lorsque le TransCap est allumé (le canal du transistor est ouvert), le polymère et l'électrode de grille de carbone stockent une charge (Q) à une tension V_{gs} donnée, donc l'énergie stockée est égale à $Q \cdot V_{gs}$. Lorsque le TransCap est éteint, le canal et la grille sont déchargés et l'énergie peut être livrée pour alimenter d'autres composants électroniques.

ABSTRACT

The ability to couple ionic and electronic transport in organic transistors, based on π conjugated organic materials for the transistor channel, can be particularly interesting to achieve low voltage transistor operation, i.e. below 1 V. The operation voltage in typical organic transistors based on conventional dielectrics (200 nm thick SiO_2) is commonly higher than 10 V. Electrolyte-gated (EG) transistors, i.e. employing an electrolyte as the gating medium, permit current modulations of several orders of magnitude at relatively low gate voltages thanks to the exceptionally high capacitance at the electrolyte/transistor channel interface, in turn due to the low thickness (ca. 3 nm) of the electrical double layers forming at the electrolyte/semiconductor interface. Electrolytes based on room temperature ionic liquids (RTILs) are promising in EG transistor applications for their high electrochemical stability and good ionic conductivity. The main motivation behind this work is to achieve low voltage operation in organic transistors by making use of RTILs as gating medium.

First we demonstrate the importance of the gate electrode material in the EG transistor performance. The use of high surface area carbon gate electrodes limits undesirable electrochemical processes and renders unnecessary the presence of a reference electrode to monitor the channel potential. This was demonstrated using activated carbon as gate electrode, the electronic conducting polymer MEH-PPV, poly[2-methoxy-5-(2′-ethylhexyloxy)-1,4-phenylene vinylene] channel material, and the ionic liquid [EMIM][TFSI] (1-ethyl-3-methylimidazolium bis(trifluoromethylsulfonyl)imide), as gating medium. Using high surface area gate electrodes resulted in sub-1 V operation and charge carrier mobilities of $(1.0 \pm 0.5) \times 10^{-2}$ $cm^2V^{-1}s^{-1}$.

A challenge in the field of EG transistors is to decrease their response time, a consequence of the slow ion redistribution in the transistor channel upon application of electric biases. We systematically investigated EG transistors employing RTILs belonging to the same family, i.e. based on a common anion and different cations. The transistor characteristics showed a limited cation influence in establishing the *p*-type doping of the conducting polymer. Interestingly, we observed that the transistor response time depends on at least two processes: the redistribution of ions from the electrolyte into the transistor channel, affecting the gate-source current (I_{gs}); and the redistribution of charges in the transistor channel, affecting the drain-source current (I_{ds}), as a

function of time. The two processes have different rates, with the latter being the slowest. Incorporating propylene carbonate in the electrolyte proved to be an effective solution to increase the ionic conductivity, to lower the viscosity and, consequently, to reduce the transistor response time.

Finally, we were able to demonstrate a multifunctional device integrating the transistor logic function with that of energy storage in a supercapacitor: the TransCap. The polymer/electrolyte/carbon vertical stacking of the EG transistor features the cell configuration of a hybrid supercapacitor. Supercapacitors are high specific power systems that, for their ability to store/deliver charge within short times may outperform batteries in applications having high power demand. When the TransCap is ON (open transistor channel), the polymer and the carbon gate electrodes store charge (Q) at a given V_{gs}, hence the stored energy equals $Q \cdot V_{gs}$. When the TransCap is switched OFF, the channel and the gate are discharged and the energy can be delivered back to power other electronic components.

EG transistors, making use of activated carbon as gate electrode and different RTILs as well as RTIL solvent mixtures as electrolyte gating medium, are interesting towards low voltage printable electronics. The high capacitance at the interface between the electrolyte and the transistor channel enables energy storage within the EG transistor architecture.

TABLE OF CONTENTS

LIST OF TABLES

LIST OF FIGURES

LIST OF SYMBOLS AND ABBREVIATIONS

A	active surface area
AM-OLED	active-matrix organic light-emitting diode
[BMIM]	1-butyl-3-methylimidazolium
BPhen	4,7-diphenyl-1,10-phenanthroline
C	capacitance
CB	conduction band
CE	counter electrode
C_i	capacitance density
CV	cyclic voltammetry
e	elementary charge
E	electric field
E_a	activation energy
EDL	electrical double layer
E_F	Fermi level
E_g	energy gap
EG	electrolyte-gated
EG-OLET	electrolyte-gated organic light-emitting transistor
EIS	electrochemical impedance spectroscopy
[EMIM]	1-ethyl-3-methylimidazolium
E_{OFF}	energy used to bring the transistor to the OFF state
E_{ON}	energy used to bring the transistor to the ON state
EQE	external quantum efficiency
[FAP]	tris(pentafluoroethyl)trifluorophosphate

F8BT	poly(9,9′-dioctylfluorene-co-benzothiadiazole)
Fc	ferrocene [bis(n5-cyclopentandienyl)iron]
FOTS	(tridecafluoro-1,1,2,2-tetra-hydrooctyl) trichlorosilane
G-EML	graded emissive layer
GOx	glucose oxidase
HMDS	hexamethyldisilazane
HOMO	highest occupied molecular orbital
I	current
I_{ds}	source-drain current
IP	ionization potential
IPA	isopropyl alcohol
k_B	Boltzmann constant
L	transistor channel length
LUMO	lowest unoccupied molecular orbital
m	mass of the electron
m^*	effective mass
MDMO-PPV	poly(2-methoxy-5-(3’,7’-dimethyloctyloxy)-1,4-phenylenevinylene)
MEH-PPV	poly[2-methoxy-5-(2′-ethylhexyloxy)-1,4-phenylene vinylene]
MISFET	metal-insulator semiconductor field-effect transistor
$[N_{1113}]$	N-trimethyl-N-propylammonium
NMP	N-methyl pyrrolidone
OFET	organic field-effect transistor
OLED	organic light-emitting diode
OLET	organic light-emitting transistor

p	hole sheet charge carrier density
P	power
P3HT	poly(3-hexylthiophene)
PBS	phosphate buffered saline
PC	propylene carbonate
PCBM	[6,6]-phenyl-C61-butyric acid methyl ester
PDIF-CN2	N,N''-bis(n-alkyl)-(1,7 and 1,6)-dicyanoperylene-3,4:9,10-bis(dicarboximide)
PDMS	poly(dimethylsiloxane)
PEDOT:PSS	poly(3,4-ethylenedioxythiophene):poly(styrenesulfonate)
PEO	poly(ethylene oxide)
PS-PEO-PS	poly(styrene-block-ethylene oxide-block-styrene)
PS-PMMA-PS	poly(styrene-b-methylmethacrylate-b-styrene)
PTFE	polytetrafluoroethylene
PVA	poly(vinyl alcohol)
[PYR_{14}]	1-butyl-1-methylpyrrolidinium
Q	sheet charge density
RT	room temperature
RE	reference electrode
RFID	radio-frequency identification
r_q	root mean square roughness
RTILs	room temperature ionic liquids
r_v	sweep rate
[TFSI]	bis(trifluoromethanesulfonyl)imide

T	temperature
t	time
TCTA	4,4′,4″-tris(carbazol-9-yl) triphenylamine
TIPS PENTACENE	6,13-bis(triisopropylsilylethynyl)pentacene
TPBi	2,2′,2″-(1,3,5-benzinetriyl)-tris(1-phenyl-1-H-benzimidazole)
VB	valence band
V_{cell}	cell voltage
V_{ds}	source-drain voltage
V_{fb}	flat-band potential
V_{gs}	gate-source voltage
VL	vacuum level
V_t	threshold voltage
W	transistor channel width
WE	working electrode
XPS	X-ray photoelectron spectroscopy
μ	mobility
μ_{FET}	field-effect transistor mobility
μ_o	mobility prefactor
Φ	metal workfunction
χ	electron affinity

LIST OF APPENDICES

CHAPTER 1 INTRODUCTION

1.1 Overview

Organic electronic materials consist of π-conjugated molecules and polymers.[2] Interest in organic electronic molecules is related to their tunable physico-chemical properties by chemical synthesis. For instance, light-emission can be achieved for virtually any color of the visible spectrum by tuning the molecular structure of organic electroluminescent materials.

In the 70's, electrically conducting polymers exhibiting conductivities in the order of 30 S cm^{-1} were discovered.[1] Later on, the first organic transistor was developed by in-situ polymerization of polyacetylene and polythiophene semiconducting thin films in the transistor channel.[2]

Organic electronic materials can be deposited over large areas from solution, e.g. using roll-to-roll processes.[3–5] Since no covalent bond needs to be broken or re-formed during deposition, these materials offer high degree of mechanical flexibility and can be formed using a small energy input, i.e. with temperature < 200 °C, offering a route towards large area flexible organic electronics.

1.2 Research problem

Despite impressive improvements in material synthesis a number of challenges are open in the field of organic electronics. The charge carrier mobility typically seen in organic semiconductors remains low, i.e. mobilities in the range of 0.1-10 $cm^2V^{-1}s^{-1}$ are considered state-of-the-art.[6–8] Many organic semiconductors are not stable in ambient conditions partly because of their relatively low ionization potential (IP) of around 4.8 eV.[3,9,10] Therefore they have to be processed in inert N_2 atmosphere. Silanol groups present at SiO_2 interfaces can quench *n*-type conductivity in organic semiconductors that do not have sufficiently large electron affinities, i.e. <3.85 eV.[11,12]

From a device point of view, the operating voltage of organic transistors making use of a conventional 200 nm-thick SiO_2 gate dielectric, is as high as 20-30 V.[6] One strategy to lower the operation voltage is to use high-k dielectric materials.[13–17]

In order to achieve low voltage operation, an interesting approach, for its compatibility with flexible electronics, is the use of electrolytes as gating medium. Coupling electrolytes and organic semiconductor channel materials can result in capacitances in the order of mF cm^{-2} at voltages below 2 V.[18] Since the transistor current modulation is directly proportional to the capacitance, coupling electrolytes and organic semiconductor channel materials results in low voltage operation.

The principle of electrolyte-gating in a transistor channel has been known since almost sixty years, having been proposed by Shockley, Brattain and Bardeen.[19,20]

Wrighton and coworkers deeply investigated microelectrochemical transistors based on the electrolyte-gating principle.[21–25] Ion-sensitive field-effect transistors,[26–29] ion sensors[30–32] and electrochemical transistors,[21,25,33–37] have been demonstrated over the past 30 years.

More recently, Frisbie et al employed electrolyte-gated organic transistors to achieve low voltage electronics.[38,39] Indeed, electrolyte-gating can be used to lower the operation voltage in organic transistors and as a *tool* to investigate the charge transport properties of organic semiconductor systems.

Another important advantage of electrolyte-gated transistors includes inherent low source and drain contact resistance.[40] In electrolyte-gated organic thin film transistors the contact resistance has been shown to be orders of magnitude lower than in conventional organic transistors. This may be due to electrical double layer assisted charge injection, similar to what is observed in light-emitting electrochemical cells, where the active material comprises a blend of an ion-conducting electrolyte and a conjugated polymer.[41]

Despite the impressive capacitance values achievable in electrolyte-gated transistors, their response time is limited by ionic transport. For instance, while SiO_2 can be polarized in the order of 10^{-13} s, the polarization of electrolytes is limited by the ionic transport to set up the electrical double layers, usually in the order of a few seconds. These topics will be reviewed with further detail in Section 3.3.

1.3 Motivation

The main motivation of this work is to achieve large current modulation in organic electronic films using the configuration of electrolyte-gated (EG) transistors. Electrolyte-gating has been

revived with the appearance of a new class of electrolytes: room temperature ionic liquids (RTILs). RTILs exhibit high thermal stability, large electrochemical stability windows and good ionic conductivities. At present, most of the research efforts in the field of EG transistors focus on the transistor electrolytes and channel materials. Such efforts are presented in Chapter 3. Objectives

The specific objectives of this Ph. D. work are:

(1) To investigate the effect of the physicochemical properties of the electrolyte in establishing the transistor characteristics.

Strategy: The use of room-temperature ionic liquids belonging to the same family, i.e. sharing a common cation/anion, can elucidate the role of the doping ion and of the physicochemical properties of the electrolyte in the doping process.

Hypothesis: The molecular structure of the ions and the electrolyte physicochemical properties play an important role in the doping process. Electrolytes with high ionic conductivity and low viscosity should be able to dope faster the transistor channel. Bulky ionic structures should limit the permeation of ions into the transistor channel.

(2) To shed light on the importance of the nature and surface area of the gate electrode on the transistor drain-source current modulation and the operation voltage of the transistor.

Strategy: In situ electrochemical characterizations in the EG transistor channel, i.e. using the transistor channel as working electrode and the gate as counter electrode and reference electrode or using a third electrode as reference, can be an effective approach to investigate the electrolyte/gate and electrolyte/channel interfaces.

Hypothesis: The surface area and the nature of the gate electrode play an important role to avoid non-reversible electrochemical processes at the gate/electrolyte interface and to establish high current modulation at low voltages.

(3) To explore the possibility to combine energy storage function within the EG transistor structure.

Strategy: The EG transistor structures with high capacitance at the interface between the electrolyte and the transistor channel enables energy storage.

Hypothesis: The energy stored in EG organic transistors can be recovered to power other electronic components and is of interest for energy autonomous devices.

As a general strategy for the above objectives we make emphasis on polymer channel materials, for their simple processability and on room temperature ionic liquids as gating media, for their electrochemical stability and high ionic conductivity.

1.4 Organization of the work

In Chapter 2, we present an introduction to organic semiconductors and we introduce organic transistors and their figures of merit. In Chapter 3, we introduce the electrolyte-gated transistor structure and the electrolytes that can be employed as gating media. In the same chapter, we include a literature review about recent reports on electrolyte-gated organic transistors. Chapter 4 has been published as an article whose title is “Low voltage electrolyte-gated organic transistors making use of high surface area activated carbon gate electrodes” by J. Sayago, F. Soavi, Y. Sivalingam, F. Cicoira and C. Santato, in the Journal of Materials Chemistry C, 2014, 2, 5690. It discusses the importance of using gate electrodes with high surface area to supply the charge required to modulate the conductivity in the transistor channel with sub-1 V electrical biases. Chapter 5 was published as an article whose title is “Electrolyte-gated polymer thin film transistors making use of ionic liquids and ionic liquid-solvent mixtures”, by J. Sayago, X. Meng, F. Quenneville, S. Liang, É. Bourbeau, F. Soavi, F. Cicoira and C. Santato, in the Journal of Applied Physics, 2015, 117, 112809. It presents a systematic study of the effect of RTILs based on a common anion and RTIL-solvent mixtures on the transistor performance. Chapter 6 was published as an article whose title is “TransCap: a monolithically integrated supercapacitor and electrolyte-gated transistor” by J. Sayago, U. Shafique, F. Soavi, F. Cicoira and C. Santato, in the Journal of Materials Chemistry C, 2014, 2, 10273. It introduces the TransCap, a multifunctional Transistor-superCapacitor that combines the transistor logic function with the energy storage capability of supercapacitors. In Chapter 7, we include preliminary results of *n*-type EG PCBM transistors. Chapter 8 is a general discussion about the elements constituting the present work as a whole and Chapter 9 presents conclusions and recommendations for future work. An appendix

with supplementary information for Chapters 4-8 and a list of other publications and conferences is included.

CHAPTER 2 ORGANIC SEMICONDUCTORS

Organic materials, mainly composed of carbon atoms, are typically poor electronic conductors because electrons are confined locally in strong covalent sigma bonds. Nevertheless, organic compounds can become electronically conductive if they possess a carbon structure with regular alternation of single (σ) and double (σ and π) bonds, which is referred to as conjugation.

To illustrate the concept of conjugation, we refer to the molecular structure of benzene, Fig. 2.1. One 2s- and two 2p-carbon orbitals hybridize to form three sp^2 hybrid orbitals on the same plane. The remaining p_z-orbitals are perpendicular to that plane. The overlap of the hybridized orbitals of one atom with the hybridized orbitals of neighboring atoms leads to the formation of σ bonds while the overlap of p_z-orbitals generates π-bonds. If p_z-orbitals overlap along a ring or an extended carbon chain, the electrons are delocalized and can participate in charge carrier conduction. The overlap of two p_z-orbitals results in one bonding π molecular orbital, with lower energy than the atomic orbitals and one anti-bonding π* molecular orbital with higher energy than the atomic orbitals. The highest occupied molecular orbital (HOMO) is the occupied π-orbital with the highest energy and the lowest unoccupied molecular orbital (LUMO) is the unoccupied π*-orbital with the lowest energy. The energy gap between the HOMO and LUMO is the band gap (E_g), in this case, of benzene. The energy level of the HOMO and LUMO with respect to the vacuum level corresponds to the ionization potential and the electron affinity of the organic molecule.

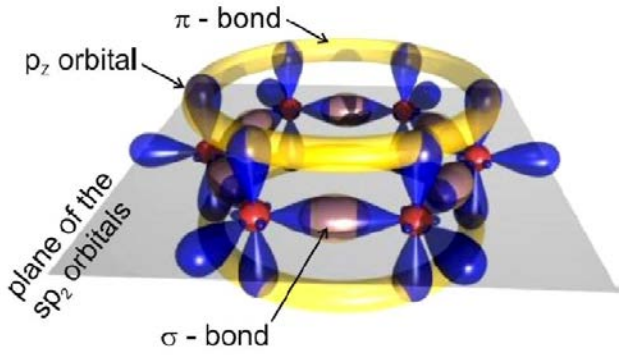

Figure 2.1. Molecular orbitals of benzene.[42] Reprinted with permission.

In solid conjugated materials, both small molecules and polymers, charge carriers can move not only at the intramolecular level but also at the intermolecular level. The transition in the electronic structure from a single molecule (i.e. benzene) to a molecular solid is illustrated in Figs. 2.2a-c. When the intermolecular interactions are weak (van der Waals interactions, with typical energy < 0.2 eV), the electronic properties of the organic semiconductors are largely determined by the energy levels of the single molecules. As illustrated in Figs. 2.2a and 2.2b, the HOMO and LUMO levels of individual molecules merge into HOMO and LUMO bands for the organic solid.[43] On the other hand, strong intermolecular interactions can result in long-range order with an important effect on the electronic properties of the solid. In this case, the HOMO and LUMO bands merge into a valence band and a conduction band with a much lower band gap, as illustrated in Fig. 2.2c.

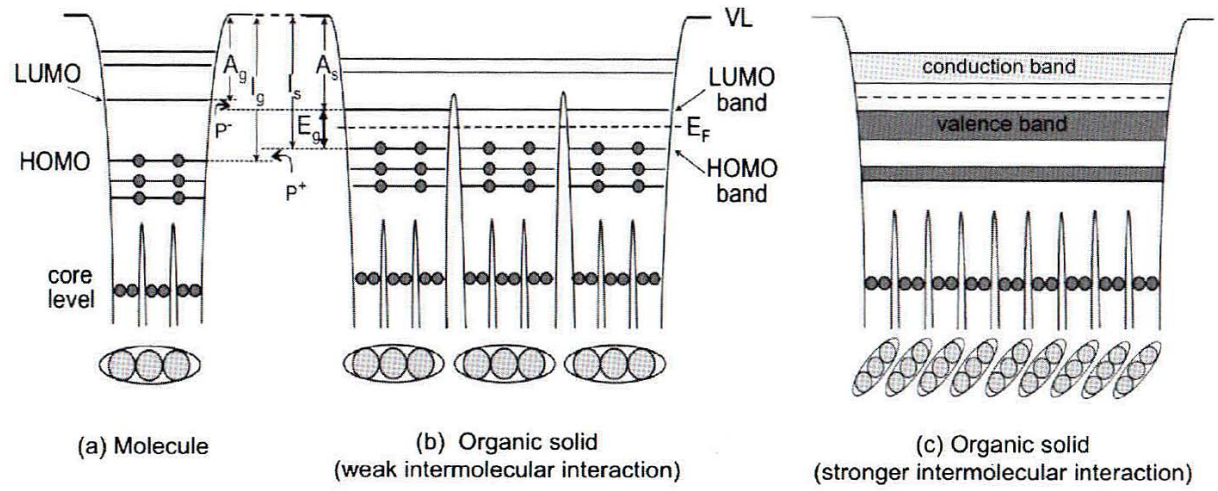

Figure 2.2. Energy level diagram of (a) an isolated molecule, (b) organic solid with intermolecular interactions extending over a few molecules and (c) solid with intermolecular interactions extending over many molecules, compared to (b). The electron affinity, A, and ionization potential, I, are indicated for the solid (s) and gas (g) phase. P is the polarization energy, E_g the band gap, E_F the Fermi level and VL is the vacuum level.[43] Reprinted with permission.

2.1 Molecular structures

Organic semiconductors materials can be small molecules or polymers. Fig. 2.3 presents the molecular structure of common repeating units found in organic semiconductor materials.

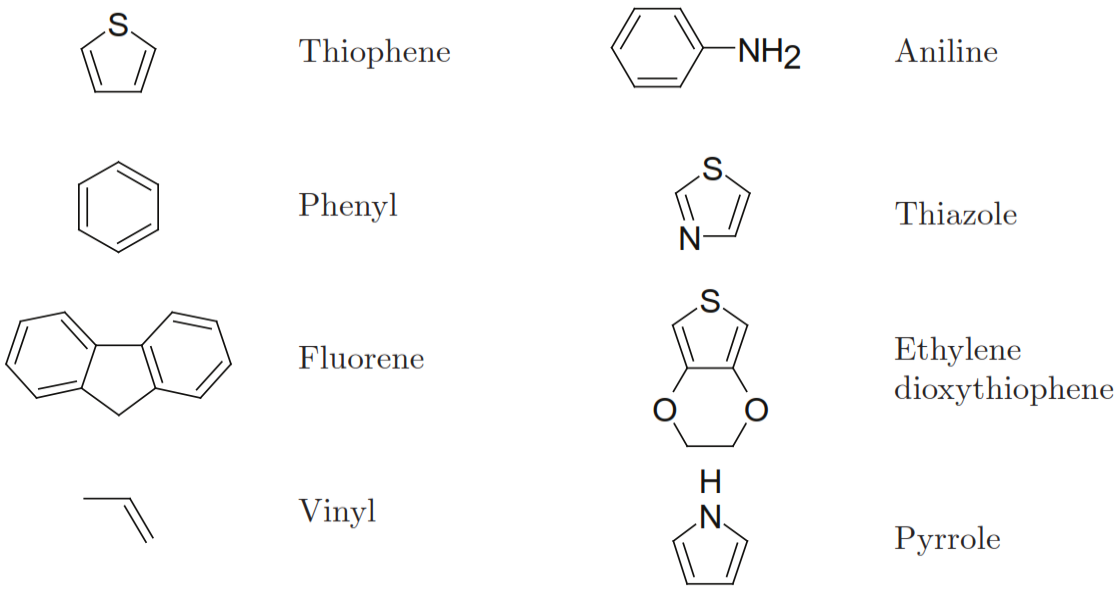

Figure 2.3. Molecular structure of common units in organic semiconductors.[44] Reprinted with permission.

2.1.1 Small molecules

A category of organic semiconductors are π-stacked conjugated small molecules. Small molecules can form single crystals through π-π orbital overlap resulting in relatively high charge carrier mobility, i.e. 20 $cm^2V^{-1}s^{-1}$.[45]

Charge transport in single crystal organic semiconductors is favoured by their highly regular, grain boundary-free structure. Particularly interesting small molecules in single crystal systems, for their good transport properties, are pentacene and rubrene, whose molecular structures are illustrated in Fig. 2.4.

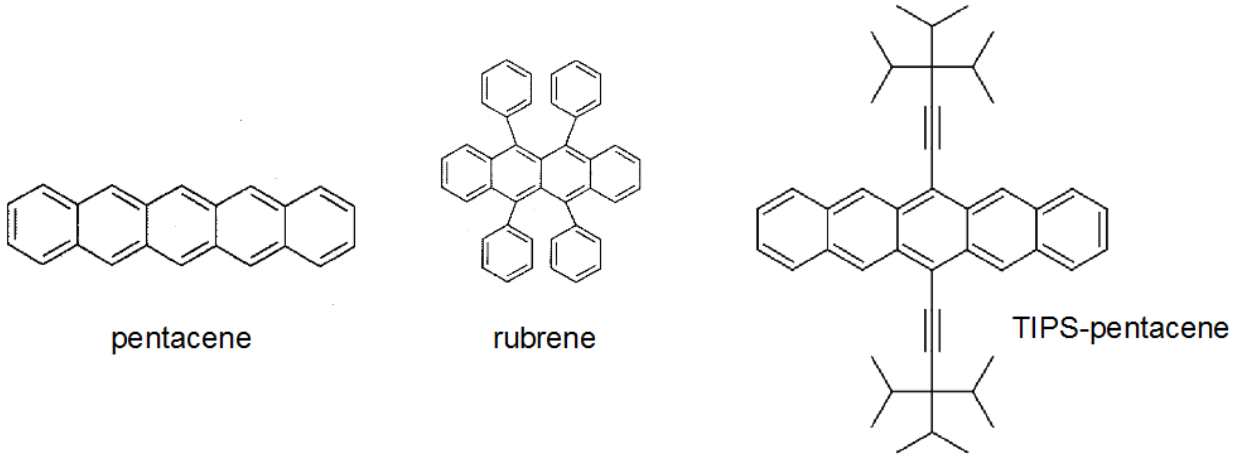

Figure 2.4. Molecular structure of pentacene, rubrene and TIPS-pentacene.[44] Reprinted with permission.

Pentacene is one of the most popular organic semiconductor materials used nowadays. It consists of five benzene rings linearly fused together, that are relatively easy to pack into ordered films. Pentacene thin films can reach charge carrier mobilities exceeding 1 $cm^2V^{-1}s^{-1}$.[3,46] It has been shown that polymorphic crystal growth can disrupt charge carrier transport due to the presence of grain boundaries.[47] Because pentacene is not soluble, it can only be deposited by vacuum processes. However, synthetically attaching proper groups to the 6,13 positions of pentacene, such as in TIPS pentacene (Fig. 2.4), solubility in common organic solvents can be achieved.[44] Rubrene is a fused ring semiconductor, illustrated in Fig. 2.4, which has attracted significant interest in its single crystal form. Rubrene holds the record for *p*-type charge transport in organic electronics with hole mobilities greater than 20 $cm^2V^{-1}s^{-1}$.[45]

One example of *n*-type molecule is PCBM, illustrated in Fig. 2.5. Its lower LUMO level compared to C60 and C70 analogues allows easy electron injection. The electron mobility of PCBM thin films is ca 10^{-3} $cm^2V^{-1}s^{-1}$.[48,49]

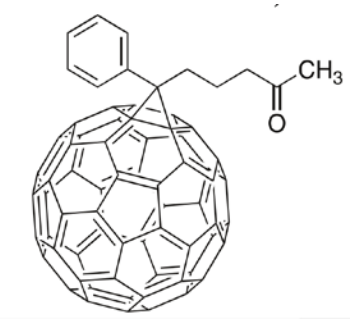

Figure 2.5. Molecular structure of PCBM.[49] Reprinted with permission.

2.1.2 Polymers

Thin films of organic semiconducting polymers are particularly interesting for printable electronics since polymers can be designed to be soluble in different organic solvents and yield cost-effective deposition over large-areas, i.e. by roll-to-roll printing.[38]

One of the most popular conjugated polymers is poly(3-hexylthiophene), P3HT, a polythiopene derivative that employs alkyl side chains to improve its solubility without significantly disturbing its conjugated backbone.[44] The molecular structure of conjugated polymers can be engineered to control the position of the solubilizing groups and yield head-tail head-tail (HT-HT) regioregular structures, as shown in Fig. 2.6a.[50,51] Regioregular P3HT can self-organize into lamellar sheets, Fig. 2.6b, and feature charge carrier mobilities of up to 1 $cm^2V^{-1}s^{-1}$.

The charge carrier mobility is not only affected by the film morphology but also by the molecular weight. Experimentally, it was observed that the mobility of spin-casted P3HT films could be increased from 10^{-6} $cm^2V^{-1}s^{-1}$ to 10^{-2} $cm^2V^{-1}s^{-1}$ by varying the molecular weight, from ca 3 kDa to 30 kDa.[52]

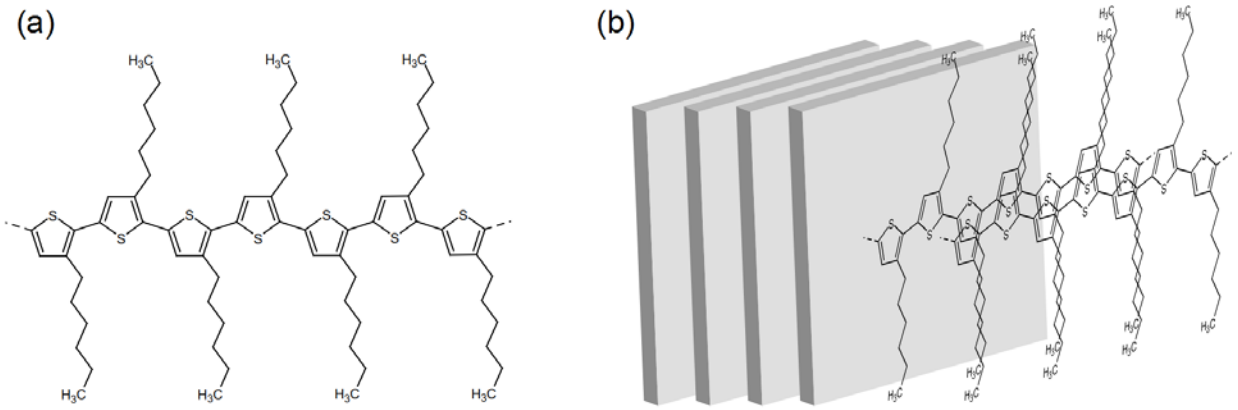

Figure 2.6. (a) Molecular structure of P3HT and (b) lamellar thin film stacking.[53] Reprinted with permission.

At laboratory scale, P3HT thin films can be formed by spin-coating solutions of P3HT in high boiling point solvents, such as 1,2-dichlorobenzene, to promote slow drying and self-assembly on a flat SiO_2 substrate.[54] Often the substrate is pre-treated with hexamethyldisilazane (HMDS), which creates a nonpolar hydroxyl-free surface that the hexyl groups of P3HT prefer. Thermal treatment under vacuum or inert N_2 atmosphere is commonly employed to remove solvent traces and to reverse possible *p*-doping that O_2 could induce.[55,56]

A. Polyphenylene vinylene light-emitting polymers

The demonstration of light-emitting diodes using electroluminescent polyphenylene vinylene (PPV) conjugated polymers in the 90's paved the way towards polymer light-emitting devices.[57] Since then, PPVs have been popular materials for their wide range of colour emission, from orange to green.[58] A popular PPV, for its availability, processability and well known properties, is poly [2-methoxy-5-(2'-ethylhexyloxy)-1,4-phenylene vinylene] (MEH-PPV), illustrated in Fig. 2.7.[59,60]

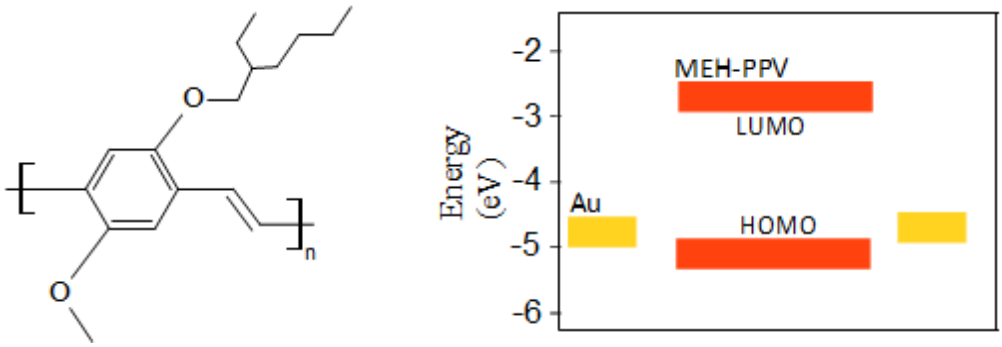

Figure 2.7. Molecular structure of MEH-PPV (left) and energy levels (right). The energetic levels were taken from Osikowicz et al.[60]

2.1.3 Thin film morphology and its correlation with the film electrical and optical properties

The molecular arrangement in organic semiconductor materials has an important effect on the film morphology and its electric and optical properties. Crystalline structures commonly feature high charge carrier mobilities but their processing commonly requires vacuum systems. Solution processing techniques, such as spin-coating, drop-casting, dip-coating and ink-jet printing, are generally simpler but the organic semiconductor has to be soluble.[38] This is commonly achieved through molecular functionalization by adding alkyl chains or other bulky substituent groups. On the other hand, these groups can induce high steric hindrance limiting close intermolecular packing and resulting in poor charge carrier mobilities.[61] The incorporation of semiconducting polymer films as active materials in electronic devices continues to be major research topic. The challenge relies on developing semiconducting polymers with high charge carrier mobility while keeping good processability and mechanical properties. Polymers usually cannot be grown into highly ordered single crystals. On the other hand, polymers may have the advantage of fast charge carrier transport along their conjugated backbone structure,[62] except for some cases where backbone tilting defects give rise to a distribution of shallow trap states in the gap and reduce the charge carrier mobility.[63]

A. Small molecule thin films

Physical vapor transport (PVT) of small molecules in a stream of high-purity noble gas (i.e. argon, helium) through horizontal reactors can produce highly pure single crystals.[64,65] The reactor chamber is set with a narrow temperature gradient and the starting material is placed in the hottest region.

As an example of solution-processed small molecule thin films, we consider PCBM. Crystalline organization of PCBM from solution was reported by Yang et al. by using different solvents and different deposition techniques.[66] PCBM films were obtained by spin-coating and, alternatively, from slow solvent evaporation in an atmosphere saturated with vapor of the corresponding solvent. The solvent-evaporation kinetics of film deposition played a major role in establishing the crystalline structure of the thin films. Spin-coated films (fast deposition) resulted in densely distributed PCBM nanocrystalline films with homogeneous morphology as illustrated in Fig 2.8a. By slow solvent evaporation conditions, large PCBM crystallites were observed, Fig. 2.8b.

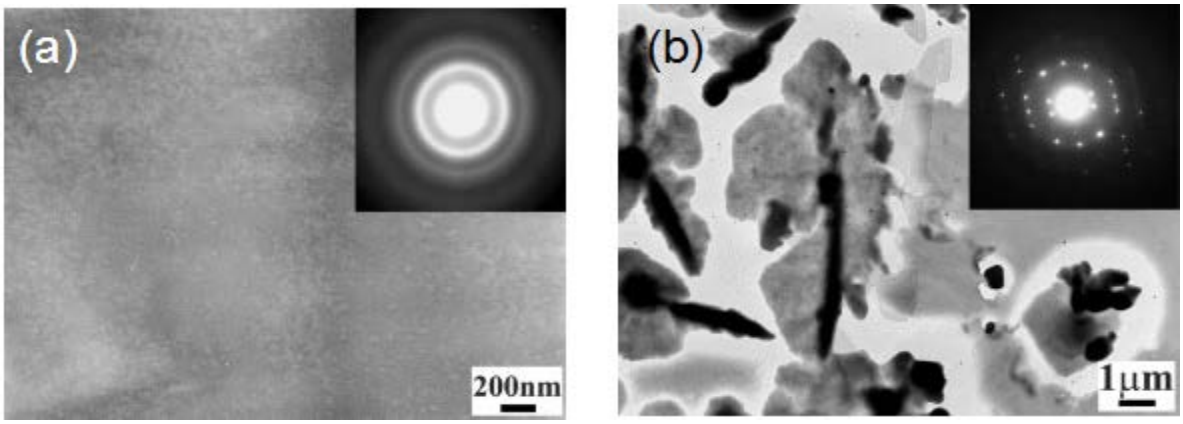

Figure 2.8. Transmission electron microscopy (TEM) bright-field images of PCBM films obtained from chlorobenzene solutions via spin-coating (a) and slow deposition from solvent-vapor saturated atmosphere from the same solvent (b). In the inset, selected-area electron diffraction patterns show the higher crystalline structure in (b) compared to (a).[66] Reprinted with permission.

Single crystal films of 2,7-dioctyl[1]benzothieno[3,2-b][1]benzothiophene (C8-BTBT) were obtained via ink-jet printing from solutions comprising a solvent and an anti-solvent (a liquid in which the semiconductor is insoluble).[67] The solvent and anti-solvent were 1,2-dichlorobenzene (DCB) and N,N-dimethylformamide (DMF), both miscible with one another. This technique results in slower evaporation rates, about 10-50 times slower than in the case without the anti-solvent. Synchrotron single-crystal X-ray diffraction was used to determine the crystallinity of the thin films. Film thicknesses about 30-200 nm were obtained with mobilities exceeding 16 $cm^2V^{-1}s^{-1}$.

Solvent vapor annealing of spin-coated thin films of C8-BTBT, an air stable and high-mobility semiconductor, has been reported.[68] C8-BTBT was first spin-coated on SiO_2 substrates pre-treated with PMMA and then annealed for 10 h in chloroform vapors, resulting in single-crystal structures. Band-like charge transport (see Section 2.3.2) was observed with hole mobilities up to 9 $cm^2V^{-1}s^{-1}$.

Single crystals of 3,11-didecyldinaphtho[2,3-d:2',3'-d']benzo[1,2-b:4,5-b']dithiophene [C10-DNBDT] were obtained by a modified edge-casting solution crystallization technique.[69] The substrate, a 100-nm thick thermally oxidized SiO_2 layer, was treated with a phenyl-substituted silane-based self-assembled monolayer [trimethoxy(2-phenylethyl)silane, β-PTS] to increase the wettability of the solution on the substrate. A mobile solid blade edge with a replenishing mechanism was used to supply solution at the same rate as the solvent evaporates resulting in inch sized single crystals, as confirmed by X-ray diffraction measurements. The *p*-type field-effect transistor mobility was 9.5 $cm^2V^{-1}s^{-1}$ in the saturation regime and 8.2 $cm^2V^{-1}s^{-1}$ in the linear regime.

B. Polymer films

The processing conditions affecting the film morphology may affect different functional film properties, in different manners. Important factors, that will be discussed in this section, include the substrate chemistry and substrate morphology, the solution properties (concentration, solvent type and viscosity), the deposition conditions (atmosphere and temperature) and post-thermal treatments commonly employed to increase molecular ordering and to remove solvent traces.[70,71] Hence it is paramount to understand the interplay between processing conditions, morphology

and structure of the films for the realization of high performance organic electronic materials and devices.

The correlations between morphology and electrical and optical properties in polymer thin films deposited from solution have been reviewed, among others, by Yang et al.[59,72]

Effect of the solution properties on the polymer film morphology

Molecules in solutions tend to aggregate when the concentration attains a critical value. The origin of molecular aggregation is the presence of intermolecular forces between polymer chains and polymer chain-solvent molecules.[59] The solution viscosity is proportional to the intermolecular forces between the solvent molecules, i.e. higher solution viscosity suggests higher solvent intermolecular forces.

Shi et al proposed a method for characterizing the solution viscosity as a function of the solution concentration. The method is based on the reduced viscosity η/η^*, where η is the viscosity of the polymer solution and η^* is that of the solvent, at room temperature.[73] A plot (Fig. 2.9) of the reduced viscosity of the polymer solution vs the polymer concentration (wt %) reveals three regimes. A linear regime at low concentration (i.e. <0.4%) where the polymer chains are not aggregated. A second linear region at high concentration (i.e. >0.9%) resulting in heavily aggregated polymer chains. The middle curved region can be defined as the region of concentration for loose aggregation.

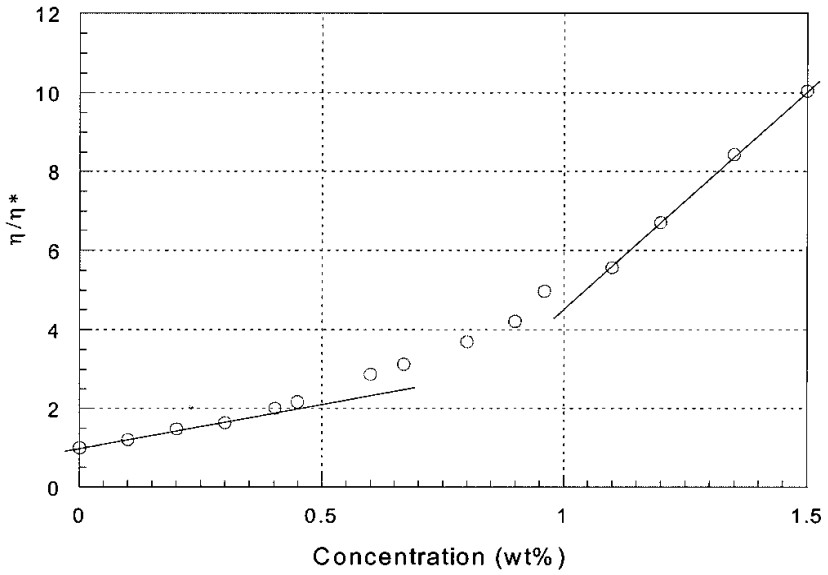

Figure 2.9. Reduced viscosity η/η* of MEH-PPV solutions in cyclohexanone (η* is 1.85 cp) vs concentration of the polymer solution.[73] Reprinted with permission.

The dependence of aggregation on solution concentration was observable by UV-Visible absorption spectroscopy.[73] High concentrations, 1 wt%, resulted in an absorption λ_{max} located at 496 nm while small concentrations, 0.3 wt%, resulted in a red shift of λ_{max}, at 510 nm, thus suggesting larger conjugation lengths for the latter. The optical properties at small and high concentrations were weakly influenced by the rotation spin speed applied during deposition suggesting that in these regimes the polymer stacking was stable enough to prevent changes by the centrifugal force or during the solvent evaporation. As the concentration approached the region for loose aggregation (0.7 wt%) the λ_{max} in the electroluminescence spectra red-shifted from ca 499 nm to ca 509 nm with increasing spin speed from 2000 rpm to 8000 rpm. During spin-coating, the centrifugal force and the radial flow of the solvent tend to stretch the polymer chains radially against the cohesive forces of the solution. If the centrifugal force is larger than the cohesive force of the solution, more extended (less coiled) conformations of the polymer molecules can be expected, resulting in more extended conjugation. Lower spin rates result in a more dense and thick films.

The solvent properties also play an important role on the conformation of MEH-PPV films.[73] Thin films deposited using non-aromatic solvents result in more hydrophilic film surfaces suggesting that the film is more polar compared to those deposited using aromatic solvents. Since the polar components of MEH-PPV come from its C-O bonds, the surface polarity depends on how many C-O bonds are available on the surface to interact with water molecules during the hydrophilicity test. The more parallel conformation of the aromatic ring to the film surface (Fig. 2.10) exposes both oxygen atoms resulting in a more polar surface compared to a perpendicular conformation that only exposes one of the two oxygen atoms on the surface. Therefore, films deposited with non-aromatic solvents probably have a more parallel conformation than films deposited with aromatic solvents.

The solvent evaporation rate during deposition can also affect the conformation of MEH-PPV films.[59] Lower solvent evaporation rates give to the polymer chains more time to relax into their more thermodynamically favorable conformation, i.e. parallel to the surface for glass substrates, as illustrated in Fig. 2.10.[59] Treating the substrate surface with a self-assembled monolayer, i.e. octadecylmercaptan (ODM), can lower the substrate surface energy facilitating the parallel conformation of the film over the substrate.[74]

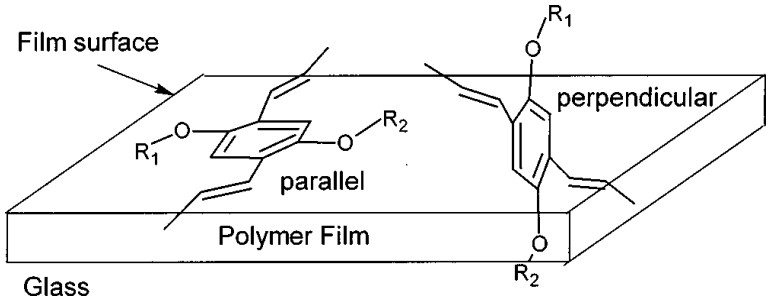

Figure 2.10. Parallel and perpendicular orientations of the MEH-PPV aromatic ring on the glass substrate surface.[59] Reprinted with permission.

B. Effects of the post-deposition thermal treatment on the emission spectra

Post-deposition thermal treatments of polymer thin films can dramatically change their morphology. At temperatures above the glass transition temperature T_g, i.e. the temperature where the polymer evolves from a hard, glassy material to a soft, rubbery material, i.e. 75 °C for MEH-PPV, polymer chains tend to relax to more thermodynamically stable conformations.[72]

As illustrated in Fig. 2.11a, higher annealing temperatures result in red-shift MEH-PPV emission spectra and lower photoluminescence (PL) intensity. The lower PL intensity at higher temperatures has been attributed to interchain interactions leading to quenching of emission. A weaker effect of the temperature was observed on the normalized PL characteristics of BCHA-PPV, Fig 2.11b. Compared to MEH-PPV, BCHA-PPV is a poly(p-phenylene vinylene) with larger side groups. The bulky side groups inhibit interchain interactions making BCHA-PPV less sensitive to the thermal treatment.

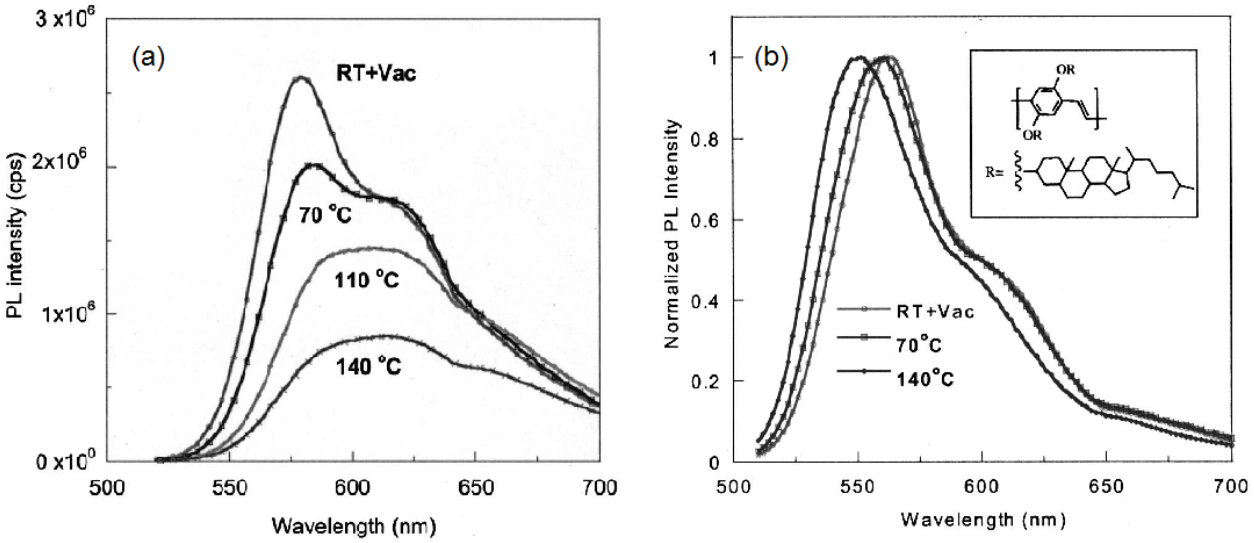

Figure 2.11. (a) Photoluminescence (PL) spectra of MEH-PPV film after subsequent 2h thermal treatments at different temperatures, increasing from room temperature to 140 °C. (b) Normalized PL spectra of poly(2,5-bis(cheolestranoxy)-1,4-phenylene vinylene) (BCHA-PPV) film processed at different temperatures. The molecular structure of BCHA-PPV is shown in the inset.[72] Reprinted with permission.

2.2 Novel organic semiconductor processing techniques

Deposition methods to attain specific morphologies non-achievable by traditional deposition techniques such as spin-coating or drop-casting, are under development.

Molecular alignment using zone-casting, a deposition technique from solution, was reported by Tsao et al.[75] A solution is spread out by means of a nozzle. The support moves after a critical concentration is attained (after solvent evaporation) this way forming an aligned thin film.

Polymer nanofiber films can be created by the electrospinning process.[76] The main advantage of electrospinned layers is the possibility to create fibers with high surface-to-volume ratio. The process of electrospinning is illustrated in Fig. 2.12. It uses an electrostatic force to spin polymer fibers from a nozzle of a syringe containing a polymer solution onto a substrate. The needle is maintained at a certain voltage with respect to the target substrate, by a power supply. When the electrostatic force overcomes the surface tension of the polymer solution, the liquid spills out of the spinneret and forms fine filaments, which are collected on the substrate. This method allows to produce fibers with diameters ranging from 2 nm to several microns and gives a unique opportunity to control the size of the voids between fibers.[77]

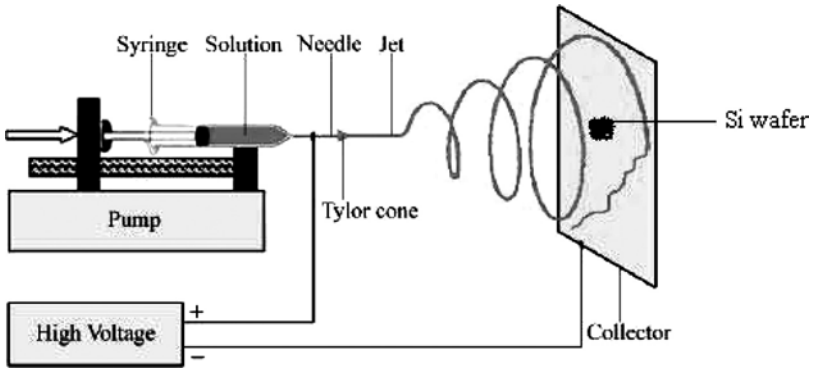

Figure 2.12. Schematic representation of the electrospinning set-up.[78] Reprinted with permission.

Controlled alignment and patterning of single *p*- and *n*- type polymer nanowires was demonstrated using an electrospinning variant, high-speed electrohydrodynamic organic nanowire printer. Single nozzle electrospinning of P3HT/PEO solutions resulted in field-effect mobilities of 3.8 $cm^2V^{-1}s^{-1}$.[79]

2.3 Charge transport in organic semiconductors

One of the figures of merit to quantify charge transport is the charge carrier mobility. The charge carrier mobility (μ) is the ratio between the average charge carrier speed (v) and the electric field (E) in the material.

$$\mu = \frac{v}{E}. \qquad \text{Eq. (1)}$$

Different mechanisms have been proposed to describe charge transport in organic semiconductors. They will be briefly reviewed in what follows.

In semiconductors such as Si or Ge, characterized by a regular lattice arrangement of atoms, coulombic interactions between electrons and holes are weak (with energy <100 meV) due to strong dielectric screening, and electrons and holes are nearly free (bounded in a crystalline structure) to move at room temperature.[80]

Charge carrier transport in such materials has been modelled employing the concept of "bands" described at the beginning of the present chapter. The band transport model is valid only when the charge carrier mean free path (distance between scattering events) is larger than the crystalline lattice constant.[80]

In the band transport model, the mobility depends on the temperature (T) as: [81]

$$\mu \propto T^{-n} \qquad \text{with n ~ 1-2} \qquad \text{Eq. (2)}$$

For example, Fig. 2.13 shows a plot of the mobility as a function of the temperature for polycrystalline pentacene- and single crystal pentacene-based transistors (see also section 2.4.1.). The mobility of single crystal pentacene (dots) can be fitted well to Eq. (2), thus indicating band transport. The mobility of polycrystalline pentacene (squares) first increases with temperature to a maximum value of ca 0.4 cm^2Vs^{-1} at ca 240 K and then sharply decreases as a function of temperature as opposed to single crystal pentacene organic transistors.

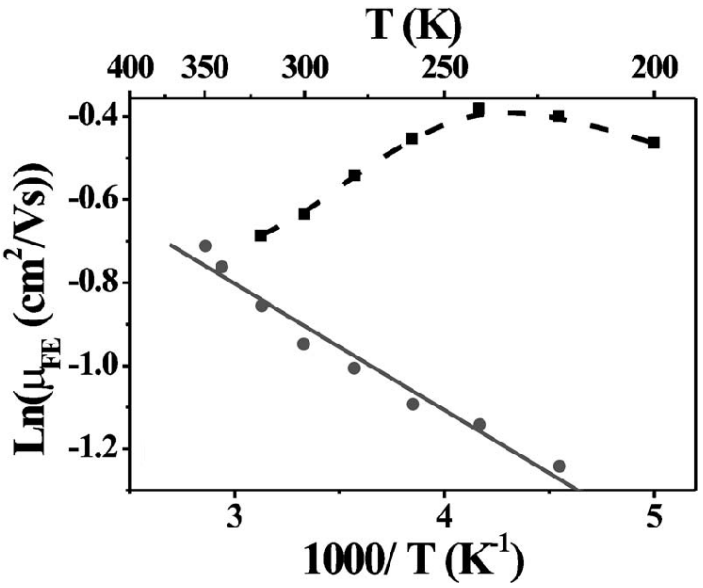

Figure 2.13. Field-effect mobility (μ_{FE}) as a function of the inverse temperature for single crystal pentacene organic transistors (dots) and polycrystalline pentacene organic transistors (squares).[82] Reprinted with permission.

The band transport behaviour is rarely observed in organic semiconductors, except for some organic single crystals. Organic semiconductors are commonly characterized by a Gaussian distribution of the HOMO and LUMO levels.[80] Amorphous and polycrystalline organic solids usually show considerable spectral broadening as schematically illustrated in Fig. 2.14.

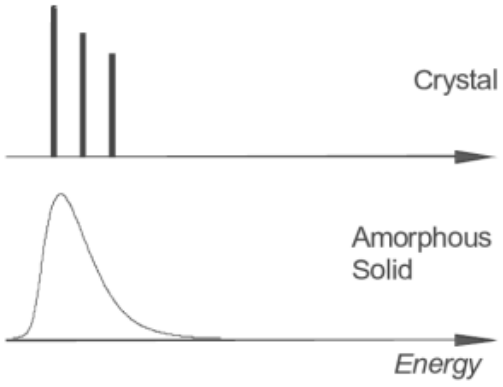

Figure 2.14. Schematic representation of optical spectra of crystal and amorphous solid organic molecules.[83] Reprinted with permission.

Charge carriers in amorphous and polycrystalline organic semiconductors usually hop between different sites and the mobility dependence on the temperature is described by an Arrhenius-type relation[84]

$$\mu = \mu_o \exp\left(\frac{-E_a}{k_B T}\right) \qquad \text{Eq. (6)}$$

with a prefactor μ_o and an activation energy E_a (k_B is the Boltzmann constant).

One notable limitation of the hopping transport model is to consider E_a constant while experimentally it has been observed that E_a decreases with the increase of the applied gate voltage (V_{gs}).[85,86] Because the charge carrier density increases with the increase of V_{gs}, affecting other material properties as well, reviewed in Section 2.4, it is reasonable to propose a correlation between the activation energy and the charge carrier density.[87]

The multiple trap and release transport model, originally conceived to model the mobility in hydrogenated amorphous silicon thin films, predicts a mobility dependence upon temperature and gate voltage, as observed experimentally in organic transistors.

Horowitz et al developed a semi-empirical mobility expression for organic transistors as a function of the gate-source voltage (V_{gs}).[85]

$$\mu = \mu_o \frac{N_C}{N_{to}} \left(\frac{C_i V_{gs}}{e N_{to}}\right)^{\frac{T_C - T}{T}} \qquad \text{Eq (7)}$$

where N_C is the effective density of states in the transport energy level, N_{to} is the surface density of traps at the semiconductor-insulator interface of the transistor channel, C_i is the specific capacitance of the insulator, e is the elementary charge and T_C is a characteristic temperature related to the width of the exponential trap distribution.

2.4 The organic field-effect transistor

The organic transistor emulates, with organic semiconducting materials, the structure of the metal-insulator-semiconductor field-effect transistor (MISFET) that is a key component in most electronic devices, for example, microprocessors, memory devices, active-matrix displays.

Modern computing power is based on single-crystalline silicon semiconductors that can reach carrier mobilities in the order of 10^2-10^3 $cm^2V^{-1}s^{-1}$. Although organic transistors, with an organic semiconductor channel, cannot compete with these mobilities, they may be employed in alternative applications such as sensors or radio-frequency identification (RFID) tags or in applications where mechanical compliance is required.[3,53]

The typical structure of an organic transistor and the energy levels for the metal-insulator-semiconductor junction are illustrated in Fig. 2.15a and Fig. 2.15b.[88] The transistor structure consists of an organic semiconductor included between source and drain electrodes and stacked with a dielectric and gate electrode. The region delimited by the source (S) and the drain (D) electrodes defines the transistor channel, with a geometry characterized by the interelectrode distance (channel length, L), the electrode width (channel width, W) and the channel thickness (t). Upon application of an appropriate gate-source bias (V_{gs}), electronic charge carriers can be induced in the transistor channel and move under the action of a source–drain bias (V_{ds}). The current flowing between S and D (I_{ds}) is modulated by V_{gs}. The source electrode is usually the common ground.[5]

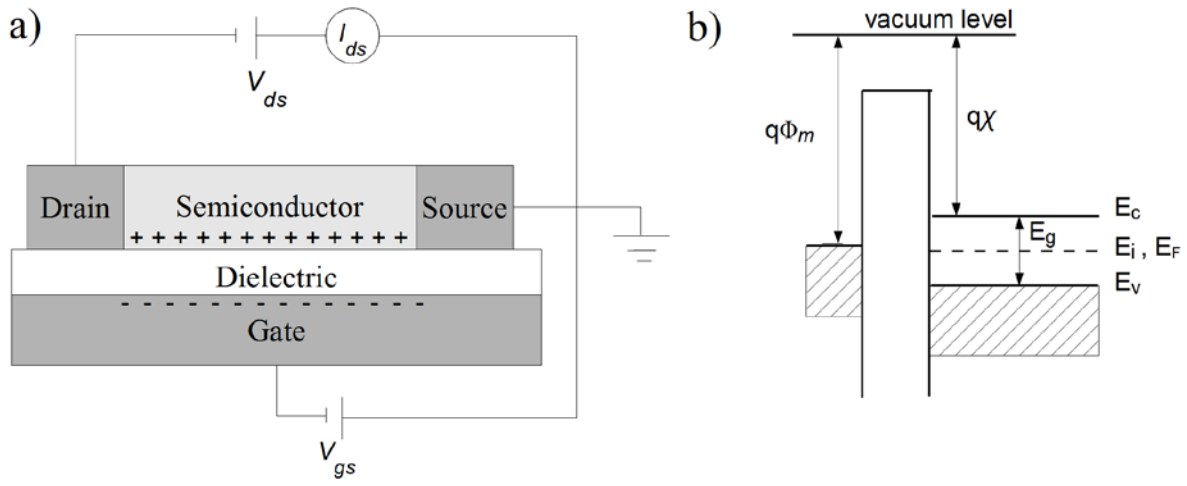

Figure 2.15. (a) Structure of a metal-insulator-semiconductor field-effect transistor and (b) ideal band diagram of the metal-insulator-semiconductor junction at equilibrium. The Fermi level (E_F) and the intrinsic level (E_i) are located close to the midgap (E_g/2) for an intrinsic semiconductor.

A. The field-effect

The energy levels of an ideal metal-insulator-semiconductor junction are shown in Fig. 2.15b for an intrinsic (non-doped) semiconductor. The junction is termed ideal because the bands are flat for an unbiased junction. This is the case when Eq. (6) is fulfilled.

$$\Phi_m = \chi + \frac{E_g}{2} + \Phi_b \qquad \text{Eq. (6)}$$

where Φ_m is the metal workfunction, χ is the electron affinity, E_g is the semiconductor band gap, Φ_b is the potential difference between the Fermi level and the intrinsic level (for an intrinsic semiconductor, Φ_b=0 and the Fermi level is located at the same energy than the intrinsic level). In the non-ideal case there is a mismatch between the metal workfunction and the semiconductor Fermi level resulting in a band curvature at the dielectric-semiconductor interface; a small potential termed flat-band voltage, V_{fb}, must be applied at the gate electrode to get the ideal (flat-band) condition.

When the metal-insulator-semiconductor junction (non-doped) is biased with a negative bias (Fig. 2.16) the bands bend upward near the dielectric-semiconductor interface and the valence band moves closer to the Fermi level causing an accumulation of holes at the interface. A similar description can be proposed for a positive applied bias for the accumulation of electrons.

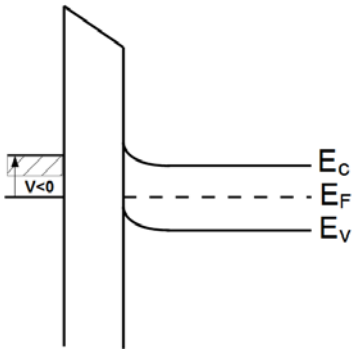

Figure 2.16. Energy band diagram for a negatively polarized metal-insulator-semiconductor junction.

2.4.1 Current-Voltage characteristics in organic field-effect transistors.

Organic transistors typically operate under accumulation of charge carriers.[89] The metal-insulator-semiconductor junction induces a sheet charge density (Q that can be expressed in C cm^{-2}), determined by the capacitor relationship

$$Q = C_i (V_{gs} - V_t), \qquad \text{Eq. (7)}$$

where C_i is the capacitance density (expressed in F cm^{-2}) of the gate dielectric and (V_{gs}-V_t) is the gate voltage applied beyond the threshold voltage. The threshold voltage (V_t) is the gate voltage at which a perceptible current begins to flow in the device.[89] With source and drain electrodes with workfunctions that match the HOMO and LUMO of the channel organic material, the I_{ds}-V_{ds} relation is generally linear, i.e. it follows Ohm's law. As the V_{ds} is increased, the channel current (I_{ds}) increases until the field from the drain-source bias cancels the field from the gate-source bias. At that point, the change of I_{ds} vs V_{ds} slows down and the device enters the saturation regime. Fig. 2.17 shows the typical output characteristic, I_{ds}-V_{ds} for increasing V_{gs} values, the linear and saturation regimes are indicated.

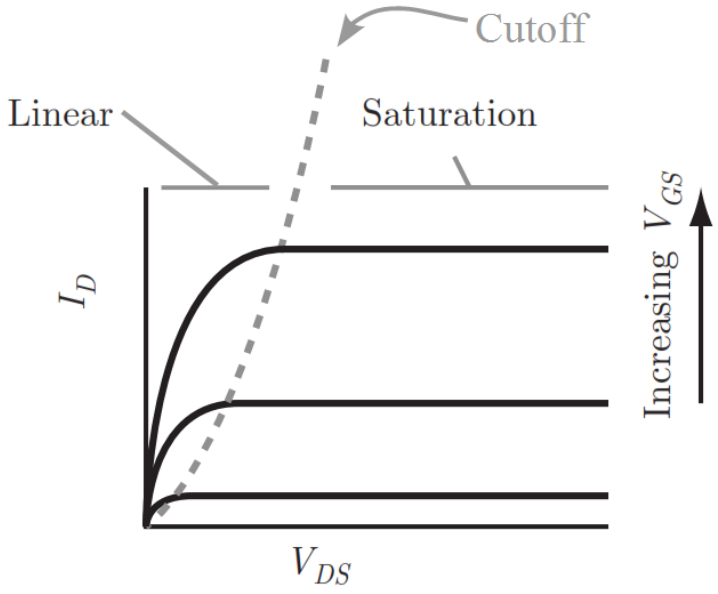

Figure 2.17. Schematic diagram of the transistor output characteristics. The transistor linear and saturation operation regimes and the cutoff line separating both regions are indicated.[89] Reprinted with permission.

In the linear region, where $V_{gs}>V_t$ and $V_{gs}-V_t > V_{ds}$, the transistor I_{ds} can be expressed as the amount of charge contained in the channel swept at the speed (v) of the charge carrier movement.[89] Under the action of a V_{ds}, the sheet charge density (Q expressed in C cm^{-2}) contained along the transistor channel width, W, yields a I_{ds}

$$I_{ds}(linear) = QWv$$

$$= QW\mu E \qquad \text{Eq. (8)}$$

where E is the electric field in the channel, i.e. V_{ds}/L .

$$I_{ds}(linear) = QW\mu\frac{V_{ds}}{L} \qquad \text{Eq. (9)}$$

Combining Eq. (7) and Eq. (9) results in

$$I_{ds}(linear) = \frac{W}{L}\mu C_i(V_{gs} - V_t)V_{ds} \quad \text{for } V_{ds} \le (V_{gs} - V_t) \qquad \text{Eq. (11)}$$

where L is the transistor channel length.

In the saturation regime, $V_{ds}\geq V_{gs}-V_t$, the electric field in the transistor channel is deduced from the quotient of the integration of the potential gradient along the channel length and the interelectrode length, i.e. $E= V_{ds}/2L$. In this regime, the I_{ds} is limited to the saturation value and the transistor current-voltage relation can be determined by substituting $V_{ds}= V_{gs}-V_t$ in Eq. (11).

$$I_{ds}(saturation) = \frac{W}{2L}\mu C_i(V_{gs} - V_t)^2 \quad V_{ds} \ge (V_{gs} - V_t) \qquad \text{Eq. (12)}$$

The equations to relate the I_{ds} vs V_{ds} are derived in the gradual channel approximation, based on the assumption that the gradient of the electric field between the drain and source electrodes is much smaller than that perpendicular to the insulator-semiconductor interface. This is generally true when the channel length is much larger than the insulator thickness. Also the mobility is assumed to be constant with the charge carrier density.

Besides the mobility (μ), the key figures of merit to characterize transistors are the threshold voltage (V_t), the ON/OFF ratio, and the transconducatance (g_m).

The threshold voltage (V_t) is generally used to specify the gate voltage at which current begins to flow, this is, at the onset of accumulation. To determine the threshold voltage, the linear part of the $I_{ds}^{1/2}$-V_{gs} curve is extrapolated to intercept the V_{gs} axis, as illustrated in Fig. 2.18.

A semi logarithmic plot of I_{ds} vs V_{gs} allows determining the onset voltage at which the drain current abruptly increases above the off level, where I_{ds} is set due to the charge carriers accumulated by the gate voltage.[90]

The ON/OFF ratio, as its name implies, is the ratio between the highest current level achieved by transistor in its "on" state (I_{ON}), divided by the lowest current measured when the transistor is "off" (I_{OFF}). The ON/OFF ratio indicates the degree at which the conductivity of the transistor channel can be modulated. A high ratio between the ON and OFF conditions is desirable. In inorganic transistors, the ON/OFF ratio is in the order of 10^6-10^8. In organic transistors the ON/OFF ratio is usually 10^4-10^6.[53] In both cases the I_{ON} is limited by the dielectric strength, i.e. ca 5 - 7 MV cm^{-1} for SiO_2.[91]

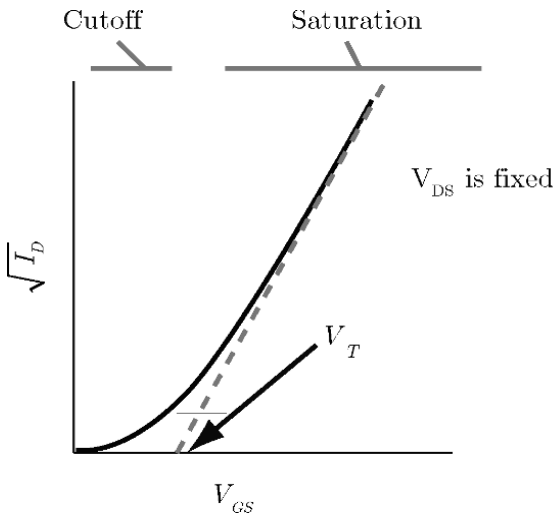

Figure 2.18. Illustration of the $I_{ds}^{1/2}$-V_{gs} transistor characteristics showing the extrapolation of $I_{ds}^{1/2}$, to obtain V_t in the V_{gs} axis.[89] Reprinted with permission.

The channel transconductance is a measure of how the drain-source current is modulated by the gate-source voltage.

The channel transconductance, g_m, is given by

$$g_m = \left| \frac{\partial I_{ds}}{\partial V_{gs}} \right| = \frac{W}{L} \mu C_i \left(V_{gs} - V_t \right) \quad \text{for a constant } V_{ds,} \qquad \text{Eq. (11)}$$

in the saturation regime, or

$$g_m = \frac{W}{L} \mu C_i V_{ds} \qquad \text{Eq. (12)}$$

in the linear regime.

The transconductance per unit channel width (g_m/W) of common EG transistors, reviewed in the next chapter, is in the order of 10 mS cm^{-1}, almost two orders of magnitude higher than that in organic thin film transistors.[92] The higher transconductance in EG transistors has been attributed to the high C_i at the interface between the electrolyte and the transistor channel, in the order of 10 μF cm^2, roughly two orders of magnitude higher than that of 200 nm of SiO_2.[93,94]

CHAPTER 3 ELECTROLYTE-GATED ORGANIC TRANSISTORS

3.1 Electrochemical capacitors

Later in this work (Chapter 6) we will present the similarity between a supercapacitor and an electrolyte-gated (EG) transistor using a polymer channel and a room temperature ionic liquid gating medium.

Supercapacitors can be used in electric circuits and electronic devices to temporarily store electrical energy and then deliver it back in the form of high-electric power.[95] Flexible supercapacitors exhibiting high power density and mechanical compliance are suitable as power back-ups in stretchable electronics.[96]

Electrochemical capacitors (EC), also known as supercapacitors or ultracapacitors, can be fully charged or discharged in seconds. Consequently, the power delivery or uptake, ca 10 kW kg^{-1}, in EC is high but the energy density, ca 5 Wh kg^{-1}, is low compared to batteries with power and energy densities of 2 kW kg^{-1} and 180 Wh kg^{-1}, respectively.[97,98]

Several types of ECs can be distinguished depending on the charge storage mechanism as well as the active materials employed.[97] Electrical double layer capacitors (EDLCs) use carbon-based active materials with high surface area. Another group of ECs are known as pseudo-capacitors or redox supercapacitors that use fast and reversible surface or near-surface reactions for charge storage.

Examples of pseudocapacitive materials are conducting polymers, transition metal oxides, carbons enriched in heteroatoms and microporous carbons with electrosorbed hydrogen.[98] Electrically conducting polymers, such as polypyrrole, polyaniline or polythiophene, can store and release charges through redox processes associated with the π-conjugated polymer chains.

In a simplified view, the Helmholtz model describes the electrode/electrolyte interface when the electrode is polarized. Ions move toward electrodes of opposite polarity. Eventually, ions form a charged layer at the electrode, termed the Helmholtz plane. The Helmholtz plane and the electrode surface form two parallel, oppositely charged layers, known as EDL. The value of *d* for the capacitance in the EDL is in the order of 3 nm, thus the capacitance per unit area of the

electrode/electrolyte interface can be 100 times greater than the analogue capacitor using a 200 nm SiO_2 dielectric.[99]

The capacitance per unit area can be defined by

$$C = \frac{\varepsilon_o \varepsilon_r}{d} \qquad \text{Eq. (19)}$$

where d is the distance between the ions and the electrode, ε_o is the vacuum permittivity and ε_r is the relative permittivity of the electrolyte. The capacity of the EDL is 10-20 μF cm^{-2}.

An important enhancement in the capacitance can be obtained if a reversible Faradaic process takes place apart from electrostatic processes.[98] The pseudocapacitance involves two processes i. double-layer charging or discharging of EDLs and ii. an electrochemical redox process.[100] The pseudocapacitance in electrically conducting polymers can attain values of 2 mF cm^{-2} or 200 F g^{-1}.[98,101]

3.1.1 Electrochemical Impedance Spectroscopy

Electrochemical Impedance Spectroscopy (EIS) is an electrochemical characterization technique that allows to model a device with an equivalent electric circuit by assigning resistive or capacitive components, connected in series or in parallel. Typical synousoidal perturbations of 5-20 mV at frequencies between kHz and mHz are applied to the electrochemical cell. In *in situ* EIS of EG transistors, the transistor channel is taken as working electrode (WE) and the gate electrode as counter electrode (CE). In Fig. 3.1 we propose a device equivalent electric circuit that includes electrolyte and electronic resistances (R_e), double layer capacitance, (C_{dl}), charge transfer resistance (R_{ct}) and a Warburg function (Z_w) that accounts for the diffusion of charged species in the electrode.

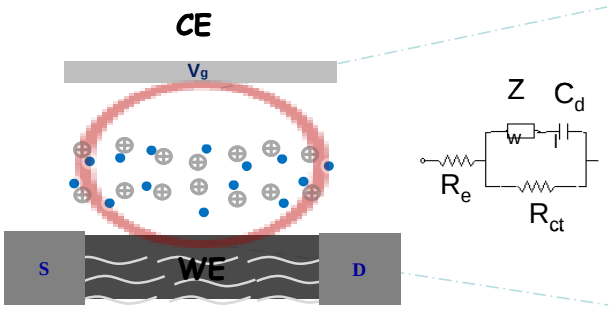

Figure 3.1. Scheme of an electrolyte gated transistor and its equivalent electrochemical cell electric circuit

3.1.2 Cyclic voltammetry

Cyclic voltammetry (CV) is an technique useful to identify the redox potentials of the electroactive species of an electrochemical cell. The current of an electrochemical cell is measured as a function of an applied referenced potential linearly increasing (forward step) or decreasing (backward step), possibly for a number of cycles. A typical cyclic voltammogram recorded for a single reversible cycle is shown in Fig. 3.2.

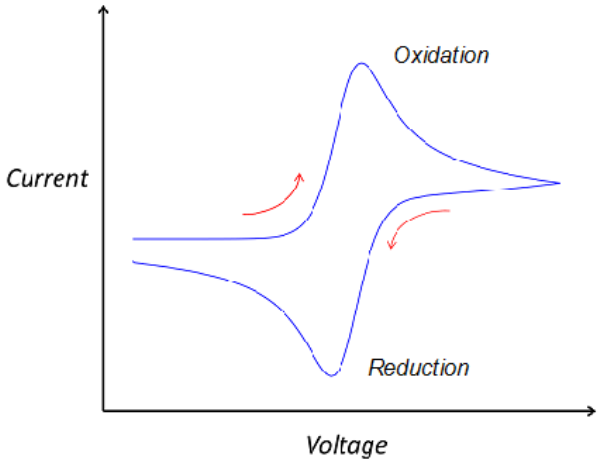

Figure 3.2. Typical cyclic voltammetry shape for a single CV cycle

Capacitive currents flow continuously charging and discharging the electrodes by the formation of electrical double layers (EDL). When the potential reaches specific values, the species in solution undergo a charge transfer process resulting in Faradaic current flow. Oxidation and reduction peaks characterize a redox system. If the surface concentrations of oxidized and reduced species at the electrodes remain in equilibrium throughout the potential scan, the redox process is reversible.

3.2 Electrolyte-gated transistor device structure and working mechanism

As its name implies, electrolyte-gated (EG) organic transistors consist of a semiconductor, small molecule or polymer, included between source and drain electrodes and coupled with a gate electrode via an electrolyte (Fig. 3.3). The electrolyte is the gating medium.[38,39,102]

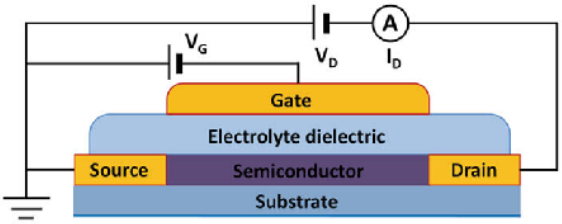

Figure 3.3. Schematic device structure of the electrolyte-gated organic transistor.[38] Reprinted with permission.

Two possible working mechanisms in *p*-type electrolyte-gated organic transistors are illustrated in Figs. 3.4a and 3.4b. If the channel material is impermeable to the electrolyte species upon application of a gate voltage, an electrical double layer is formed at the electrolyte-semiconductor channel interface, Fig 3.4a.[17] This process can modulate the I_{ds} by the field-effect; since there is no charge transfer process, this mechanism is referred to as electrostatic doping.[103] V_{gs} drops at the EDLs whose thickness leads to high capacitance density values, in the order of μF cm^{-2}. High capacitance results in high charge density in the semiconductor channel at relatively low voltages.

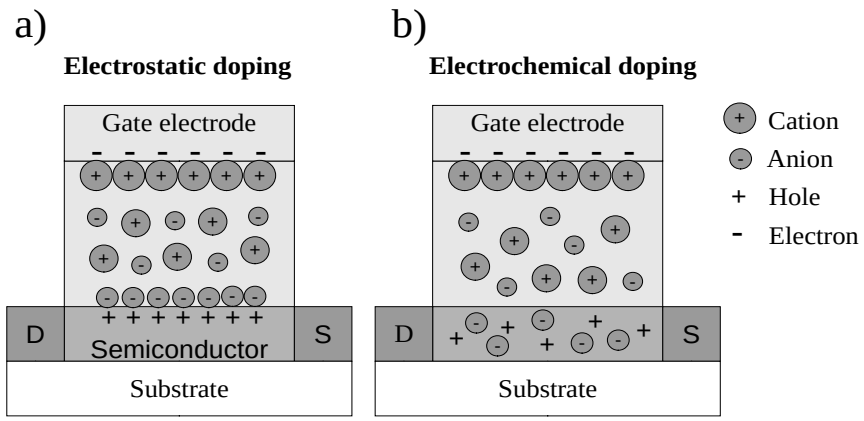

Figure 3.4. Schematic of the working mechanism of a *p*-type electrolyte-gated transistor. a) electrostatic doping characterized by the formation of electrical double layers and b) electrochemical doping, where ion incorporation in the transistor channel takes place.

If the channel material is electrochemically active and permeable to ions, which is usually the case in polymer channel materials,[104–107] upon application of V_{gs} a Faradaic process occurs under conditions close to reversibility (i.e. with comparable oxidation and reduction charge density, Q).[108] This is the working principle governing organic electrochemical transistors, Fig 3.4b. Complex phenomena such as semiconductor swelling, morphological and structural changes come into play during electrochemical doping. Frisbie et al, reported a change of volume of the film upon electrochemical doping of up to 15 % in [EMIM][FAP]-doped P3HT films with a charge density of 1.8×10^{21} holes cm^{-3} (~0.45 charge per thiophene ring).

3.3 Electrolyte materials as gating media

Conduction of electric current can be electronic or ionic depending on the nature of the charge carrier involved. Electrolytes are ionic conductors.[108] This section is about electrolytes that satisfy a criteria to be employed as gating medium in EG organic transistors. Electrolytes must have an appropriate anodic and cathodic limit (electrochemical stability window, ESW) compatible with the voltages applied to the electrodes of the transistor. The ionic conductivity and viscosity of the electrolyte need to be considered as the transistor electric characteristics depend on these properties, in particular, the transistor response time.[99,109–111]

Fig. 3.5 illustrates different kind of electrolytes classified from left to right according to their liquid-like to solid-like properties: electrolyte solutions, ionic liquids, ion gels, polyelectrolytes and polymer electrolytes.

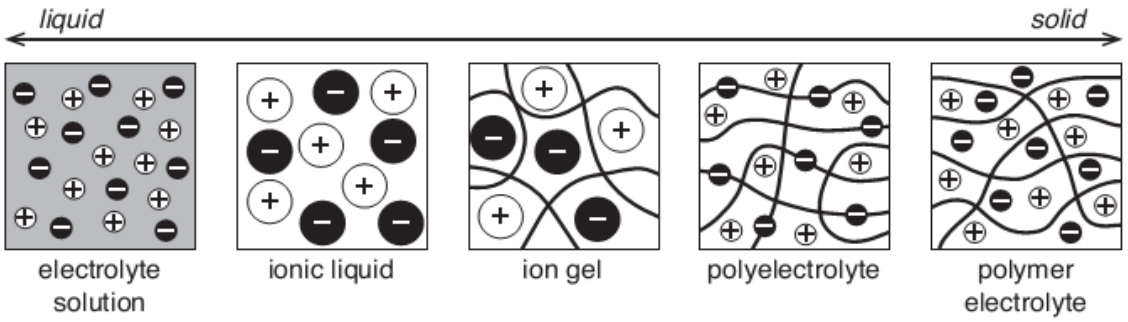

Figure 3.5. Schematic illustration of different types of electrolytes.[112] Reprinted with permission.

3.3.1 Electrolyte solutions

Electrolyte solutions are formed by mixing a salt and a polar solvent. The salt dissociation results in the formation of cations and anions that participate in ionic conduction as a function of their mobility leading to conductivities of 10-200 mS cm^{-1}.[113,114] Common sources of ions are $LiClO_4$, $LiCF_3SO_3$ and KCF_3SO_3. The role of the solvent is to dissolve the salt and to provide specific bulk properties such as ionic conductivity, density, viscosity and thermal stability. For obvious reasons, water has been the solvent of choice for applications in bioelectronics.[102,115,116] High boiling point and low vapor pressure solvents, i.e. propylene carbonate, ethylene carbonate or dimethyl sulfoxide, are used for applications other than bioelectronics for their excellent stability up to 70 °C. The ionic conductivities of electrolyte solutions is 1-10 mS cm^{-1}.[103,103,117,118] Electrochemical stability windows of 2.5-2.7 V are possible with propylene carbonate and tetra alkylammonium tetra fluoroborate salts.[119] Low volatile solvents such as those in the family of glycols can result in negligible mass losses up to 200 °C but provide reduced conductivity at RT (~10^{-5} Scm^{-1}).[118]

3.3.2 Room temperature ionic liquids

Room temperature ionic liquids (RTILs) are materials solely composed of ions whose melting point is below 100 °C.[120] The cations are commonly bulky and asymmetric with more than one heteroatom (Fig. 3.6).[121,122] Other quaternary ammonium or cyclic amine cations are also employed. They can be aromatic (e.g. pyridium) or saturated (e.g. piperidinium, pyrrolidinium).[123] Common anions are PF_6^-, BF_4^-, SbF_6^-, and bis(trifluoromethanesulfonyl)imide ([TFSI]). RTILs based on imidazolium cations and [TFSI] anion usually have a limited degree of inter-ionic interaction resulting in higher ionic conductivity and lower viscosity.[124] Moreover the hydrophobic properties of [TFSI] facilitate its drying, i.e. [EMIM][TFSI] can reach a water content of less than 20 ppm when set in a vacuum of 10^{-4} Torr at 100 °C.[120]

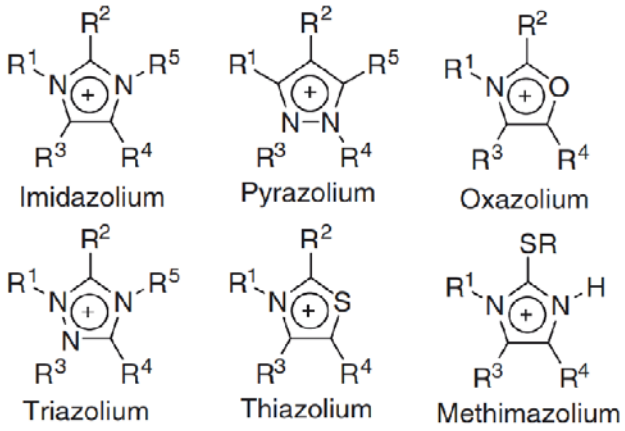

Figure 3.6. Molecular structure of commonly used cations in ionic liquids.[125] Reprinted with permission.

A number of RTILs with *task specific* physicochemical properties are possible by tuning the molecular structure, i.e. a polymerized ionic liquid triblock copolymer with single cation conducting properties for *n*-type transistors was recently developed.[126] Depending on the anion and cation, RTILs can show negligible volatility up to 300 °C,[127] wide electrochemical stability window, up to 5 V[123] and relatively high ionic conductivity, in the range of 0.1-20 mS cm^{-1} at room temperature.[123] The ionic conductivity of RTILs is commonly lower than that of aqueous solutions but can be comparable to that of lithium ion based organic electrolytes; for instance

$LiPF_6$ in ethylene carbonate and 1,2-dimethoxyethane (1 mol dm^{-3}) has a conductivity of 15 mS cm^{-1} at room temperature. An important increase in conductivity can be achieved in solution. For instance the conductivity of [EMIM][BF_4] increases four times when diluted in acetonitrile.[123]

The RTIL viscosity, which is the resistance of a fluid to deform under sheer stress or tensile stress,[128] is related to a combination of electrostatic interactions, including effects due to ion size and polarizability, van der Waals interactions and hydrogen bonding.[129] RTIL electrolytes have higher viscosity (10-1000 cP at RT) than common electrolyte solutions based on organic solvents (0.3-5 cP at RT).[130] Some physicochemical properties and anodic and cathodic limits of RTILs of interest for EG transistors, based on imidazolium cations and the [TFSI] anion, are summarized in Table 3.1. The physicochemical properties of a number of RTILs are available in the literature.[123,127,131]

Table 3.1: Physicochemical properties and anodic and cathodic limits of ionic liquids of interest in electrolyte-gated organic transistors.[132]

	[EMIM][TFSI]	**[BMIM][TFSI]**	**[PYR_{14}] [TFSI]**
Melting point (°C)	***-3***	***-4***	***-18***
Density (g/cm^3)	***1.52 (20 °C)***	***1.44 (19 °C)***	***1.40 (23 °C)***
Ionic conductivity (mS/cm)	***6.63 (20 °C)***	***3.41 (20 °C)***	***2.12 (20 °C)***
Viscosity (mPa s)	***39.4 (20 °C)***	***49 (25 °C)***	***94 (20 °C)***
Anodic and cathodic limits* (V)	***2.6; -2.1***	***2.5; -2.1***	***2.8; -2.5***

*measured with platinum working electrode, glassy carbon as counter electrode and Ag/AgCl as reference electrode.

3.3.3 Ion gels, polyelectrolytes and polymer electrolytes

Incorporating a polymer backbone can make the electrolyte structures more solid and easy to handle. A polymer electrolyte consists in a polymer matrix with sufficiently strong polar chemical moieties to solvate ions in the solid state. Poly(ethylene oxide) is a commonly used solvating polymer matrix. The ion gel alternative is a polymer/electrolyte blend which can be described as a liquid electrolyte swollen by polymer network.[112] As one would expect, the ionic conductivity of polymer electrolytes, i.e. <1 mS cm^{-1},[133] is lower than that of ion gels which have an ionic conductivity comparable to the corresponding pure electrolyte.[110,134] Polymer electrolytes commonly have more mechanically stable structure.[135] Polyelectrolytes are polymers with an electrolyte group bonded covalently to the repeating unit along the molecular backbone. The electrolyte group can dissociate when in contact with a polar solvent resulting in a charged polymer chain and oppositely charged ions. Thus polyelectrolytes transport only one type of ion. Polyelectrolytes are characterized with low ionic conductivities in the range of 10^{-5} to 10^{-3} S cm^{-1}.[136]

3.3.4 Ionic conduction and ionicity

The Nernst-Einstein equation relates the molar conductivity (Λ, in S cm^2 mol^{-1}) to the diffusion coefficient of the cation (D^+) and the anion (D^-) constituting the salt, in m^2s^{-1}.

$$\Lambda = \frac{N_A e^2}{k_B T}\left(D^+ + D^-\right) \qquad \text{Eq. (15)}$$

where e is the elementary charge, N_A is the Avogadro number, k_B is the Boltzmann constant and T is the absolute temperature.

Substituting in Eq. (15) the Stokes-Einstein equation, $D = \frac{k_B T}{6\pi\eta r}$; for the cation, D^+, where η is the electrolyte viscosity and r is the radii of the cation, r^+; and for the anion, D^-, where r^- is the radii of the anion, leads to the Walden rule

$$\Lambda\eta = k_{(T)} \qquad \text{Eq. (16)}$$

where $k_{(T)}$ is a temperature dependent parameter, i.e.

$$k(t) = \frac{N_A e^2}{k_B T}\left(\frac{k_B T}{6\pi}\left(\frac{1}{r^+} + \frac{1}{r^-}\right)\right) \qquad \text{Eq. (17)}$$

A comparison of the calculated molar conductivity Λ and the measured one Λ_m, is interpreted in terms of a deviation Δ

$$\Lambda_m = (1-\Delta)\Lambda \qquad \text{Eq. (18)}$$

where (1-Δ) is the *ionicity*. In ionic liquids, complex ion-ion interactions may result in ionic stable aggregates that may be regarded as neutral and do not participate in ionic conduction. The ionicity in RTILs can reach values between 0.5 and 0.8.[137]

3.4 Electrolyte-gated organic transistors: literature

In the 80s', Wrighton et al. investigated reversible electrochemical oxidation of conducting polymers (polyaniline, polyacetylene, polythiophene, polypyrrole) to amplify chemical signals and to investigate the correlation between the electrochemical potential and the electronic conductivity in polymers.[21,22,25,33,138–140] Finite potential windows of high conductivity were observed for a number of conjugated polymers (i.e. polyaniline, polythiophene, polypyrroles and polyacetylene) following redox processes.

At present, the topic of electrolyte-gated (EG) organic transistors has been revived due to the discovery of printable electrolytes that can offer fast-response, i.e. 1 kHz,[109] and unprecedented thermal and electrochemical stability.[38] Such properties are of interest for potential applications in flexible displays.

A number of ion-gel gated polymer transistors with improved polarization response times and solid-like mechanical properties have been reported by the groups of Frisbie and Lodge.[99,99,99,109,141–144] The ion gels consist of a polymer network swollen with an ionic liquid. The polymer network, is an ABA triblock copolymer where B block is soluble in the ionic liquid and the A block is not.[145] Block polymers are macromolecules containing two or more different monomer repeating units and they are covalently bonded in contiguous sequences (or blocks).

For example, imidazolium-based ionic liquids can be gelled in the triblock copolymers PS-PEO-PS, or PS-PMMA-PS, Fig. 3.7, by self-assembly.[109] The ion gels contain a modest quantity of polymer, ca 4 % wt, resulting in self-contained mechanical integrity without compromising the RTIL ionic conductivity. Ion-gel gated polymer transistors reached operation frequencies higher than 1 kHz.[109] High frequencies, >1 kHz, and low gate voltages, <1 V, tend to favour electrostatic doping mechanism while low frequencies and high gate voltages favour electrochemical doping.[99] The switching speed of these devices may be determined by the polarization response time of the electrolyte gel and not by the carrier mobility in the semiconductor channel.[109] Processes affecting the response time in EG organic transistors will be discussed in Chapter 5.

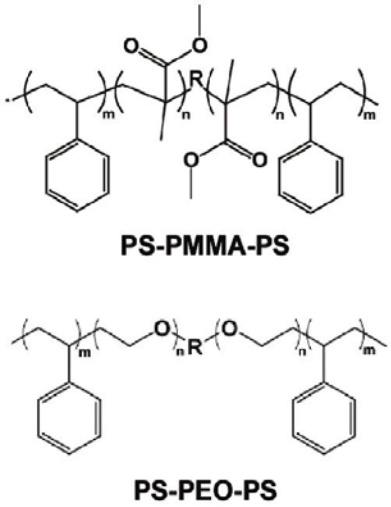

Figure 3.7. Chemical structure of two triblock copolymers, poly(styrene-b-methylmethacrylate-b-styrene) (PS-PMMA-PS) and poly(styrene-block-ethylene oxide-block-styrene) (PS-PEO-PS).[99] Reprinted with permission.

Aerosol jet printing deposition technique has been used to fabricate fully printed ion-gel gated polymer transistors on polyimide substrates, Figs 3.8a.[143] Inks of Au nanoparticles were used to print the source and drain electrodes on polyimide substrate, P3HT channel material was printed over the source and drain electrodes, ion gel constituted of [EMIM][TFSI] ionic liquid and PS-PMMA-PS block copolymer was used as gating medium, and PEDOT:PSS was printed over the ion gel and used as gate electrode. The all-printed electrolyte-gated transistor showed a hole

mobility of 1.8 $cm^2V^{-1}s^{-1}$, ON/OFF ratio of 10^5 and sub-2 V operation, as deduced from the transfer characteristics, Fig. 3.8b.

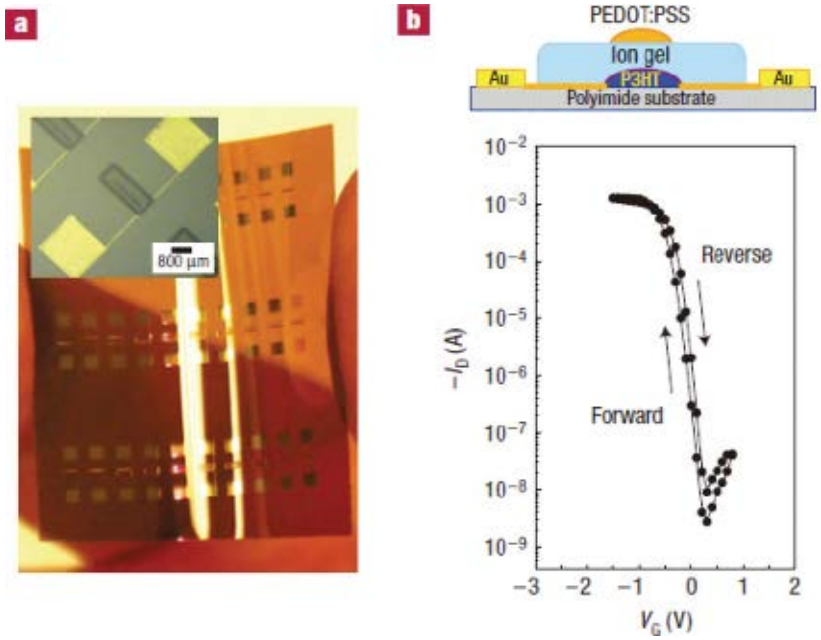

Figure 3.8. Printed ion-gel gated polymer transistor. (a) Image of the aerosol-printed ion-gel polymer transistor array on a flexible polyimide substrate. The device channel length was 20 µm and channel width was 1400 µm. (b) Transfer characteristic (V_{ds}= -1 V) and, on top, the device schematic cross-section diagram for devices employing P3HT channel material.[143] Reprinted with permission.

Another important objective is to demonstrate *n*-type electrolyte-gated transistors. *N*-type and *p*-type EG transistors would enable the design of complementary circuits made from *n*-type and *p*-type transistors.[146] The typical digital design style of a complementary circuit uses symmetrical paths of *p*-type and *n*-type transistors set in series. Since one transistor of the pair is always off for any applied gate voltage, the series combination consumes power momentarily only during switching between ON and OFF states, thus resulting in more limited power dissipation, relative to unipolar circuits.

Ono et al. reported *n*-type N-methyl-N-propyl pyrrolidinium bis(trifluoromethanesulfonyl) amide ([PYR_{13}][TFSI])-gated transistors with single crystal N,N''-bis(n-alkyl)-(1,7 and 1,6)-

dicyanoperylene-3,4:9,10-bis(dicarboximide) (PDIF-CN2) channel material.[147] The device structure consisted of a pre-moulded stamp of poly(dimethylsiloxane) (PDMS, Sylgard 184, Dow corning Corp) coated with Ti/Au, 2 nm/20 nm, source and drain electrodes and bridged with a pre-laminated single-crystal of PDIF-CN2.[147,148] The thin space between the source and drain electrodes and the gate electrode was used as control gate dielectric. The space was filled with [PYR_{13}][TFSI] to complete the electrolyte-gated transistor structure, structure shown in Fig. 3.9 (top). Fig. 3.9 (bottom) shows the transfer characteristic, I_{ds}-V_{gs}, for V_{ds}=0.1, 0.2, 0.3, 0.4 and 0.5 V; it includes the transfer characteristic of the control device employing air as gate dielectric and on bottom, the gate current I_{gs}-V_{gs}. The device operation was stable in ambient air conditions with electron mobility up to 5 $cm^2V^{-1}s^{-1}$ and threshold voltage close to 0.1 V. The absence of redox peaks in the I_{gs}-V_{gs} plot could indicate an electrostatic doping process.

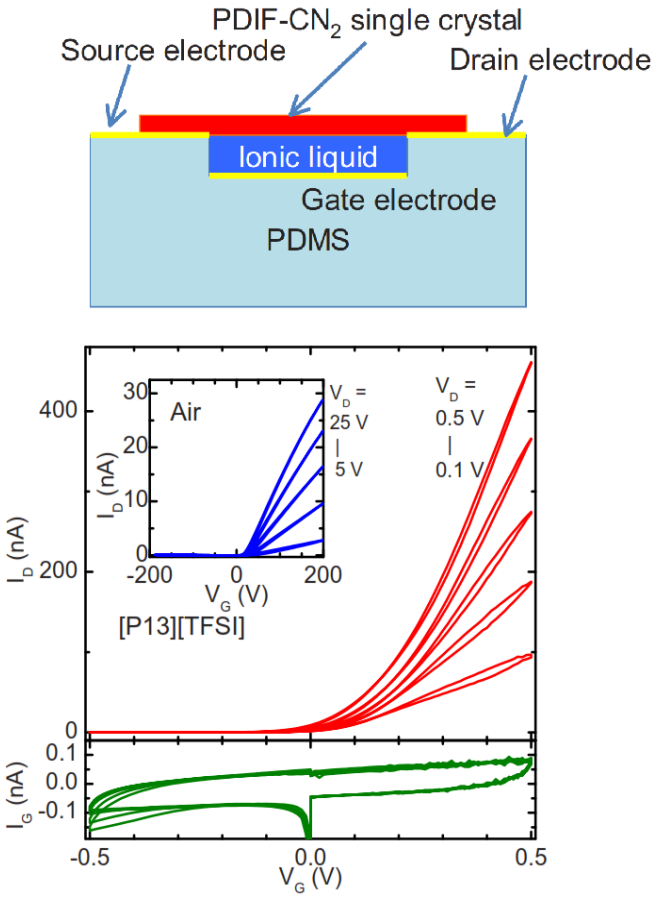

Figure 3.9. Schematic illustration of the *n*-type electrolyte-gated single crystal transistors (top). A PDMS stamp moulded from a SU-8 photoresist relief was used as a substrate defining the drain-

source interelectrode distance. L= 149 μm, W= 1 mm, and distance between the crystal and the recessed gate, d= 25 μm. Control devices were obtained by coating the substrate with a Ti/Au layer of 2/20 nm/nm, with a collimated flux of metal, and attaching a laminated single crystal on top of the channel. The final device structures were obtained by incorporating [PYR_{13}][TFSI] ionic liquid as gating medium; the cross-section schematic of the final device is shown. Transfer characteristics (bottom) and gate current, measured with V_{ds} =0.1, 0.2, 0.3, 0.4 and 0.5 V. The transfer characteristics of transistors employing air as gate dielectric are shown in the inset.[147] Reprinted with permission.

All organic, all printed ion gel-gated transistors were fabricated on flexible poly(ethylene 2,6-naphthalate) (PEN) substrates by sequential aerosol jet printing of PEDOT:PSS source and drain electrodes, P3HT channel material and [EMIM][TFSI]/PS-PMMA-PS ion-gel gating medium.[142] Discrete transistors and printed circuits for more complex functions operated at supply voltages below 2 V and high switching frequencies, 1-10 kHz. The typical transfer characteristics, I_{ds}-V_{gs}, for a constant V_{ds}= -1 V, acquired with a sweeping rate of 50 mVs^{-1} are presented in Fig. 3.10. The ON/OFF ratio was ca 10^5 for V_{gs}= -1 V which demonstrates that the conductivity of PEDOT:PSS is high enough to serve as electrode material which can be important from a cost perspective. Negligible current hysteresis between the forward and reverse V_{gs} sweeps suggests that PEDOT:PSS is stable with the ion-gel.

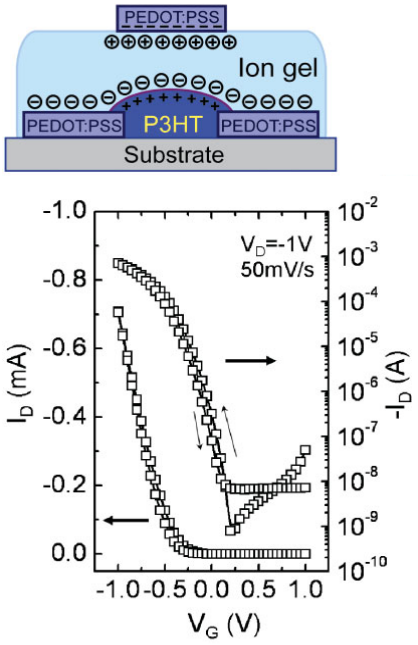

Figure 3.10. All-organic, all-printed ion-gel gated P3HT transistor on flexible poly(ethylene naphthalate) substrates; device schematic (top) and transfer characteristics (bottom), I_{ds}-V_{gs}, for V_{ds}= -1V. The source and drain electrodes were made of PEDOT:PSS with an interelectrode distance, L= 50 μm, and width, W= 500 μm.[142] Reprinted with permission.

Fundamental studies on the charge carrier transport properties of P3HT and the light-emitting polymers, MEH-PPV and F8BT, were carried out by Paulsen et al.[87] In particular, the conductivity was investigated at high charge carrier density. The experimental configuration employed by Paulsen et al. was a microelectrochemical transistor (Fig. 3.11), previously proposed by Wrighton et al.[21] Transistor transfer curves and cyclic voltammograms were obtained using such a configuration. A Pt mesh electrode immersed in the electrolyte served as the gate and the counter electrode. Ag quasi reference electrode was also immersed in the electrolyte. Source and drain electrodes, together with the open transistor channel, served as the working electrode. The polymers were spin coated on substrates pre-patterned with Au source and drain electrodes, L= 250 μm and W= 7.5 mm. The ionic liquid, 1-ethyl-3-methylimidazolium tris(pentafluoroethyl)trifluorophosphate ([EMIM][FAP]), was deposited on the polymer thin film and served as the gate electrolyte.

The volumic charge carrier density (p_{3D}) was obtained by dividing the total gate-induced charge (Q) by the unit charge, the thickness of the film (t = 50 nm) and the area of the polymer film in contact with electrolyte (A=0.709 cm^2).[149,150] Q, in coulombs, was obtained by integrating the gate current (I_{gs}) vs the gate voltage and dividing the result by the sweeping rate (r_v = 50 mVs^{-1})

$$p_{3D} = \frac{Q}{eAt} = \frac{\int I_{gs} dV_{gs}}{r_v eAt} \qquad \text{Eq. (21)}$$

The mobility was obtained using a similar equation to Eq. (9) for a volumic charge carrier density

$$\mu = \frac{L}{tW} \frac{I_{ds}}{V_{ds} e p_{3D}} \qquad \text{Eq. (22)}$$

The peak charge carrier density (p) for the MEH-PPV EG transistors was estimated as 5.4×10^{20} cm^{-3}, for a V_{gs} near 2 V. The mobility, deduced using Eq. (22), was 0.08 cm^{2}V^{-1}s^{-1}, for a V_{gs} near 2 V. For F8BT transistors, the peak mobility was 0.07 cm^2 V^{-1}s^{-1} and p was 1×10^{21} cm^{-3}, for a V_{gs} near 2.6 V. In agreement with previous studies,[151,152] as the charge carrier density is increased, an increase in mobility and conductivity is first observed, followed by a peak and eventual decrease upon further increase of the charge density. Overall, the peak in mobility and conductivity versus charge carrier density was confirmed for a number of polymer semiconductors with different morphology and chemical structures gated with room temperature ionic liquids.

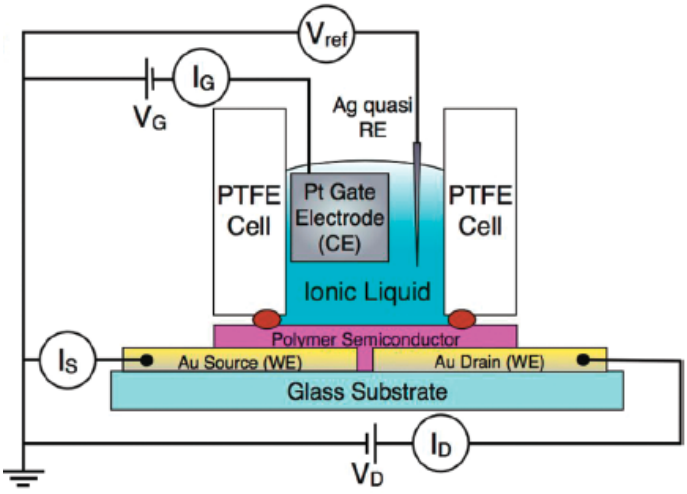

Figure 3.11. Device structure of a microelectrochemical transistor including: source and drain electrodes, which, taken together with the open transistor channel, behave as the working

electrode of the electrochemical cell, and a gate electrode, which behaves as the counter electrode in the electrochemical cell. The microelectrochemical transistor includes a reference electrode immersed in the electrolyte-gating medium.[87] Reprinted with permission.

Organic electrochemical textile transistors, a creative device architecture towards “smart fabrics”, were reported by Hamedi et al.[153,154] The electrolyte-gated transistors were based on P3HT and imidazolium ionic liquids. The device schematic and electric characteristics are shown in Figs. 3.12a and 3.12b. The source and drain electrodes were produced by weaving a fiber mesh and coating a layer of Au (100 nm); the fibers were then unweaved and immersed in a P3HT solution and pulled out at a constant speed forming a thin film layer of P3HT over the surface. Au wires were sewed perpendicularly and used as gate electrodes. A mixture of [BMIM][TFSI] ionic liquid and the polymerized ionic liquid poly(1-vinyl-3-methylimidazolium bis(trifluoromethanesulfonimide)) was introduced at the junction and used as gating medium. Interestingly, transient measurements, Fig. 3.12a, showed that the transistor channel was open in two regimes; i) the fast regime which can be associated to a field-effect transistor operation with response times in the order of 3-5 ms, enabling kHz frequency operation; and ii) a slow regime with a response time of ca 2 s. The electrochemical textile transistors operated below |-1 V| and provided ON/OFF ratios of ca 1000 at V_{ds} = -1 V, as shown in Fig. 3.12b.

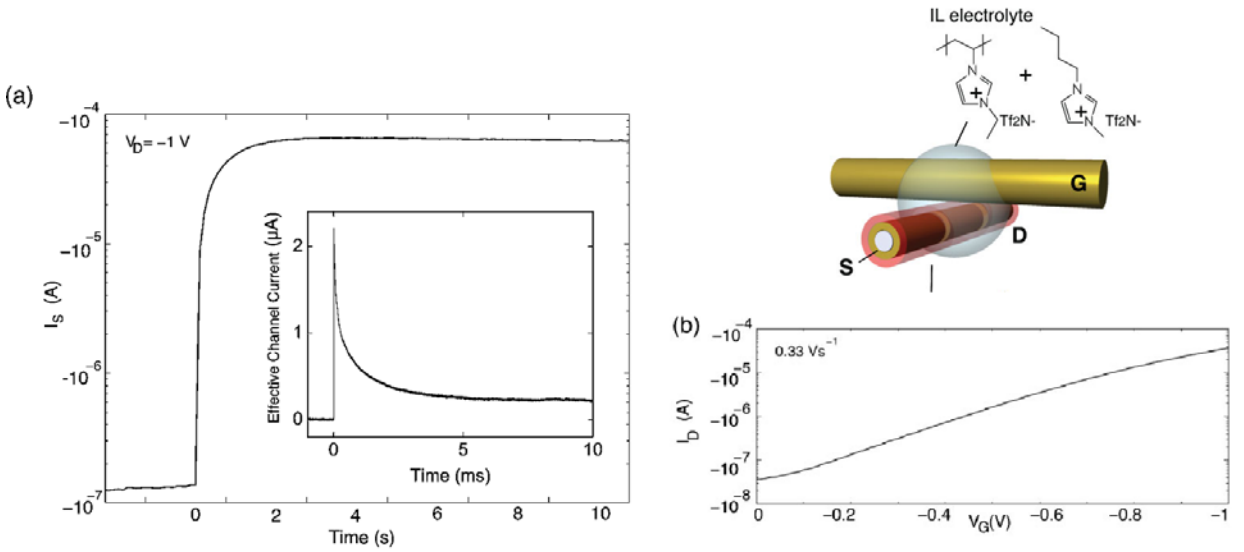

Figure 3.12. Transistor schematic formed at a fiber junction connected via an ionic liquid electrolyte (top right). (a) transient plot, I_{ds} vs time, measured by applying a gate voltage step from 0 to -1 V; in the inset, the transient plot at ms scale is shown to demonstrate electrostatic doping. (b) Transfer characteristics, I_{ds}-V_{gs}, for V_{ds}= -1 V, measured with a V_{gs} sweep at 0.33 V s^{-1}.[153] Reprinted with permission.

CHAPTER 4 ARTICLE 1: LOW VOLTAGE ELECTROLYTE-GATED ORGANIC TRANSISTORS MAKING USE OF HIGH SURFACE AREA ACTIVATED CARBON GATE ELECTRODES

This chapter was published as an article in the *J. Mater. Chem. C*, 2014, **2**, 5690.

4.1 Authors

Jonathan Sayago,[a] Francesca Soavi,[b] Yuvaraj Sivalingam,[a] Fabio Cicoira[c] and Clara Santato[a]

[a]Département de Génie physique, École Polytechnique de Montréal, C.P. 6079, Succ. Centre Ville, Canada.

[b]Department of Chemistry "Giacomo Ciamician", Università di Bologna, Via Selmi, 2, Italy.

[c]Département de Génie chimique, École Polytechnique de Montréal, C.P. 6079, Succ. Centre Ville, Canada.

4.2 Abstract

In electrolyte-gated transistors, the exceptionally high capacitance of the electrical double layer forming at the electrolyte/transistor channel interface permits current modulations of several orders of magnitude, at relatively low gate voltages. The effect of the nature of the gate electrode on the performance of electrolyte-gated transistors is still largely unclear, despite recent intensive efforts. Here we demonstrate that the use of high surface area, low cost, activated carbon gate electrode enables low voltage (sub-1 V) operation in ionic liquid-gated organic transistors and renders unnecessary the presence of an external reference electrode to monitor the channel potential, thus dramatically simplifying the device structure. We used the organic electronic polymer MEH-PPV (poly[2-methoxy-5-(2'-ethylhexyloxy)-p-phenylene vinylene), as the channel material, and the high ionic conductivity, low viscosity ionic liquid [EMIM][TFSI] (1-ethyl-3-methylimidazolium bis(trifluoromethylsulfonyl)imide), as the electrolyte gating material. We believe that this will prove to be the first of a new generation of low voltage electrolyte-gated transistors for applications in organic printable electronics.

4.3 Introduction

Electrolyte-gated (EG) transistors[38,102,155] make use of electrolytes, such as polymer electrolytes, ionic liquids and ion gels,[156] to replace conventional dielectrics in large area, flexible electronic applications.[5,157] EG transistors exhibit current modulations of several orders of magnitude at relatively modest gate voltages, exploiting the exceptionally high capacitance of the electrical double layer formed at the electrolyte/transistor channel interface. Different doping mechanisms, including electrostatic and Faradaic (the latter being commonly referred in the electrolyte gating literature as electrochemical doping), have been proposed to explain the gating process in EG transistors. While both processes can be reversible, the former does not involve charge transfer and takes place in the immediate vicinity of the surface of the channel material, whereas the latter involves charge transfer and takes place in the bulk of the channel material.

A number of channel materials have been used in EG transistors, including organic single crystals,[147,151,158] organic thin films of small molecules and polymers,[87,104,106,152,159] thin films of metal oxides,[118,160–164] InN,[165] CdSe,[166] and PbSe.[167] The nature of the channel material is one of the key factors establishing the type of doping mechanism. For channel materials based on organic polymers, it is mainly Faradaic. For this class of channel materials, the doping charge and the (pseudo)capacitance are about two orders of magnitude larger than for electrostatically doped, non-porous materials.[168] Importantly, because of the Faradaic nature of the doping, in polymer channels the level of the doping and, hence, the current modulation depend upon the channel electrical potential. As a consequence, to optimize the current modulation in EG transistors based on organic polymer channels, it is of the utmost importance to carefully monitor and set the channel potential vs an additional reference electrode. Further, it is necessary to monitor the voltage in order to ensure its compatibility with the electrochemical stability window of the electrolyte.

The effect of the nature of the gate electrode on the performance of EG transistors is still largely unclear, at present, despite recent intensive efforts.[159,169] However, a judicious choice of the gate electrode material can limit undesirable electrochemical reactions at the gate electrode, detrimental for the device stability. In addition, gate electrodes with high specific surface area are desirable for high current modulations in transistor channels prone to bulk electrochemical doping, such as organic polymers. Indeed, high surface area gate electrodes featuring high double

layer specific capacitances should be non-limiting in terms of their capability to supply within a narrow potential excursion the charge required to dope organic polymer transistor channels.

High surface area, low cost electrodes made of activated carbon (1000 - 2000 $m^2 \cdot g^{-1}$) have been successfully employed in double-layer supercapacitors.[168,170] They store charge by a fast, highly reversible electrostatic process described by $Q = C\Delta Vm$, where Q is the stored charge, C is the specific capacitance (ca 100 - 200 $F \cdot g^{-1}$ for optimized high surface area carbon), ΔV is the electrode potential excursion, and m is the mass of the electrode material. Gate electrodes based on activated carbon with high mass and specific capacitance are attractive candidates for application in EG transistors. Indeed, within a relatively low ΔV (a few mV), they can store electrostatically an amount of charge that, counterbalanced at the transistor channel, leads to its effective doping. At the same time, the low value of ΔV employed opens the possibility to use the carbon gate electrode as a quasi reference electrode.[171] The use of high surface area activated carbon gate electrodes represents an exciting approach to achieve low voltage channel modulations. A *caveat*, of course, has to be considered for this approach. The redox activity of the channel material has to take place at low potentials vs the carbon quasi reference electrode (i.e. to demonstrate EG transistors with sub-1 V operation voltage, the redox activity of the polymer has to take place at potentials lower than 1 V vs the carbon quasi reference electrode).

In this work we demonstrate that the use of a high surface area, low cost, activated carbon gate electrode makes low voltage (sub-1 V) operation in ionic liquid-gated organic transistors possible and renders unnecessary the presence of an external reference electrode to monitor the channel potential. We use the organic electronic polymer MEH-PPV, poly[2-methoxy-5-(2′-ethylhexyloxy)-1,4-phenylene vinylene],[87,159] channel material. The electrolyte gating material is the high ionic conductivity, low viscosity ionic liquid [EMIM][TFSI] (1-ethyl-3-methylimidazolium bis(trifluoromethylsulfonyl)imide). We believe that this will prove to be the first of a new generation of low voltage EG transistors for applications in organic printable electronics.

4.4 Results and discussion

The structure of the EG transistors investigated in this work is shown in Fig. 4.1. The MEH-PPV thin film, deposited on the source-drain pre-patterned SiO_2 substrate (source-drain distance, L, 10

μm and electrode width, *W*, 4 mm) is vertically stacked with the activated carbon gate and separated from it by a Durapore® filter soaked in the ionic liquid electrolyte.[172] An additional activated carbon electrode, the quasi reference electrode,[171] is placed to the side of the activated carbon gate electrode. The activated carbon gate electrode, with a high specific capacitance of about 100 $F \cdot g^{-1}$ in [EMIM][TFSI],[170,173] supplies the charge required to dope the MEH-PPV channel by a fast, highly reversible electrostatic process.

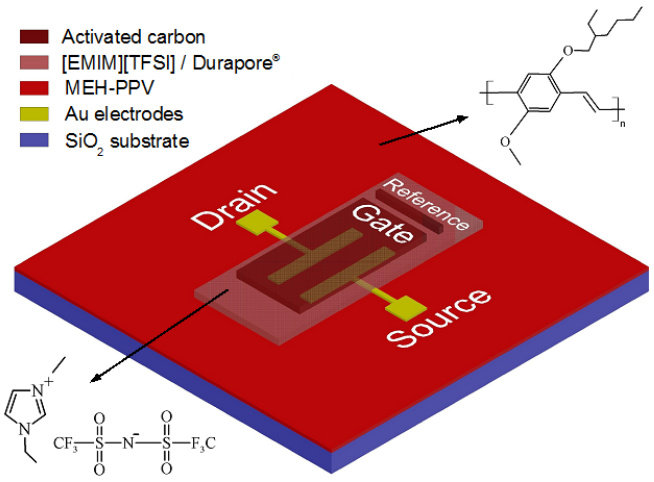

Figure 4.1. Device structure of the [EMIM][TFSI]-gated MEH-PPV transistors making use of an activated carbon gate electrode, in this work. The structure includes an activated carbon quasi reference electrode. A separator (Durapore® membrane filter, 9 mm × 4 mm × 125 μm) was soaked with [EMIM][TFSI] and placed on top of the MEH-PPV transistor channel (source-drain interelectrode distance, *L*, 10 μm, and electrode width, *W*, 4 mm). Two conducting carbon papers coated with activated carbon were set in contact with the separator and used as the gate (6 mm × 3 mm × 170 μm) and quasi reference (6 mm × 1 mm × 170 μm) electrodes. The molecular structures of the polymer MEH-PPV and the [EMIM][TFSI] ionic liquid are shown.

We used about 1 mg of activated carbon per cm^2 of geometric area of the gate electrode in order to keep its potential within a few tenths of mV vs that of the reference electrode, during channel modulation. This, in turn, creates the possibility of using the activated carbon gate electrode itself as a quasi reference electrode for channel potential modulation, therefore rendering the use of the

external quasi reference electrode unnecessary during transistor measurements. To verify that the carbon gate electrode can behave as a quasi reference electrode we performed a cyclic voltammetry survey. Fig. 4.2a shows cyclic voltammetry plots obtained using the MEH-PPV thin film as the working electrode and the activated carbon gate as the counter electrode (CE). The black curve was obtained using a supplementary, relatively small, activated carbon quasi-reference electrode (RE) whereas the dashed red curve was collected considering the gate electrode as both the CE and the quasi RE. In the latter case, the working electrode potential corresponds to $-V_{gs}$ (V_{gs} being the gate-source voltage). The voltammetric cycles performed in the two cases (with lateral quasi reference or without i.e. with the gate acting as the quasi reference) almost overlap.[1] More important, Fig. 4.2a shows that the MEH-PPV doping process takes place between about 0.3 V and 1 V vs the activated carbon quasi reference electrode, suggesting that a gate-source voltage bias lower than 1 V is necessary for the operation of the EG transistor.

[1] The values of the current obtained with the additional quasi reference electrode are slightly higher than those obtained using the gate electrode as the quasi reference electrode. This result can be explained by considering that in the former case the values of the current are affected by the polymer channel electrode capacitance (C_c) whereas in the latter case the values are affected by the total capacitance of the gate electrode/electrolyte/channel system (C_{gs}). C_{gs} corresponds to the capacitances of the gate (C_g) and polymer channel electrodes connected in series such that $C_{gs}^{-1} = C_g^{-1} + C_c^{-1}$.

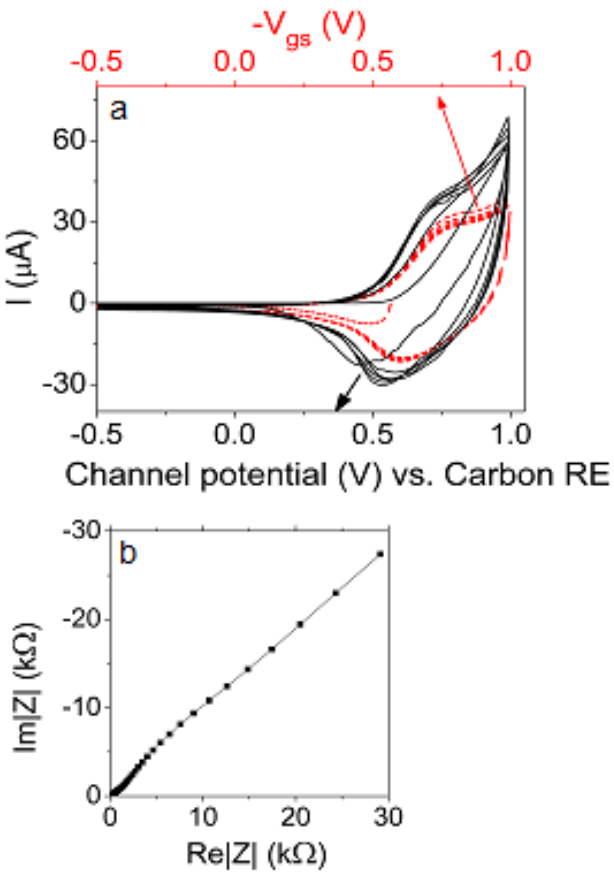

Figure 4.2. Electrochemical characteristics of [EMIM][TFSI]-gated MEH-PPV transistors. (a) Cyclic voltammetry at 50 $mV \cdot s^{-1}$ obtained using the polymer film as the working electrode, the activated carbon gate electrode as the counter electrode and a second activated carbon electrode as the quasi reference electrode (black, solid line) or the carbon gate electrode itself as both the counter and the quasi reference electrode (red dotted line). In the latter case, the potential of the transistor channel corresponds to $-V_{gs}$ (V_{gs} being the gate-source voltage). (b) Nyquist plot of the MEH-PPV working electrode at 0.8 V vs activated carbon, with the activated carbon gate electrode as the counter electrode and the small-sized activated carbon electrode as the quasi reference electrode.

The cyclic voltammetry plots obtained using the quasi reference electrode (solid curves in Fig. 4.2a) show that the absolute value of the current increases for the first two voltammetric cycles, after which, from the third to sixth cycle, they almost overlap. The increase in the current from the first to the second cycle is attributable to an increased possibility for ions of penetrating the

polymer after swelling caused by doping (forward cycle) and dedoping (backward cycle) of the polymer. From the slope of the linear plot of the doping charge (obtained by the integral of the current during the third cycle over time) vs channel potential, we obtained a pseudocapacitance of 0.83 mF. Electrochemical impedance spectroscopy is a relevant technique to study the mechanism and the limiting steps of the doping process of the polymer channel. Fig. 4.2b shows the Nyquist plot of the MEH-PPV transistor channel, obtained at 0.8 V vs the activated carbon quasi reference electrode. The impedance of the channel is a 45 ° transmission line typical of diffusion controlled processes related to the diffusion of the doping ions from the viscous ionic liquid into the polymer channel. This suggests that the time response of the transistor is affected by ion diffusion. The pseudocapacitance obtained at 10 mHz is 0.6 mF, slightly lower than the limit capacitance deduced by cyclic voltammetry. The Bode plot (Annex A, Fig. S1) indicates that the pseudocapacitive behaviour of the polymer becomes predominant in the channel impedance at frequencies lower than 10 Hz, thus indicating a time response of the device > 100 ms.

The electrochemical experiments suggested the possibility of operating our polymer transistors at unprecedented low voltages and the device characterization experiments indeed confirmed the interest of using activated carbon gate electrodes. The output curves (I_{ds}, drain-source current, vs V_{ds}, drain-source voltage, for increasing values of $|V_{gs}|$, Fig. 4.3a) show that, for our *p*-type MEH-PPV transistors, the saturation regime is achieved at V_{ds} values as low as -0.2 V. The transfer characteristics of the device in the saturation regime (Fig. 4.3b) show that the behavior of the gate-source, I_{gs}, current is in agreement with the cyclic voltammetry measurements. The conduction onset is located at about -0.72 V in the forward sweep and -0.44 V in the backward sweep. The hysteresis observed in the transfer curve is attributable to the slow diffusion of the doping ions in the polymer channel, already discussed for the Nyquist plot (Fig. 4.2b). Indeed, the hysteresis decreased with decreasing the sweep rate, such that, at 10 $mV \cdot s^{-1}$, the conduction onset is located at -0.66 V in the forward sweep and -0.56 V in the backward sweep (inset Fig. 4.3b). The transistor current ON/OFF ratio (calculated from I_{ds} at V_{gs} = 1 V (ON) and 0 V (OFF)) was approximately 5×10^3 (Annex A, Fig. S2).

For our [EMIM][TFSI]-gated MEH-PPV transistors, the hole carrier mobility (μ) was obtained from:

$$\mu = \frac{L}{W}\frac{I_{ds}}{V_{ds} e p} \qquad (1)$$

where e is the elementary charge and p is the charge carrier density (cm^{-2}), deduced from:

$$p = \frac{Q}{eA} = \frac{\int I_{gs} dV_{gs}}{r_v e A} \qquad (2)$$

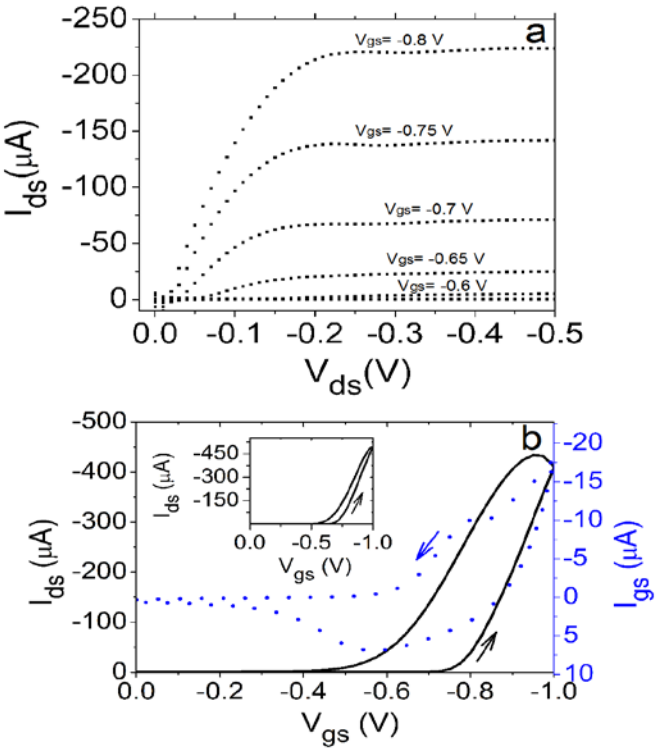

Figure 4.3. Device characteristics of [EMIM][TFSI]-gated MEH-PPV transistors making use of activated carbon for the gate and the quasi reference electrode: (a) output characteristics (I_{ds} vs V_{ds} for V_{gs} = 0, -0.6, -0.65, -0.7, -0.75 and -0.8 V); (b) transfer characteristics in the saturation regime (V_{ds} = -0.3 V), I_{ds} (left axis, solid line) and I_{gs} (gate-source current, right axis, dotted line) plotted vs V_{gs}, sweep rate 50 mV·s^{-1}. Inset: transfer characteristics in the saturation regime (V_{ds}=-0.3 V), for a sweep rate of 10 mV·s^{-1}.

where I_{gs} is the gate-source current (measured during the linear transfer curve, V_{ds} = -0.1 V, Annex A, Fig. S3, r_v is the sweep rate, and A is the active channel surface area (18 mm^2, surface

area of the polymer in contact with the electrolyte, in turn in contact with the gate electrode).[87,141,174] The hole mobility we obtained was $(1.0 \pm 0.5) \times 10^{-2}$ $cm^2 \cdot V^{-1} \cdot s^{-1}$, in agreement with the literature.[175]

4.5 Conclusions

In conclusion, we have demonstrated sub-1 V electrolyte-gated transistors making use of high surface area activated carbon as the gate electrode material, [EMIM][TFSI] as the electrolyte gating medium, and MEH-PPV as the organic polymer channel material. The use of the high surface area carbon gate electrode in contact with the ionic liquid renders unnecessary the use of a reference electrode in the device structure. Indeed, the gate electrode itself can be employed as quasi reference electrode. The processability of both the carbon gate electrode and polymer channel is of relevance for the development of flexible miniaturized devices. For the simple architecture and the low operation voltages, we believe that the devices we report have the potential to advance the development of low cost, large area electronics.

4.6 Experimental

Substrates were cleaned by sequential ultrasonic baths in isopropyl alcohol (IPA, J.T. Baker, microelectronic grade, 5 min), acetone (J.T. Baker, microelectronic grade, 10 min), and IPA (5 min), followed by a 5 min dehydration process at 120 °C in N_2 atmosphere consisting of 3 purging cycles of low pressure (20 Torr) and high pressure (500 Torr). Drain and source contacts of Ti/Au, 5/40 nm/nm, were photolithographically patterned on SiO_2 substrates (channel width, *W*, 4000 μm and length, *L*, 10 μm). 5 mg of MEH-PPV (Sigma Aldrich, 55 kDa) in 1 mL of toluene (Sigma Aldrich) were mixed and stirred overnight in a N_2 glove box (O_2, $H_2O \leq 5$ ppm) keeping the temperature at about 40 °C. MEH-PPV thin films were deposited by spin coating the solution at 1000 rpm. Afterwards, films were thermally treated at 70 °C for 3 hours. [EMIM][TFSI] (IoLiTec, >99%, ionic conductivity 6.63 $mS \cdot cm^{-1}$ and viscosity 39.4 mPa·s at 20 °C)[132] was purified under vacuum (~10^{-5} Torr) at 80 °C overnight prior to use, and stored (for a maximum period of 2 days) in the N_2 glove box. The device fabrication was completed by sandwiching a Durapore® GVHP filter separator soaked in the ionic liquid between the MEH-PPV thin film and the activated carbon gate electrode. An activated carbon quasi reference electrode was placed on the side of the carbon gate electrode (see Fig. 4.1). The gate and quasi

reference electrodes were prepared using carbon paper (Spectracorp 2050) coated with an ink of activated carbon (PICACTIF SUPERCAP BP10, Pica, 28 $mg \cdot mL^{-1}$) and polyvinylidene fluoride (PVDF, KYNAR HSV900, 1.4 $mg \cdot mL^{-1}$) binder in N-methyl pyrrolidone (NMP, Fluka, > 99.0%) solvent. The coating was followed by thermal treatment at 60 °C for several hours to remove the solvent.

The characterization of the EG transistors was carried out in a N_2 glovebox (H_2O, $O_2 \leq 5$ ppm). The electrochemical tests were performed using a PARSTAT 2273 (Princeton Applied Research) multichannel potentiostat equipped with impedance modules. Electrochemical impedance spectroscopy (EIS) was performed at frequencies from 20 kHz to 10 mHz and an oscillation amplitude of 10 mV. Transistor device characteristics were measured using a B1500A Agilent semiconductor parameter analyzer.

4.7 Acknowledgements

The authors are grateful to Y. Drolet, J. Bouchard and Dr K. Laaziri for technical support. This work was financially supported by NSERC (Discovery grants, CS and FC) and FQRNT (Nouveau Chercheur, CS). JS acknowledges financial support by CONACYT and CMC Microsystems. F.S. acknowledges financial support by Università di Bologna (Researcher Mobility Program, Italian-Canadian cooperation agreement).

CHAPTER 5 ARTICLE 2: ELECTROLYTE-GATED POLYMER THIN FILM TRANSISTORS MAKING USE OF IONIC LIQUIDS AND IONIC LIQUID-SOLVENT MIXTURES

This chapter was published as an article in the *Journal of Applied Physics*, 2015, **117**, 112809.

5.1 Authors

J. Sayago,[a] F. Soavi,[b] Y. Sivalingam,[a] F. Cicoira[c] and C. Santato[a]

[a]Département de Génie physique, École Polytechnique de Montréal, C.P. 6079, Succ. Centre Ville, Canada.

[b]Department of Chemistry "Giacomo Ciamician", Università di Bologna, Via Selmi, 2, Italy.

[c]Département de Génie chimique, École Polytechnique de Montréal, C.P. 6079, Succ. Centre Ville, Canada.

5.2 Abstract

Electrolyte-Gated (EG) transistors, making use of electrolytes as the gating medium, are interesting for their low operation voltage. Furthermore, EG polymer transistors offer the advantage of solution processing, low cost and mechanical flexibility. Despite the intense research activity in EG transistors, clear guidelines to correlate the properties of the materials used for the transistor channel and electrolytes with the doping effectiveness of the transistor channel are yet to be clearly established. Here we investigate the use of room temperature ionic liquids (RTILs) based on the [TFSI] anion (namely, [EMIM][TFSI], [BMIM][TFSI] and [PYR_{14}][TFSI]), to gate transistors making use of MEH-PPV as the channel material. Morphological studies of MEH-PPV and RTIL films showed a certain degree of segregation between the two components. All the EG transistors featured clear drain-source current

modulations at voltages below 1 V. Polar solvent additives as propylene carbonate were used to improve the transistor response time.

5.3 Introduction

Electrolyte gating offers the possibility to combine low-voltage operation, cost-effective deposition techniques and mechanical flexibility in polymer transistors.[38,102,176] Electrolyte-gated (EG) polymer transistors can operate at low electrical biases (about 1-2 V) due to the high pseudo-capacitance of the electrolyte/transistor channel interface, a fast and reversible Faradic process. EG polymer transistors have been demonstrated with a number of electrolytes, i.e. saline aqueous solutions, polymer electrolytes, Room Temperature Ionic Liquids (RTILs) and ion gels.[38,99,109,142] The use of RTILs is attractive for their relatively high conductivity, ranging between 0.1 - 10 $mS \cdot cm^{-1}$, their negligible volatility and their high electrochemical stability window, up to ca 5 V.[124,177,178] Furthermore, the availability of RTILs with different molecular structures and chemico-physical properties offers the possibility to specifically control the interactions between the ions constituting the RTIL and the polymer channel in view of an optimized doping. Unluckily, clear guidelines to correlate the characteristics of a certain electrolyte with its doping effectiveness are yet to be established. Therefore, systematic comparisons of the performance of EG transistors making use of RTILs belonging to the same family (i.e. having a common cation/anion), and based on the same polymer channel, are highly desirable. The knowledge gained from such a systematic study is expected to be extremely valuable to improve EG polymer transistors characteristics such as their response time and operation voltage. One key challenge in the field of EG transistors is indeed the relatively slow device response time, a consequence of the ion redistribution taking place in the electrolyte and the transistor channel upon application of the electrical bias and governing the mechanism of gating.[109,110]

In this work, we investigate EG transistors making use of several RTIL electrolytes as the gating medium. For our investigations, we considered RTILs based on the bis(trifluoromethanesulfonyl)imide [TFSI] anion. We selected such RTILs because of their high ionic conductivity and hydrophobicity.[123,179] This last property is of primary importance for the characterization of EG transistors making use of moisture-sensitive channel materials, such as

MEH-PPV. The use of RTILs with the same anion and different cations aims at revealing the possible effect of a different molecular structure for the ions on the doping of the channel.[176,180–182]

The well known organic electronic polymer MEH-PPV, poly[2-methoxy-5-(2′-ethylhexyloxy)-1,4-phenylene vinylene],[87,159] was employed as the transistor channel material. High surface area, low-cost electrodes made of activated carbon (1000 - 2000 $m^2 \cdot g^{-1}$) were used as the gate electrode to efficiently dope the transistor channel and monitor its potential.[183] After carrying out a systematic study on three different RTILs making use of the [TFSI] anion we explored the use of RTIL and propylene carbonate (PC) mixtures to decrease the RTIL viscosity and increase its ionic conductivity, with the objective to improve the transistor response time.

5.4 Results and discussion

To investigate systematically the effect of different RTILs on the doping effectiveness in MEH-PPV transistors we used RTILs making use of [TFSI] as the anion and [EMIM] (1-ethyl-3-methylimidazolium), [BMIM] (1-butyl-3-methylimidazolium) or [PYR_{14}] (1-butyl-1-methylpyrrolidinium), as the cation (Fig. 5.1). [EMIM][TFSI], [BMIM][TFSI] and [PYR_{14}][TFSI] have an ionic conductivity of 6.63 (20 °C), 3.41 (20 °C) and 2.12 (20 °C) $mS \cdot cm^{-1}$ and viscosity of 39.4 (20 °C), 49 (25 °C) and 89 (25 °C) cP, respectively.[132]

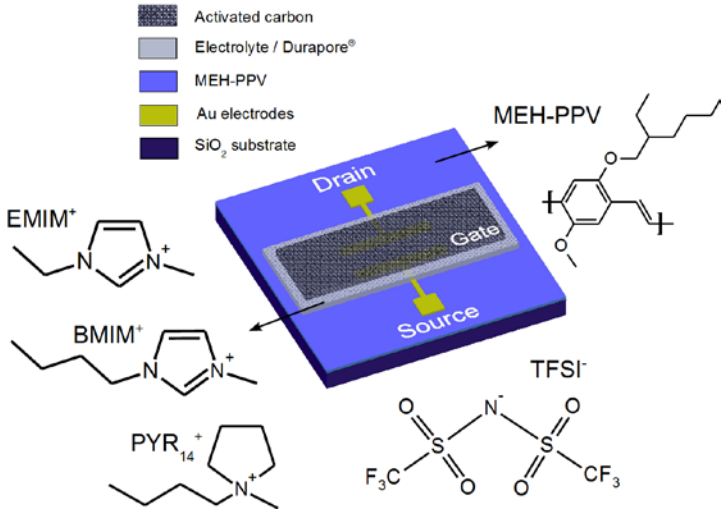

Figure 5.1. Device structure of the electrolyte-gated MEH-PPV transistors. A separator (Durapore® membrane filter, 9 mm × 4 mm × 125 μm) was soaked in the electrolyte and placed on top of the transistor channel. Carbon paper coated with activated carbon was set in contact with the separator and used as the gate electrode (6 mm × 3 mm × 170 μm). The molecular structures of the polymer MEH-PPV and the ionic species [EMIM], [BMIM] , [PYR_{14}] and [TFSI] are shown.

Initially we performed a morphological characterization, by Atomic Force Microscopy (AFM) of the films based on pure MEH-PPV as well as MEH-PPV blended with the ionic liquids. Such a characterization, which shed light onto the compatibility of the two components, is undoubtedly helpful to shed light on the factors governing the doping process. The compatibility (miscibility) between the semiconducting polymer and the ionic liquid is indeed expected to affect the degree of electrochemical doping in the polymer film.

AFM height images of films of MEH-PPV (Fig. 5.2a) and MEH-PPV:RTIL with 1:0.5 molar ratio (Figs. 5.2b-5.2d) show that the films cover completely the substrate surface. In the AFM images of the two-component films, segregation of the components is observable (*vide infra*).[184,185] The corresponding height profiles (Figs. 5.2f-5.2h) show the presence of circular domains that can be as large as 2 μm in diameter and 110 nm high (Fig. 5.2g). Furthermore, Figs. 5.2a-5.2d show the presence of MEH-PPV islands, with typical height of 5-10 nm and diameter of 0.5-1 μm (Figs. 5.2e-5.2g).[186] The film roughness (r_q) was 6 nm, 10 nm, 12 nm and 5 nm for MEH-PPV, MEH-PPV:[EMIM][TFSI], MEH-PPV:[BMIM][TFSI] and MEH-PPV:[PYR_{14}][TFSI] films on the 10 μm × 10 μm height images. When obtained from relatively smooth portions of the films (1 μm × 1 μm in size), r_q was 1±0.5 nm, for all the films. AFM phase images (Figs. 5.2i-5.2l) show relatively dark circular domains on a clear background. These domains are attributable to the RTIL component in the films. This hypothesis is corroborated by i) the molar ratio of the two components in the films and ii) the sharp colour contrast observed in the phase images.

The investigation of the morphology of the two-component (ionic liquid - MEH-PPV) films demonstrates that the ionic liquids we employed are suitable for MEH-PPV channels, in EG transistors. Indeed, the AFM images show phase separation (immiscibility) in the films.

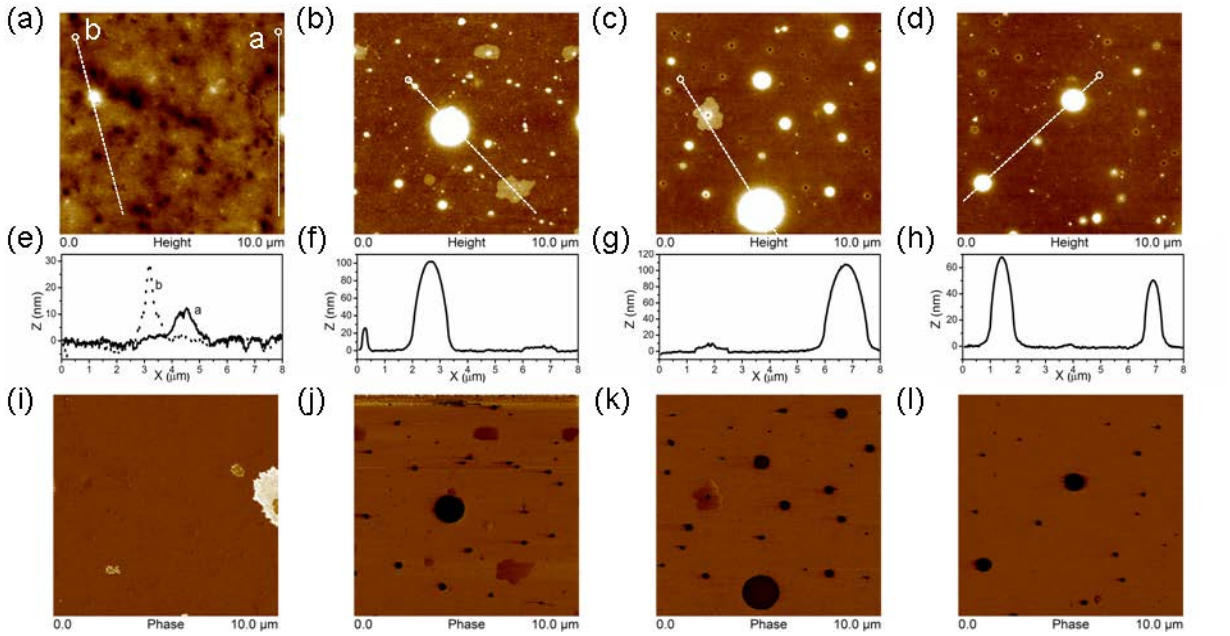

Figure 5.2. Atomic Force Microscopy height images (a-d, z-scale 10 nm), section profiles along the lines indicated in the height images (e-h), and phase images (i-l, z-scale 20°) of (a,e,i) MEH-PPV, (b,f,j) MEH-PPV:[EMIM][TFSI], (c,g,k) MEH-PPV:[BMIM][TFSI] and (d,h,l) MEH-PPV:[PYR_{14}][TFSI] films. [MEH-PPV]:RTIL molar ratio of 1:0.5.

EG transistors employing the different RTILs as gating medium adopted the structure shown in Fig. 5.1. The MEH-PPV thin film was deposited on a gold source/drain patterned SiO_2 substrate and, afterwards, vertically stacked with the RTIL, soaked in a Durapore® membrane, and an activated carbon gate contact.[183]

The output (drain-source current, I_{ds}, vs drain-source voltage, V_{ds}) and transfer (I_{ds} vs gate-source voltage, V_{gs}) characteristics of [EMIM][TFSI]-, [BMIM][TFSI]-, and [PYR_{14}][TFSI]-gated MEH-PPV transistors are presented in Figs. 5.3a-f.

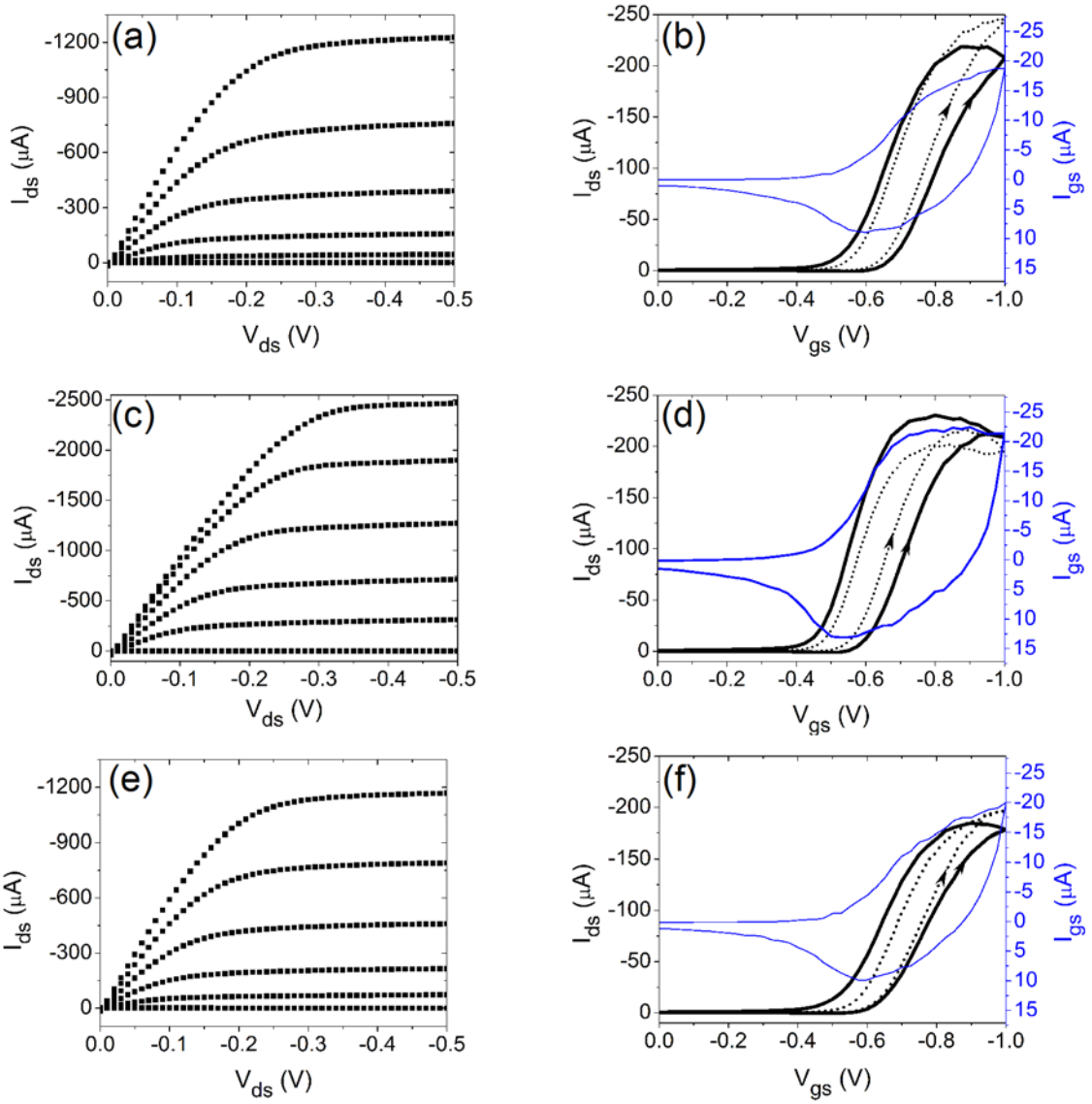

Figure 5.3. Device characteristics of electrolyte-gated MEH-PPV transistors making use of different ionic liquids. Left column: output characteristics (I_{ds} vs V_{ds} for V_{gs} = 0, -0.6, -0.65, -0.7, -0.75 and -0.8 V). Right column: transfer characteristics in the linear regime (V_{ds}= -25 mV) for V_{gs} sweeping rate of 50 mV·s^{-1} (left axis, black solid line) and for V_{gs} sweeping rate of 10 mV·s^{-1} (left axis, black dotted line) together with I_{gs} (gate-source current, right axis blue line) vs V_{gs} for V_{gs} sweeping rate of 10 mV·s^{-1}. In (a, b) the ionic liquid was [EMIM][TFSI], in (c, d) [BMIM][TFSI] and in (e, f) [PYR_{14}][TFSI].

A limited influence of the different cations constituting the RTILs is observable on the transistor output characteristic, indicating that the anion plays the key role in establishing the *p*-type doping

of MEH-PPV. The transistors operate at V_{gs} biases lower than 1 V and the saturation region starts at ca -0.25 V, for the three types of devices. This behavior is attributed to the high pseudo-capacitance at the polymer/RTIL interface and the non-limiting behavior of the high surface area gate electrode.[183] The ON/OFF ratio deduced from the forward step of the transfer curves with a V_{gs} between 0 and -1 V, V_{ds} at -25 mV, and I_{gs} sweep rate of 10 mV·s^{-1}, ranges between 2-3 × 10^3 for all the devices.

The hole carrier mobility (μ) was obtained from:

$$\mu = \frac{I_{ds}}{V_{ds} e p W} \frac{L}{V_{ds}} , \qquad (1)$$

where e is the elementary charge, L is the interelectrode distance, 10 μm, W is the electrode width, 4000 μm, and p is the charge carrier density (cm^{-2}) deduced from:

$$p = \frac{Q}{eA} = \frac{\int I_{gs} dV_{gs}}{r_v e A} , \qquad (2)$$

where I_{gs} is the gate-source current, r_v is the sweeping rate, and A is the active channel surface area (18 mm^2, surface area of the polymer in contact with the electrolyte, in turn in contact with the gate electrode).[87,183] We estimated Q from the forward sweep of the transfer curve (r_v = 10 mV·s^{-1}) as 1.7 × 10^{-4} C, 2.3 × 10^{-4} C and 1.8 × 10^{-4} C for [EMIM][TFSI]-, [BMIM][TFSI]-, and [PYR$_{14}$][TFSI]-gated MEH-PPV transistors. The charge carrier mobility (μ) was 2.5 × 10^{-2}, 1.5 × 10^{-2} and 2.0 × 10^{-2} cm^2·V^{-1}·s^{-1} for [EMIM][TFSI]-, [BMIM][TFSI]- and [PYR$_{14}$][TFSI]-gated MEH-PPV transistors. The similarity of the transistor performance observed for EG transistors using different RTILs as the gating medium is in agreement with the similarity of the results of the morphological studies. For the RTILs and the polymer considered, the electrical bias could play a key role in overcoming the presence of segregation between the RTIL and the MEH-PPV, observed in the AFM images.

The increase in I_{ds} and the lower current hysteresis at lower sweeping rates, observed in the transfer characteristics, point to ion diffusion as the limiting process during doping. Ion diffusion would therefore seem the process establishing the transistor response time.[183] As an example, upon application of V_{gs}, the redistribution of ions in the transistor channel for [BMIM][TFSI]-gated transistors results in a transient I_{gs} lasting less than 1 s and a transient I_{ds} which achieves its maximum value after ca 4 s after V_{gs} application (Fig. 5.4). This suggests that the transistor

response time depends on at least two processes: the redistribution of ions from the electrolyte into the transistor channel during doping, affecting I_{gs} vs time, and the redistribution of charges in the transistor channel, affecting I_{ds} vs time.[177] The two processes have different rate, with the latter being the slowest.[187]

To improve the kinetics of the doping process, thus reducing the transistor response time, we adopted the RTIL - solvent mixture approach. The addition of a molecular solvent to a RTIL is a valuable strategy for the increase of conductivity and the decrease of viscosity of pristine RTILs. Propylene carbonate (PC) is a very well known high-boiling point solvent used in electrolyte solutions for various electrochemical devices, including EG transistors. With PC/[PYR_{14}][TFSI] mixtures, values of the conductivity of ca. 12 $mS \cdot cm^{-1}$ and of the viscosity of ca. 6 cP are achievable, with ca. 1:1 volume ratio.[188] The use of such mixtures as the gating medium is expected to favorably affect the transistor response time and current hysteresis. We observed that after addition of PC to [BMIM][TFSI] (ca 15 µL of PC in 4.5 µL of [BMIM][TFSI]) the I_{ds} transient was at its maximum value at ca 1.5 s, after V_{gs} application, whereas the I_{gs} transient remained at 1 s. This type of result was observed with the other ionic liquids.

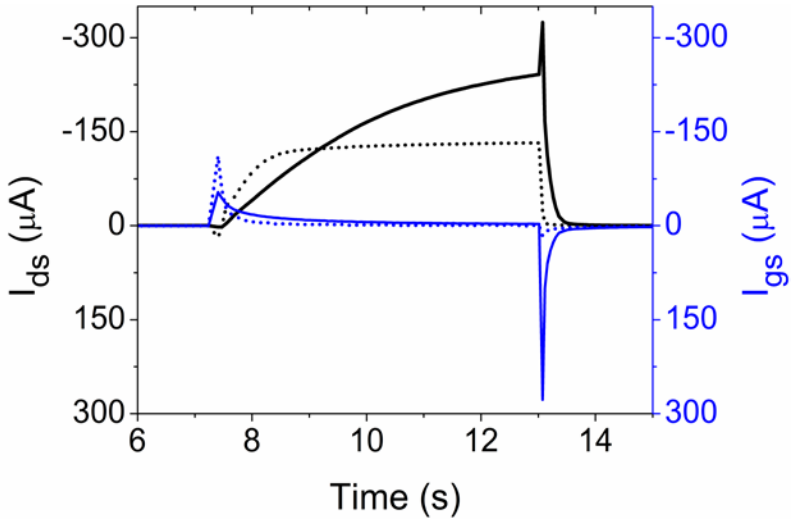

Figure 5.4. I_{ds} (left y axis) and I_{gs} (right axis) vs time for a constant V_{ds} of -300 mV applied to a [BMIM][TFSI]-gated MEH-PPV transistor before (solid lines) and after (dotted lines) addition of propylene carbonate. V_{gs} of -800 mV was applied at t=7.4 s for 5.5 s.

Afterwards, the effect of adding a polar solvent to a RTIL on the performance of MEH-PPV transistors was investigated by adding a drop of PC to the transistor that was assembled with pure [PYR_{14}][TFSI] (Fig. 5.5).

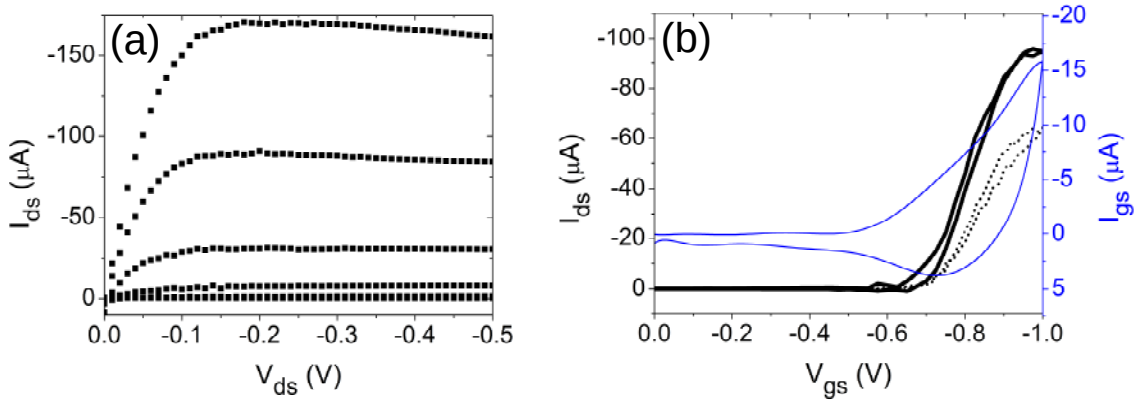

Figure 5.5. Device characteristics of the MEH-PPV transistor gated with [PYR_{14}][TFSI] and a drop of propylene carbonate (ca 15 μL of PC in 4.5 μL of [PYR_{14}][TFSI]). (a) output characteristics (I_{ds} vs $V_{ds,}$ for V_{gs} = 0, -0.6, -0.65, -0.7, -0.75 and -0.8 V) and (b) transfer characteristics in the linear regime, V_{ds}= -25 mV, for a V_{gs} sweeping rate of 50 mVs^{-1}, left axis black solid line, and sweeping rate of 10 mVs^{-1}, left axis black dotted line, and I_{gs} (gate-source current, right axis blue line) plotted vs V_{gs}.

Comparison between Figures 5.4 and 5.5 shows that PC addition lowers the V_{ds} onset for the saturation region down to -0.15 V and leads to a decrease of the current hysteresis in the transfer curves. The physicochemical properties of the solvent - RTIL mixtures, such as viscosity and ionic conductivity, determine the transistor performance. The higher conductivity of the PC - RTIL mixture with respect to that of the pristine RTIL accounts for the faster response time of the EG transistors gated using the mixture. Unluckily, I_{ds} decreases by almost one order of magnitude in the saturation regime and by a factor of two in the linear regime, possibly due to the partial dissolution of MEH-PPV in PC and to the "plasticizer" properties of this solvent. The ON/OFF ratio, Q and μ estimated from the forward transfer characteristics at r_v = 10 $mV \cdot s^{-1}$ were 1.8 × 10^3, 9.5 × 10^{-5} C and 1.2 × 10^{-2} $cm^2 \cdot V^{-1} \cdot s^{-1}$. Studies are ongoing to identify the solvent - RTIL mixture ratio to optimize the response time of the transistor without compromising the polymer film channel integrity.

5.5 Conclusions

In conclusion, we carried out a systematic comparison of the performance of transistors based on MEH-PPV channels and different ionic liquids, all of them including the [TFSI] anion, as the gating medium to understand the factors governing the doping in electrolyte-gated polymer transistors. We also included in such a comparative study a morphological characterization of pure MEH-PPV films and films produced by combining MEH-PPV and the ionic liquids in a way to gain insight into the compatibility between the ionic liquids and the polymer. A certain degree of segregation is observable in the AFM images of the two-component films. The electrical bias is expected to affect the compatibility of the two components, in turn affecting the nature and the extent of the doping. The results point to a key role played by the anion of the ionic liquid in establishing the transistor properties (the *p* doping), deduced from the similarities of the performance of transistors making use of ionic liquids constituted by the same anion. Even though the results we obtained, i.e. that anions from the bulk electrolyte determine a *p*-type doping, could have been predicted, such results are quite important. Indeed, complex intermolecular interactions between anions and cations constituting the ionic liquid, which is a solvent-free electrolyte, can affect the doping process, e.g. through the degree of ionicity of the ionic liquid.

Interestingly, during our efforts to tackle one of the key issues in the field of electrolyte-gated transistors i.e. their relatively slow response time, we observed that mixing a polar solvent with the ionic liquid increases the transistor time response. Despite its interest, such a solvent-ionic liquid mixture approach presents an enormous challenge: the solvent should be in principle orthogonal to the solvent used for the processing of the polymer film channel. The identification of suitable (orthogonal) solvents to be used in minimal amount in the mixture could represent a viable route to the improvement of the time response of electrolyte-gated transistors.

5.6 Experimental

The substrates were cleaned following sequential ultrasonic bath in isopropyl alcohol (IPA) for 5 min, acetone for 10 min and IPA for 5 min; followed by a 5 min dehydration process at 120 °C in

N_2, consisting of 3 purging cycles at low pressure (20 Torr) and high pressure (500 Torr). Drain and source contact electrodes of Ti/Au, 5/40 nm/nm, were deposited on SiO_2 substrates by e-beam physical vapor deposition and patterned using photolithography to form single channel electrodes with a channel width (*W*) of 4000 μm and length (*L*) of 10 μm. 5 mg of MEH-PPV (Sigma Aldrich, 55 kDa) were dissolved in 1 mL of toluene (Sigma Aldrich) by stirring overnight in a N_2 glove box (O_2, $H_2O \leq 5$ ppm) keeping the temperature at 40 °C. MEH-PPV thin films were deposited by spin-coating the solution at 1000 rpm for 1 min. Afterwards, films were thermally treated at 70 °C for 3 hours. [EMIM][TFSI], [BMIM][TFSI] and [PYR_{14}][TFSI] (IoLiTec, >99%) were dried under vacuum (~10^{-5} Torr) at 80 °C overnight prior to use, and stored (for a maximum period of 2 days) in the N_2 glove box. Anhydrous propylene carbonate (99.7%) was purchased from Sigma Aldrich and used as received. The device structure was completed by sandwiching a Durapore® GVHP filter membrane, soaked with the ionic liquid, between the MEH-PPV thin film and the activated carbon gate electrode. The gate electrode was prepared using carbon paper (Spectracorp 2050) coated with an ink of activated carbon (PICACTIF SUPERCAP BP10, Pica, 28 mg·mL^{-1}) and polyvinylidene fluoride (PVDF, KYNAR HSV900, 1.4 mg·mL^{-1}) binder in N-methyl pyrrolidone (NMP, Fluka, > 99.0%) solvent. The activated carbon coat was followed by a thermal treatment at 60 °C for several hours to remove the solvent. The electric characteristics of all devices were measured inside a N_2 glovebox (H_2O, $O_2 \leq 5$ ppm) using a B1500A Agilent semiconductor parameter analyzer.

MEH-PPV:IL blend films were fabricated using the following procedure: Pure RTILs ([EMIM][TFSI], [BMIM][TFSI], [PYR_{14}][TFSI]) were diluted in toluene (1:3 by volume) and then mixed with the above-mentioned MEH-PPV solution in order to get solutions with the final polymer:RTIL molar ratios of, 1:0.5. The liquid mixtures were spin-coated on the pre-cleaned patterned substrates at 1000 rpm for 60 s. Afterwards the films were thermally treated at 70 °C for 3 hours to remove the solvent.

AFM images were acquired in air ambient condition using tapping mode on a Digital Instruments Dimension 3100 (Santa Barbara, CA) combined with a Veeco Nanoscope V controller (Bruker). Tapping mode was performed at a scan rate of 1 Hz using etched silicon cantilevers (ACTA from Applied Nanostructures Inc.) with a resonance frequency around 300KHz, a spring constant ~ 40N/m and tip radius < 10nm. All images were acquired with medium tip oscillation damping (20-30%).

5.7 Acknowledgements

The authors are grateful to P. Moraille, Y. Drolet, J.-P. Lévesque and J. Bouchard, for technical assistance. This work was financially supported by NSERC (Discovery grants, CS and FC) and FQRNT (CS). JS acknowledges financial support by CONACYT and CMC Microsystems. F.S. acknowledges financial support by Università di Bologna, researcher mobility program, Italian-Canadian cooperation agreement.

CHAPTER 6 ARTICLE 3: TRANSCAP: A MONOLITHICALLY INTEGRATED SUPERCAPACITOR AND ELECTROLYTE-GATED TRANSISTOR

This chapter was published as an article in the *J. Mater. Chem. C*, 2014, **2**, 10273.

6.1 Authors

Jonathan Sayago,[a] Umar Shafrique,[a] Francesca Soavi,[b] Fabio Cicoira[c] and C. Santato[a]

[a]Département de Génie physique, École Polytechnique de Montréal, C.P. 6079, Succ. Centre Ville, Canada.

[b]Department of Chemistry "Giacomo Ciamician", Università di Bologna, Via Selmi, 2, Italy.

[c]Département de Génie chimique, École Polytechnique de Montréal, C.P. 6079, Succ. Centre Ville, Canada.

6.2 Abstract

We report the proof-of-concept of the TransCap, a monolithically integrated device that exhibits the storage properties of a supercapacitor and the low-voltage operation of an electrolyte-gated transistor. The proof-of-concept is based on coupling a polymer channel with a high surface area carbon gate, employing an ionic liquid as the electrolyte. The possibility to recover the stored energy from the TransCap permits to use it to power different microelectronic components.

6.3 Introduction

The increasing demand of energy autonomy for portable electronics is triggering intensive research efforts towards the development of self-powered, sustainable electronic devices.[189–191] Within this context, the coupling of electronic devices (sensors, transistors, etc.) with energy harvesters and small size energy storage systems (e.g. micro-batteries or micro-supercapacitors) is actively pursued.[190]

For their low-voltage operation characteristics, electrolyte-gated (EG) transistors are attractive candidates to be coupled to energy harvester/storage microsystems.[38,102,118,192,183,106,193,160] EG transistors make use of electrolytes, such as polymer electrolytes, ionic liquids and ion gels, to replace conventional gate dielectrics. Ionic liquids are particularly attractive since they are available in a wide range of different molecular structures and chemico-physical properties, thus offering the possibility to specifically control the interactions between the ions and the transistor channel, in view of an optimized doping.[176,180–182] The working principle of EG transistors is based on the high capacitance of the electrical double layer at the electrolyte/transistor channel interface. Different doping mechanisms, including electrostatic and Faradaic, have been proposed to explain the gating process. Polymer channel materials are typically characterized by Faradaic doping.

A large number of channel materials have been applied to EG transistors, including organic single crystals, organic thin films of small molecules and polymers,[87,104,106,147,152,158,159,194] thin films of metal oxides,[118,160–164] InN,[165] CdSe,[166] and PbSe.[167] EG transistors are intensively investigated because they permit current modulations of several orders of magnitude, upon application of relatively low gate voltages. Low-voltage operation is achieved by exploiting the exceptionally high capacitance of the electrical double layer forming at the electrolyte/transistor channel interface. High electrode capacitances are also exploited for charge and energy storage in electrochemical supercapacitors. Supercapacitors are high specific power systems that, for their capability to store/deliver charge in relatively short times (a few seconds), may outperform batteries in applications having high peak-to-average power demand. Different classes of supercapacitors making use of electrodes with different nature have been demonstrated. The most common supercapacitors are electrochemical double layer capacitors that use high surface area carbon electrodes, which store/deliver charge by an electrostatic process. Pseudo-supercapacitors feature battery-like electrodes (electronically conducting polymers, metal oxides) that are charged/discharged by fast and reversible redox processes. Hybrid supercapacitors feature positive and negative electrode materials of different nature that are charged/discharged via different electrostatic and faradaic modes.[97,168,195,196]

Here we report for the first time a monolithically integrated Transistor and superCapacitor (TransCap), where the typical function of a transistor is coupled with the energy storage function of a supercapacitor, within the same EG transistor structure. The proof-of-concept of the

TransCap is based on coupling a polymer channel with a high surface area carbon gate, employing an ionic liquid as the electrolyte. The p-doping that brings the polymer channel from the insulating to the conducting state is a pseudocapacitive charging process.[97,168] The high surface area gate electrode supplies the charge required to dope the transistor polymer channel by a fast, highly reversible, electrostatic process, referred to as double layer charging process, that is at the basis of the energy storage process in conventional electrochemical double layer supercapacitors. The use of a high surface area carbon gate electrode featuring a high double layer specific capacitance and employing an excess mass of carbon with respect to the amount required to balance the doping charge of the polymer is a valuable approach for an effective doping of the polymer channel.[183]

6.4 Results and discussion

The polymer/electrolyte/carbon stacking of the EG transistor features the cell configuration of a hybrid supercapacitor, where the negative carbon electrode and the positive polymer electrode are charged by an electrostatic and a faradic process, respectively. When the TransCap is ON, the polymer transistor channel is open. The *p*-doped polymer and negatively polarized carbon gate electrode are storing the charge (Q) at a given gate-source voltage (V_{gs}), hence the system is storing energy (equal to $Q \cdot V_{gs}$). When the TransCap is switched OFF, the channel and the gate are discharged and the delivered energy can be used for subsequent operation of the EG transistor itself or to power other components in the electronic system. The characteristics of the TransCap have similarities with those of floating gate transistor devices.

Specifically, we report a TransCap making use, as the channel material, of a thin film of the organic electronic polymer MEH-PPV, poly[2-methoxy-5-(2′-ethylhexyloxy)-1,4-phenylene vinylene], deposited on top of a SiO_2 substrate pre-patterned with gold drain and source electrodes (Fig. 6.1 and Annex C, for fabrication details). A high surface area carbon electrode (Brunauer-Emmett-Teller, BET, specific surface area of 1850 m^2/g) was used as the gate electrode. The room temperature ionic liquid N-trimethyl-N-propylammonium bis (trifluoromethanesulfonyl) imide ([N_{1113}][TFSI]), exhibiting remarkable electrochemical stability, was used as the gating medium.

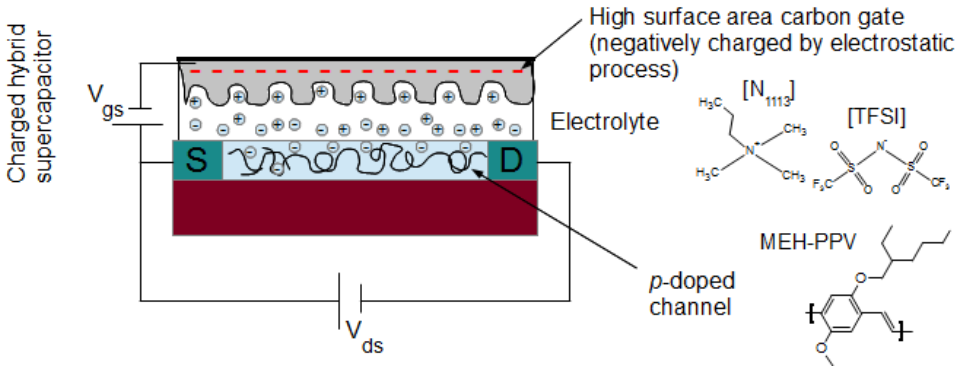

Figure 6.1. Device structure and working principle of the TransCap, whose proof-of-principle is proposed in this work. The drain (D) and source (S) electrodes and the *p*-doped MEH-PPV polymer channel are stacked with the electrolyte and the high surface area carbon gate. The polymer/electrolyte/carbon stacking features the cell configuration of a hybrid supercapacitor.

We initially performed the transistor characterization of the [N_{1113}][TFSI]-gated MEH-PPV TransCap. The output (drain-source current, I_{ds}, *vs* drain-source voltage, V_{ds}) and the transfer (I_{ds}-V_{gs}) characteristics of the TransCap (Figs. 6.2a and 6.2b) demonstrate the p-type transistor operation. In the output curves, we observe that the saturation regime is achieved at ca 0.25 V. The transistor ON/OFF ratio, calculated between V_{gs}= -0.8 V (ON state) and V_{gs}= 0 V (OFF state) at V_{ds} = -0.3 V, is about 2×10^3 (Annex C, Fig. S1). The hole mobility, determined from the transfer linear characteristics is 2×10^{-2} $cm^2 \cdot V^{-1} \cdot s^{-1}$. The hysteresis of the transistor current observed in the transfer curve (Fig. 6.2b) originates from ion diffusion during the doping and dedoping processes, in turn affecting the device response time.[187]

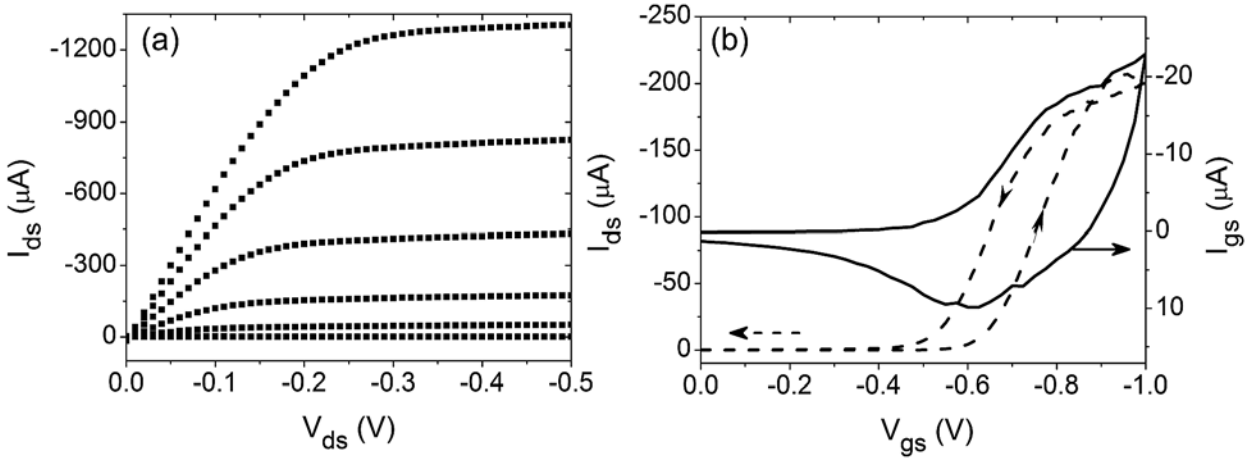

Figure 6.2. Transistor characteristics of the [N_{1113}][TFSI]-gated MEH-PPV TransCap: (a) output characteristics (V_{gs} = 0, -0.6, -0.65, -0.7, -0.75 and -0.8 V) and (b) transfer characteristics in the linear regime (V_{ds}= -25 mV) for a V_{gs} sweeping rate of 10 mV s^{-1}: I_{ds} on the left axis, dashed line, and I_{gs} on the right axis, solid line (please note that 0 V≤ V_{gs} ≤ -0.6 V do not significantly affect the transistor current).

Upon application of V_{gs}, we observed that I_{gs} decreases within 1 s whereas I_{ds} approaches its plateau value after ca 4 s (Fig. 6.3). This suggests that the transistor response time depends on two processes: the penetration of ions from the electrolyte in the polymer, which affects I_{gs} vs time, and the *p*-doping process in the polymer, which affects I_{ds} vs time.[196] While both the processes are affected by the [N_{1113}][TFSI] ionic conductivity,[170,187,196] they have different rates, with the former being the fastest. This result is not surprising if we consider that the MEH-PPV/[N_{1113}][TFSI]/carbon gate stacking has a similar configuration of a hybrid supercapacitor, which typically exhibits a relatively fast response time.[190]

The energy used to bring the transistor to the ON state (E_{ON}) and stored in the TransCap is given by the integration of I_{gs} over time multiplied by the value of V_{gs} (0.8 V); this value is of 53 μJ (Fig. 6.3). Such energy is then delivered upon switch OFF (E_{OFF}, calculated from the integration of I_{gs} over time during the switch off multiplied by 0.8 V) with an efficiency ($E_{ON}/E_{OFF} \cdot 100$) of 99.5%, due to the energy storage capability of the TransCap and the reversibility of the charging/discharging processes at the electrodes.

In our TransCap, where the carbon gate mass is in large excess with respect to that of the polymer (see ESI), the electrochemical response is mainly affected by the polymer doping/dedoping processes.

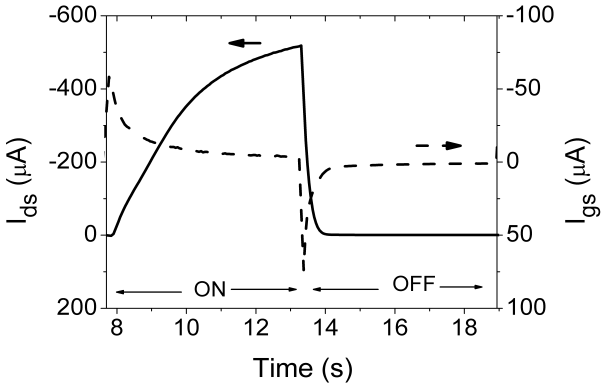

Figure 6.3. Switch ON and OFF of the $[N_{1113}][TFSI]$-gated MEH-PPV TransCap. I_{ds} (left axis) and I_{gs} (right axis) vs time for a switch ON at V_{gs} = -800 mV and switch OFF at V_{gs}=0 V. V_{ds} = -300 mV. Data taken during a sequential type of acquisition (5.5 s TransCap ON followed by 5.5 s TransCap OFF): during the first 8 s, V_{ds} = -300 mV and V_{gs} = 0 V.

To characterize the supercapacitor characteristics of the TransCap, we used the polymer transistor channel together with the drain and source electrodes as the positive electrode and the high surface area carbon gate as the negative electrode. Therefore, the supercapacitor cell voltage, V_{cell}, corresponds to $-V_{gs}$. We performed galvanostatically charge/discharge cycles (Fig. 6.4a) at a current $I = \pm 10$ μA (where $I = -I_{gs}$) up to 0.8 V, a cut-off cell voltage selected in agreement with the results reported in Fig. 6.2b. The capacitance (C) obtained by the slope of the discharge voltage profiles ($C = I\ dt/dV_{cell}$) is 0.16 mF. The delivered energy, E, and power, P, were calculated from the galvanostatic discharge curve using Eqs. (1) and (2):

$$E = I\int V_{cell}(t)\cdot dt\,, \qquad \text{Eq. (1)}$$

$$P = \frac{E}{\Delta t}, \qquad \text{Eq. (2)}$$

where Δt is the discharge time. E and P are 27.4 μJ and 4.6 μW, respectively. The capacitance, energy and power normalized to the TransCap electrode geometric area (0.36 cm^2) are 0.44 $mF\cdot cm^{-2}$, 0.02 $\mu Wh\cdot cm^{-2}$, 13 $\mu W\cdot cm^{-2}$. These values are of interest for energy autonomous electronic devices.[190]

Figure 6.4a shows that the storage capability of the TransCap permits to keep the transistor channel open even when the transistor is not connected to a power supply. This storage capability can be affected by the presence of leakage currents, resulting in discharging of the device. The leakage currents and discharge were therefore investigated using the following protocol: galvanostatic charge at 10 μA, up to a cut-off cell voltage value of 0.8 V; voltage of 0.8 V held over 10 s; rest step (I = 0 A) over 30 s; discharge at a constant current of -10 μA (Fig. 6.4b). The leakage current during the step at 0.8 V reaches 3.5 μA after 10 s, thus indicating that the energy consumption to keep the TransCap in the ON state at 0.8 V is not negligible (ca 0.43 μJ). These

values have to be taken into account if the TransCap is coupled to energy harvester systems that operate at low energy levels. On the other hand, the voltage behaviour over time during the rest step shows that the supercapacitor can keep its state of charge within a voltage drop of 1.4 % after 0.2 s (high resolution plot not shown here). After 30 s, the voltage decreases by 30% of its initial value. This result suggests that the TransCap can operate without being connected to an electric grid for relatively short times and that the transistor channel is still open (doped) at relatively long times. Any TransCap switch OFF following the rest step will provide an energy recovery with an efficiency depending on the duration of the previous rest step. The capability of the TransCap to store charge at the polymer/electrolyte/carbon interface holds promise for applications in the electronic industry, such as in displays where the transient switching of the display pixel is desired.

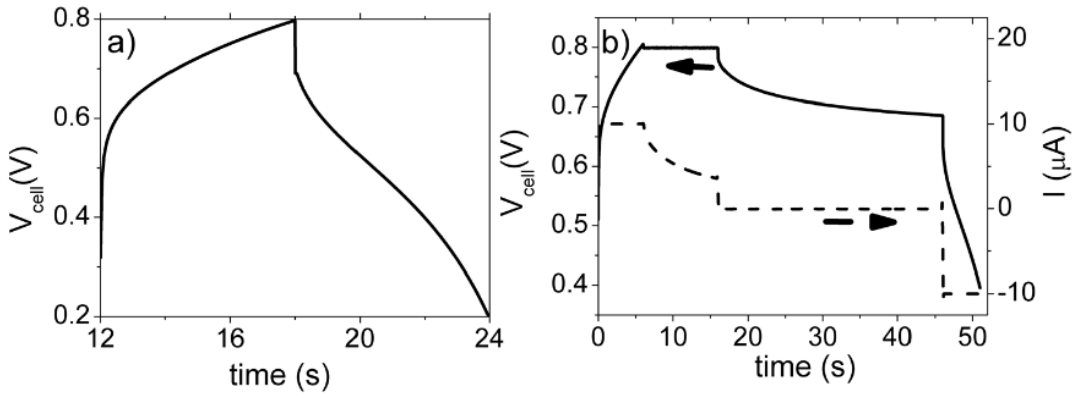

Figure 6.4. Supercapacitor characteristics of the [N_{1113}][TFSI]-gated MEH-PPV TransCap: (a) voltage profile *vs* time when the device is galvanostatically charged/discharged at ±10 μA up to 0.8 V (data taken during the second cycle of a sequential type of acquisition: 6 s TransCap ON followed by 6 s TransCap OFF); (b) voltage (left axis) and current (right axis) *vs* time upon galvanostatic charging at 10 μA up to 0.8 V, followed by 10 s at 0.8 V, 30 s rest in open circuit conditions, and galvanostatic discharge at -10 μA.

6.5 Conclusions

We report the proof-of-concept of the TransCap, a multifunctional monolithically-integrated device that combines the characteristics of an electrolyte-gated transistor and a micro-supercapacitor. The charge storage capability of the TransCap, similar to that of a floating gate

transistor design, opens the possibility to use the TransCap in memory (latch) applications. The possibility to recover energy from the TransCap permits to use the stored energy to subsequently power different microelectronic components. Remarkably, for the proof-of-concept of the TransCap we used materials such as carbon and organic electronic polymers that exhibit suitable processability characteristics for portable, low-cost, flexible electronics on plastic substrates.

6.6 Acknowledgements

The authors are grateful to Y. Drolet and J. Bouchard for their technical assistance. This work was financially supported by NSERC (Discovery grants, CS and FC) and FQRNT (Nouveau Chercheur, CS). JS acknowledges financial support by CONACYT and CMC Microsystems. FS acknowledges financial support by Università di Bologna (Researcher Mobility Program, Italian-Canadian cooperation agreement).

CHAPTER 7 COMPLEMENTARY RESULTS

7.1 *N*-type electrolyte-gated PCBM organic transistors

In section 3.3.1, we reviewed a solution-based method to deposit crystalline PCBM thin films, a well known *n*-type organic material. Incorporating crystalline PCBM thin films into electrolyte-gated *n*-type transistor structures can be valuable to correlate the morphology and the material properties with the *n*-type doping effectiveness of EG transistors. Combining *n*- and *p*-channels, are required to develop complementary circuits, of great interest in the field of organic electronics for their lower power dissipation and noise levels compared to circuits employing unipolar transistors. The influence of the cation molecular structure in the PCBM channel doping effectiveness can be studied by systematically employing electrolytes belonging to the same family, i.e. with a common cation and different anions.

Uemura et al. reported *n*-type [EMIM][TFSI]-gated C_{60} thin film transistors.[197] Figs. 7.1a and 7.1b show a schematic illustration of the device structure and a top view of the [EMIM][TFSI]-gated C_{60} transistor. C_{60} thin films were grown by vacuum deposition on SiO_2 (500 nm)/doped silicon substrates pre-patterned with Au drain and source electrodes, L = 30 μm and W = 100 μm. A PDMS well with a depth of ca 500 μm was used to contain the ionic liquid. The PDMS was coated with Au and set on top of the channel as gate electrode. Figs. 7.1c and 7.1d show the transistor transfer characteristics in the saturation region, V_{ds}= 0.5 V, and the output characteristics, for V_{gs} = 0, 0.2, 0.4, 0.8 and 1 V. Sub-1 V operation was realized with an onset voltage of ca 0.4 V. The saturation mobility was evaluated to be 0.06 $cm^2\ V^{-1}s^{-1}$ and the transconductance was 340 nS V^{-1} at V_{ds} = 0.1 V. The mobility was evaluated using a capacitance, for the electric double layer of 5 μF cm^{-2}, determined by ac impedance analysis.

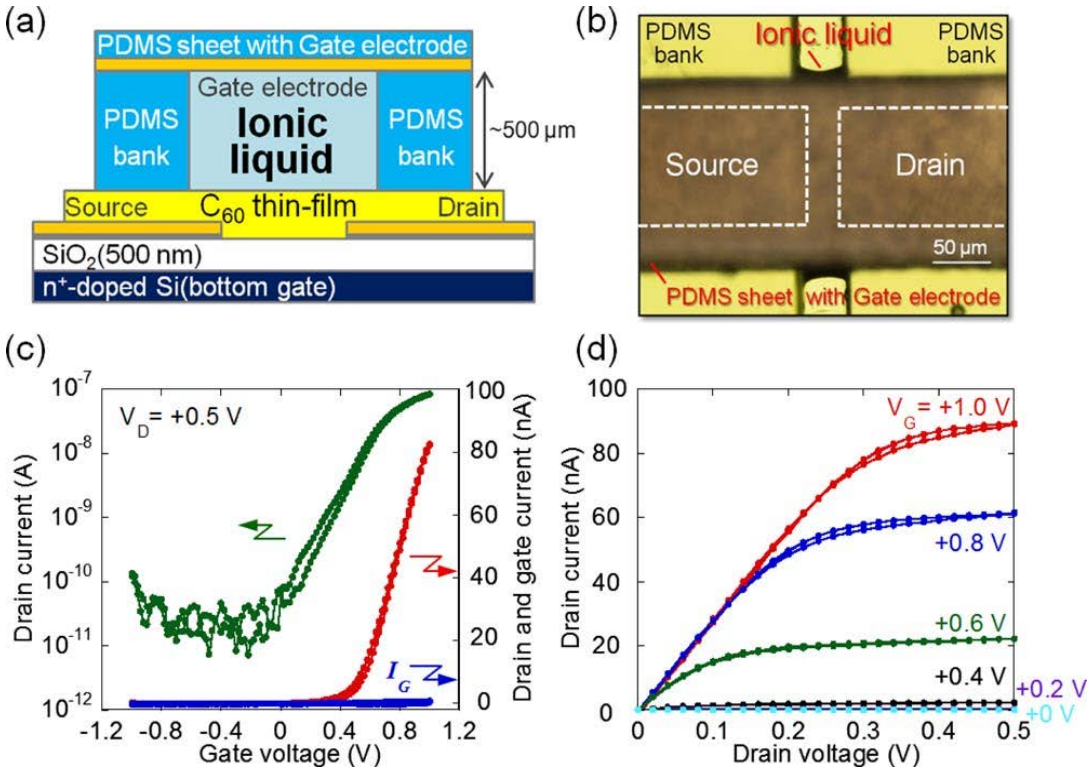

Figure 7.1. (a) Schematic illustration and (b) optical top view of the [EMIM][TFSI]-gated C_{60} transistor. (c) Transfer characteristics including the gate current plotted in the right axis and (d) output characteristics of the [EMIM][TFSI]-gated C_{60} transistor.[197] Reprinted with permission.

7.1.1 Preliminary results of electrolyte-gated transistors making use of *n*-type PCBM channel material.

In this section we present preliminary results towards *n*-type EG transistors based on PCBM thin film channel materials and [EMIM][TFSI] or [PYR_{14}][TFSI] gating medium.

PCBM thin films were spin-casted from 5 mg mL^{-1} of PCBM (Solaris Chem Inc.) in chlorobenzene onto SiO_2 substrates patterned with Au drain and source electrodes (W= 4 mm, L= 10 µm). The substrates were also patterned with parylene C (Cookson Electronics) wells with a height of 1.6 µm and an area of 980 × 5000 μm^2. The wells were employed to contain ca 100 µL of PCBM solution during deposition of the PCBM thin film at 50 °C during 2 h, as illustrated in Fig. S1, Annex D.

X-ray diffraction (XRD) spectra of the PCBM thin films was taken using Bruker D8 diffractometer equipped with a copper source for X-rays with a wavelength (Cu K_a) of 1.54 Å. The PCBM thin film XRD patterns, Fig. S2, Annex D, present three peaks at 2θ= 5.3°, 10.74° and 19.3° corresponding to a spacing between planes of atoms of 1.7 nm, 0.83 nm and 0.46 nm, in agreement with the characteristic XRD pattern of polycrystalline PCBM thin films reported in the literature.[198]

We investigated the viability of using PCBM as *n*-type channel material in EG transistors by incorporating [EMIM][TFSI] or [PYR_{14}][TFSI] RTILs as gating media and high surface area activated carbon gate electrodes, following the same procedure described in Chapters 4, 5 and 6. Cyclic voltammetry was measured in situ by employing the drain and source as WE and the gate as CE and REF within a potential range of 0 to -1.9 V vs activated carbon. The CV of [EMIM][TFSI]-gated PCBM transistors, Fig. S3a, Annex D, presents three reduction peaks at ca -1.1 V, -1.47 V and -1.85 V, in the forward potential sweep and three oxidation peaks at ca -1.7 V, -1.27 V and -0.73 V, in the backward potential sweep. The CV of [PYR_{14}][TFSI]-gated PCBM transistors, Fig. S3b, Annex D, presents three reduction peaks at ca -1 V, -1.4 V and -1.7 V, in the forward potential sweep; and three oxidation peaks at ca -1.56 V, -1.17 V and -0.72 V, in the backward potential sweep. The capacitance values for [EMIM][TFSI]- and [PYR_{14}][TFSI]-gated PCBM transistors up to 1 V, was estimated using the method described in Chapter 4, as 153 μF and 52 μF. The higher capacitance observed in devices employing [EMIM][TFSI] suggests higher permeability of [EMIM] into PCBM thin films.

The output curves (V_{gs} of 0, 0.8, 0.9 1 and 1.1 V) of [EMIM][TFSI]- and [PYR_{14}][TFSI]-gated PCBM transistors, are presented in Figs S4a and S4b, Annex D. Both devices show a typical *n*-type transistor behavior. The higher I_{ds} observed in [EMIM][TFSI]-gated transistors can be explained by the higher capacitance of the transistor channel, compared to [PYR_{14}][TFSI]-gated transistors. Figs. S4c and S4d, Annex D, present the transfer characteristics in the linear regime (V_{ds} = 200 mV) of [EMIM][TFSI]- and [PYR_{14}][TFSI]-gated PCBM transistors. The plot includes I_{gs} vs V_{gs} in the right axis. The μ of [EMIM][TFSI]- and [PYR_{14}][TFSI]-gated PCBM transistors, calculated using the method described in Chapter 4,[183] resulted in values of 8.8×10^{-4}

and 1.3×10^{-3} $cm^2 \cdot V^{-1}s^{-1}$, respectively. The ON (1 V_{gs}) / OFF (0 V_{gs}) ratio was 100 and 68 for [EMIM][TFSI]- and [PYR_{14}][TFSI]-gated PCBM transistors. The onset potential in the forward and backward sweep of the V_{gs} was 0.71 V and 0.65 V for [EMIM][TFSI]-gated PCBM transistors and 0.61 V and 0.45 V for [PYR_{14}][TFSI]-gated PCBM transistors. The higher I_{ds} hysteresis observed during the forward and backwards sweep of the V_{gs} in the transfer characteristics of [EMIM][TFSI]-gated PCBM transistors supports the hypothesis that [EMIM] is more permeable in PCBM thin films than [PYR_{14}].

Despite the typical *n*-type behavior of [EMIM][TFSI]- and [PYR_{14}][TFSI]-gated PCBM transistors, the I_{ds} and I_{gs} have comparable values in the transfer curves. The relatively low I_{ds} with respect to the I_{gs} can be related to an unfavorable energy difference between the workfunction of Au drain and source electrodes (Φ = 4.7-5.1 eV)[60] and the LUMO level of PCBM (LUMO ca 3.7 eV) to inject electrons.[199]

CHAPTER 8 GENERAL DISCUSSION

In this chapter, we try to critically discuss the elements presented in the previous chapters as a whole, including the thesis objectives, the literature presented in Chapters 2 and 3 and the results presented through Chapters 4 to 7. Although only a small part of the complex properties of EG transistors could be investigated in the present work, several insights were gained. These insights are discussed in terms of the effect of the physicochemical properties of the electrolyte in establishing the transistor characteristics, the importance of the nature and surface area of the gate electrode on the EG transistor drain-source current modulation and energy storage properties, and the properties of *n*-type PCBM EG transistors. We also review the advances and challenges to simultaneously achieve light-emission and current modulation within the EG transistor structure.

Table 8.1 compares some characteristics of EG transistors with respect to organic and inorganic transistors making use of conventional (not electrolyte) dielectrics. EG transistors typically operate at 1-2 V, however in the present thesis we demonstrate sub-1 V EG transistors. [87] We can observe that the main advantage of EG transistors rely on their low operation voltage. As opposed to that, their main limitation is related to their time low operation frequency, orders of magnitude lower.

Table 8.1: Comparison of EG organic transistors with organic and inorganic transistors making use of conventional dielectrics (not electrolyte).

	Operating Voltage	*Operation Frequency*	*Flexibility*
Organic Transistors based on 200 nm SiO_2 dielectric	20-30 V	1-20 MHz	no flexibility
Organic Transistors based on nanodielectrics	1-5 V	1-20 MHz	limited flexibility
Organic Transistors based on high-k dielectrics	1-10 V	1-20 MHz	limited flexibility
Inorganic Transistors based on 200 nm SiO_2 dielectric	1-5 V	1-2 GHz	limited flexibility
Inorganic Transistors based on high-k dielectrics	sub-1 V	1-2 GHz	limited flexibility
EG transistors with inorganic channel materials	1-2 V	1-10 MHz	can be flexible
EG transistors with organic channel materials	sub-1 V	1-10 kHz	can be flexible

8.1 The effect of the physicochemical properties of the electrolyte in establishing the transistor characteristics

The first objective in the present section is to understand whether the physicochemical properties of the electrolyte play an important role in establishing the transistor characteristics. As mentioned in Section 3.2, a number of RTILs with properties tunable by chemical synthesis are readily available. Moreover RTILs can be incorporated into a polymer matrix to form polymer electrolytes or gel electrolytes that are easier to incorporate into the device structure for their solid-like mechanical properties.

One would expect that the electrolyte properties, i.e. the ionic conductivity and viscosity, have an important effect on the performance of EG transistors, in particular in the transistor response time as reported by Frisbie et al.[109,110,144] Surprisingly, in Chapter 5 we observed similar transistor

characteristics (within one standard deviation) with transistors employing different RTILs with different physicochemical properties. The RTILs employed as gating medium were based on the common [TFSI] anion that is the doping agent in *p*-type transistor channels.

Transient transistor measurements, where we recorded the transistor I_{ds} and I_{gs} as a function of time for a given V_{gs} pulse, were useful to elucidate the doping process. We found that the redistribution of ions within the transistor channel is the limiting factor to the transistor response time. As described in Chapter 5, we observed that upon application of V_{gs} pulse in [BMIM][TFSI]-gated MEH-PPV transistors, the redistribution of ions in the transistor channel resulted in a transient I_{gs} decaying in less than 1 s and a transient I_{ds} which achieved a maximum value after ca 4 s. This suggests that the transistor response time depends on at least two processes: the redistribution of ions from the electrolyte into the transistor channel during doping, affecting I_{gs} vs time, and the redistribution of ions in the transistor channel, affecting I_{ds} vs time. The two processes have different rates, with the latter being the slowest.

8.2 The importance of the nature and surface area of the gate electrode on the EG transistor drain-source current modulation and its energy storage properties

The first approach we followed to investigate EG transistors was based on Pt gate electrodes and a device structure illustrated in Figs. 8.1a and 8.1b. A similar structure is reported by other research groups.[161,167,200] MEH-PPV was spin-coated onto SiO_2 substrates pre-patterned with Au drain and source electrodes (W= 4 mm, L= 10 μm). The substrate was pre-patterned with a sacrificial layer of parylene-C to delimit the MEH-PPV film on the transistor channel. A well of polydimethylsiloxane (PDMS) with an area of ca 0.45 × 0.28 cm^2 was prepared by moulding and attached to the transistor channel in order to contain the RTIL. Finally a Pt wire or coil was employed as gate electrode.

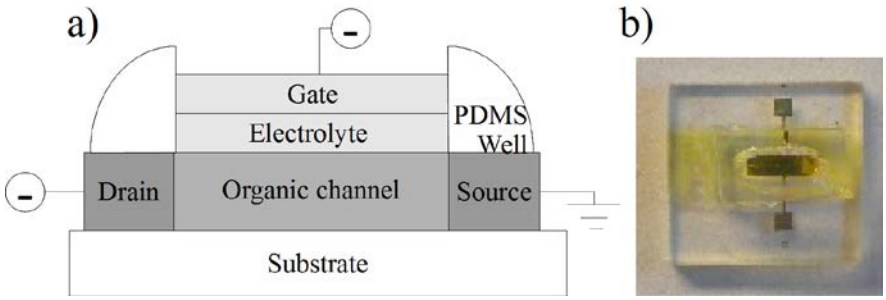

Figure 8.1. Electrolyte-gated organic transistor: a) schematic device structure and b) image (top view) of a device where are shown the transistor channel, the square-shaped source and drain electrodes, and the electrolyte, confined by a polydimethylsiloxane (PDMS) well. The substrate employed was glass or SiO_2.

MEH-PPV EG transistors based on such structure behaved as typical *p*-type transistors. However the I_{ds} showed a slow response upon application of V_{gs}, as illustrated in Fig. S1, Annex E. Our first hypothesis to explain the slow response of the I_{ds} as a function of V_{gs} was the slow reorganization of the anions in the transistor channel.

Electrochemical techniques such as cyclic voltammetry and electrochemical impedance spectroscopy were used within the EG transistor configuration to understand the electrochemical processes occurring between the transistor channel and the electrolyte and between the gate and the electrolyte. The transistor channel was set as the working electrode and the gate as the counter electrode. As discussed in Chapter 4, the nature and morphology of the gate electrode have an important effect on the performance of EG transistors. Employing high surface area gate electrodes, non-limiting in terms of their capability to supply the charge required to modulate the conductivity of the transistor channel resulted in sub-1 V operation and charge carrier mobilities of $(1.0 \pm 0.5) \times 10^{-2}$ $cm^2V^{-1}s^{-1}$. Moreover, high surface activated carbon gate electrodes limit undesirable electrochemical processes and render unnecessary the presence of a reference electrode to monitor the channel potential.

Electrochemical impedance spectroscopy (EIS) is a relevant technique to study the doping mechanism in EG transistors. Various groups suggest that the dominant doping process is electrostatic and therefore consider the transistor channel capacitance to be that of the RTIL, i.e.

10 μF cm^{-2}.[39,201–203] In [EMIM][TFSI]-gated MEH-PPV transistors the picture is quite different. The Nyquist plot (Fig. 4.2b) obtained at 0.8 V vs the activated carbon quasi reference electrode shows a 45° transmission line typical of diffusion controlled processes related to the diffusion of the doping ions from the ionic liquid into the polymer channel. Moreover, the pseudocapacitance measured with EIS or CV is in the order of 0.6-0.8 mF. The high capacitance values confirm the presence of electrochemical doping in the devices.

The high capacitance in MEH-PPV EG transistors based on high surface area activated carbon gate electrodes enables energy storage in a device we named TransCap for its Transistor-superCapacitor features. The polymer/electrolyte/carbon stack of the TransCap is analogue to the cell configuration of a hybrid supercapacitor. When the TransCap is ON the polymer and the carbon gate electrodes store charge (Q) at a given V_{gs}, hence the stored energy equals $Q \cdot V_{gs}$. When the TransCap is switched OFF the energy can be delivered back to power other electronic components. The energy and power normalized to the TransCap electrode geometric area (0.36 cm^2) are 0.02 μWh·cm^{-2} and 13 μW·cm^{-2}. These values are of interest for energy autonomous electronic devices.[204]

8.3 Properties of *n*-type PCBM EG transistors

In Chapter 7, we presented preliminary results on *n*-type EG transistors with PCBM films as channel material and [EMIM][TFSI] or [PYR_{14}][TFSI] as gating medium. Spin-casted films of PCBM presented XRD patterns characteristic of polycrystalline PCBM films. The capacitance of [EMIM][TFSI]- and [PYR_{14}][TFSI]-gated PCBM transistors, deduced from cyclic voltammetry measurements up to -1 V, normalized by the electrode geometric area (0.36 cm^2), was 425 μF cm^{-2} and 145 μF cm^{-2}. The higher capacitance in [EMIM][TFIS]-gated transistors possibly indicates a better permeability of [EMIM] into the PCBM thin films.

The output and transfer characteristics of [EMIM][TFSI]- and [PYR_{14}][TFSI]-gated PCBM transistors show typical *n*-type behavior. The charge carrier mobility of [EMIM][TFSI]- and [PYR_{14}][TFSI]-gated PCBM transistors deduced form the linear transfer characteristics, following the procedure described in Chapter 4, is 8.8×10^{-4} and 1.3×10^{-3} $cm^2 \cdot V^{-1}s^{-1}$, lower than

that reported for PCBM transistors.[49] The relatively low mobility can be related to an unfavorable mismatch between the Au workfunction (Φ = 4.7-5.1 eV)[60] and the LUMO level of PCBM, (LUMO ca 3.7 eV) to inject electrons.[199] Using metal electrodes with a workfunction closer to the LUMO level of PCBM can be an interesting strategy to improve the charge carrier injection.

8.4 Fabrication process flow

A summary of the process flow employed to fabricate MEH-PPV EG transistors is illustrated in Fig. 8.2. The process includes (i) metallization by photolithography lift-off, (ii) solution-cast of MEH-PPV films and (iii) integration of gate components. Substrates were cleaned by sequential ultrasonic baths in isopropyl alcohol (IPA, J. T. Baker, microelectronic grade, 5 min), acetone (J. T. Baker, microelectronic grade, 10 min), and IPA (5 min), followed by a 5 min dehydration process at 120 °C in N_2 atmosphere consisting of 3 purging cycles of low pressure (20 Torr) and high pressure (500 Torr). Drain and source contacts of Ti/Au, 5/40 nm/nm, were photolithographically patterned on SiO_2 substrates (channel width, W, 4000 μm and length, L, 10 μm). 5 mg of MEH-PPV (Sigma Aldrich, 55 kDa) in 1 mL of toluene (anhydrous, Sigma Aldrich) were mixed and stirred overnight in a N_2 glove box (O_2, H_2O lower than 5 ppm) keeping the temperature at about 40 °C. MEH-PPV thin films were deposited by spin coating the solution at 1000 rpm for 1 min. Afterwards, films were thermally treated at 70 °C for 3 hours. The final MEH-PPV thickness was 50 nm. The device fabrication was carried out by sandwiching a Durapore® GVHP filter separator (9 mm × 4 mm × 125 μm) soaked in the ionic liquid between the MEH-PPV thin film and the activated carbon gate electrode. The gate electrode was prepared using carbon paper (Spectracarb 2050, 3 mm × 6 mm) coated with 6 μL of an ink of activated carbon (PICACTIF SUPERCAP BP10, Pica, BET specific surface area 1850 m^2g^{-1}, 28 $mg \cdot mL^{-1}$) and polyvinylidene fluoride (PVDF, KYNAR HSV900, 1.4 $mg \cdot mL^{-1}$) binder in N-methyl pyrrolidone (NMP, Fluka, >99.0%) solvent. The coating was followed by a thermal treatment at 60 °C for several hours to remove solvent and water traces. The activated carbon mass loading was ca. 0.9 $mg \cdot cm^{-2}$. The footprint of the TransCap corresponds to the geometric area of the separator (0.36 cm^2).

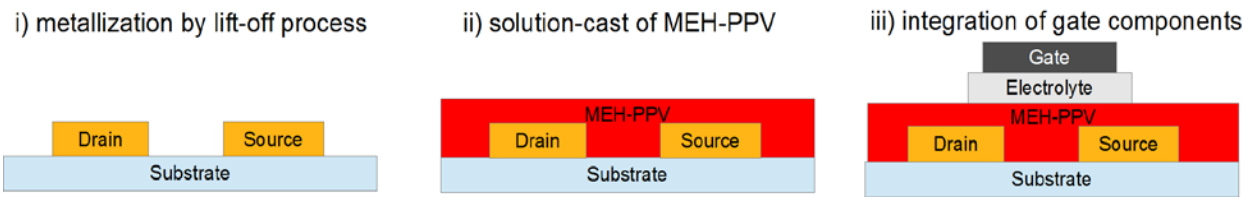

Figure 8.2. Process Flow to fabricate the MEH-PPV EG transistors. The substrate was a Si wafer (625 μm) with 200 nm dry thermal oxide (Silicon Quest International, Premium Grade). The electrolyte was [EMIM][TFSI], [BMIM][TFSI], [PYR_{14}][TFSI] [N_{1113}][TFSI] or [BMIM][TFSI]-propylene carbonate (3:1 v:v) mixture, contained in a Durapore® membrane.

The process flow employed to fabricate PCBM EG transistors is illustrated in Fig. 8.3. The process includes (i) metallization step by lift-off photolithography, (ii) sublimation of parylene, (iii) etching of parylene, (iv) cleaning, (v) solution coating of the organic semiconductor and (vi) the integration of gate components. Processes (i) and (vi) correspond to processes (i) and (iii) of the MEH-PPV EG transistor. 1.6 μm of parylene C (Cookson Electronics) was deposited using a vacuum sublimation system (Specialty Coating Systems PDS 2010) setting the deposition chamber to 135 °C and 125 Torr. The parylene was etched off the transistor channel (clearing an area of 980 x 5000 μm^2) by reactive ion etching under oxygen plasma. Substrates were cleaned by sequential ultrasonic baths in isopropyl alcohol (IPA, J. T. Baker, microelectronic grade, 5 min), acetone (J. T. Baker, microelectronic grade, 10 min), and IPA (5 min). 100 μL of PCBM solution, 5 mg of PCBM (SolarisChem Inc.) in 1 mL chlorobenzene, was spun on the parylene patterned substrate and thermally treated at 50 °C for 2 h.

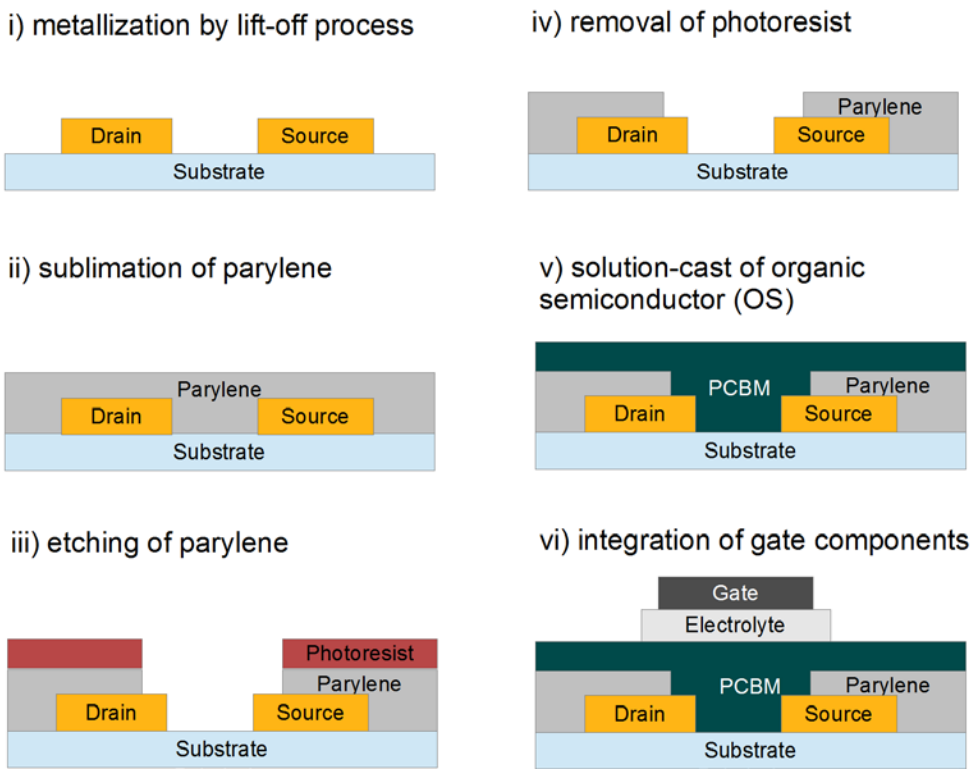

Figure 8.3. Process Flow to fabricate the PCBM EG transistors. The substrate was a Si wafer (625 μm) with 200 nm dry thermal oxide (Silicon Quest International, Premium Grade). Drain and source electrodes were 5 nm/40 nm of Ti/Au. The electrolyte was [EMIM][TFSI], or [PYR_{14}][TFSI], contained in a Durapore® membrane.

Devices with the same structure were fabricated in independent fabrication runs. A number of figures of merit to assess the reproducibility of the devices can be used: ON-OFF, V_{th}, mobility. Actually we could go far beyond these figures of merit considering e.g. also the number of cycles needed to activate the channel material in order to have a reproducible response of the transistor. The device fabrication and characterization, including fabrication of the thin film channel material, was carried out using the same experimental conditions (dry N_2 with H_2O < 5 ppm and O_2 < 5). The handling of the devices was carried out following the same sequence of events and timing to assess the reproducibility of the results. Typically 3 devices formally identical were fabricated and characterized. The performance of devices following the same fabrication process and characterization protocol were in agreement with an error lower than 10%.

We would like to point out that a number of source of error are possible for our research: i.e. the deposition of the organic semiconductor is highly sensitive to the processing conditions as discussed in Chapter 2.

Within the context of this Thesis we did not perform a detailed characterization of the device stability. Studies are ongoing in the group to assess the morphological and structural changes in the transistor channel material accompanying the electrical bias of the device; both shelf-life and operational stability studies are ongoing. Nevertheless we can say that if devices are stored and characterized in the glove box (dry N_2 with H_2O < 5 ppm and O_2 < 5) within the range of electrical bias reported in this Thesis, the transistor behavior can be observed after a few months from fabrication, for about 5-50 doping-dedoping cycles.

8.5 Towards electrolyte-gated organic light-emitting transistors: advances and challenges

Modulated light-emission has been reported in organic transistors making use of an organic light-emitting active layer, i.e. organic light-emitting transistors (OLETs).[6,130,205–214] Fundamental investigations on how charge carriers are injected, transported, and radiatively recombined in the channel to produce light in conditions of high charge carrier density and high exciton density as well as high current density, can be systematically investigated using OLETs as an optoelectronic characterization tool.[215–219,209,220] Interestingly, high current density (~33 kA cm^{-2}) has been observed in single crystal OLETs,[220] with no detrimental effect on the emission efficiency.[221,222] One goal in the field of organic electroluminescent semiconducting materials is to resolve the fundamental relationship between charge carrier density, charge carrier mobility and light-emission efficiency. High brightness, low voltage operation and device stability are all desirable characteristics in display technology. Organic light-emitting materials are of interest for potential applications in flexible displays,[208,223,224] solid-state lighting,[225,226] organic lasers,[227–230] and organic electroluminescent sensors.[231]

Interest in OLETs naturally extends towards electrolyte gated (EG-) OLETs, such that several groups are exploring the electrolyte-gating approach to simultaneously modulate the transistor current and the light generated.[92,104,159,216,232–234]

Liu et al. reported spatial control in the *p*-*n* junction in an organic light-emitting electrochemical transistor based on a thin film of MEH-PPV as the light-emitting polymer and a blend of PEO and KCF_3SO_3 as the electrolyte gating medium.[104] Bottom Au contacts served as drain and source electrodes (L=500 μm). Poly(3,4-ethylenedioxythiophene):poly(styrenesulfonate) (PEDOT:PSS) was laminated on top of the electrolyte and used as top gate electrode (Fig. 8.4a).

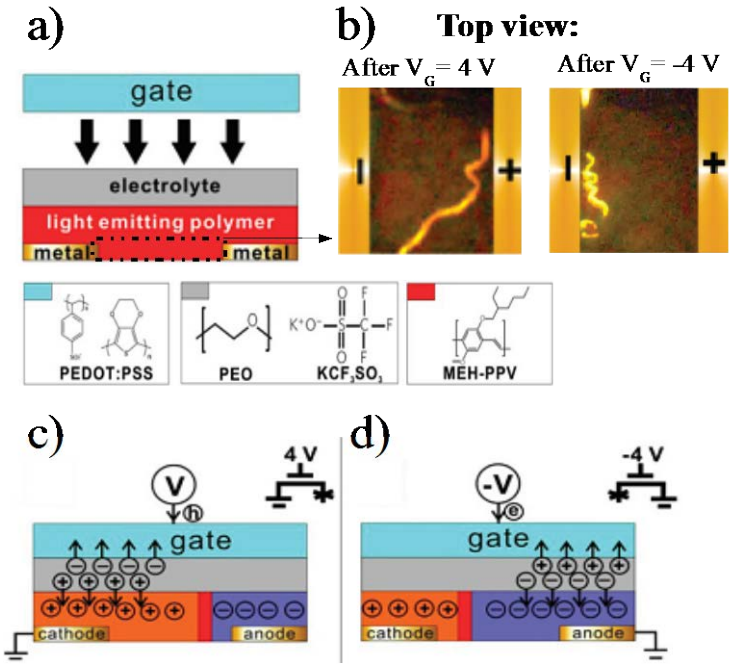

Figure 8.4. Organic light-emitting electrochemical transistor: a) device structure based on a PEDOT:PSS gate electrode, a KCF_3SO_3-PEO electrolyte, a MEH-PPV light-emitting polymer semiconductor, and Au source and drain bottom electrodes; b) top view of the transistor channel, upon application of a cathode-anode voltage of 4 V a gate bias (V_G) of 4 V (left) and -4 V (right); c) and d) proposed working principle for the light-emitting transistor upon application of positive (c) and negative d) gate bias. Adapted from.[104] Reprinted with permission.

As illustrated in Fig. 8.4b, the position of the light-emitting region within the EG-OLET transistor channel could be controlled by the polarity and magnitude of the applied gate bias which induced a preferential penetration of cations (anions) in the polymer affecting the length of the *n*- (*p*-) type doped regions. The device was operated in different modes. In the *n*-doped mode,

Fig. 8.4c, a positive bias was applied between the gate and the cathode (4 V) followed by the diffusion of cations from the electrolyte into the MEH-PPV extending the *n*-doping of the polymer. In the *p*-doped mode, Fig. 8.4d, a negative bias was applied between the gate and the anode (-4 V) such that anions from the electrolyte diffused into the MEH-PPV extending the *p*-type doping region. The ON/OFF ratio in the transistor ranged from 10 to 100 and the gate threshold bias was -2.3 V.

In 2010, Yumusak et al. reported a similar OLET but in this case no spatial control of the light-emitting region was reported.[233] The OLET structure, Fig. 8.5a, consisted of a film of poly(2-methoxy-5-(3',7'-dimethyloctyloxy)-1,4-phenylenevinylene) (MDMO-PPV) light-emitting polymer blended with $LiCF_3SO_3$ and poly(ethylene oxide) PEO. The film was deposited on conductive glass (SnO_2:In/glass) patterned with Au drain and source electrodes and coated with poly(vinyl alcohol) (PVA). *P*-type output transistor characteristics were achieved as shown in Fig. 8.5b.

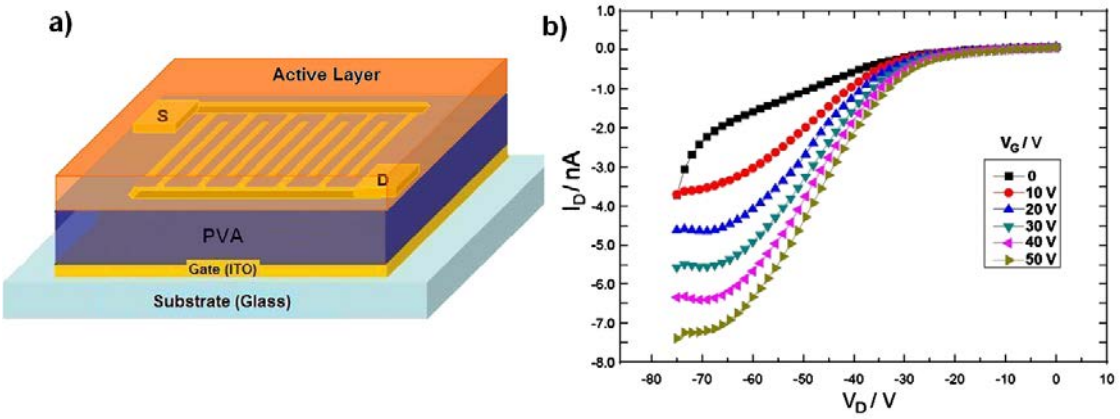

Figure 8.5. a) Device structure and b) p-type output characteristics of the organic electrochemical light-emitting field-effect transistor.[233] reprinted with permission.

Bhat et al. investigated ion-gel gated transistors making use of the light-emitting polymer poly(9,9′-dioctylfluorene-co-benzothiadiazole) (F8BT).[159] F8BT was spin-coated from xylene solution (4 mg mL^{-1}), annealed at 290 °C for 30 min resulting in polycrystalline F8BT films. The

film was deposited on glass substrates patterned with Au source and rain electrodes with L= 40 μm and W= 2 cm. The ion-gel was spin-coated from a solution constituted of [EMIM][TFSI] / poly(styrene-block-ethylene oxide-block-styrene) (SOS) / anhydrous acetonitrile with a wt % ratio of 9.3/0.7/90. Then the structure was annealed at 70 °C for about 15h in nitrogen atmosphere. A film of PEDOT:PSS drop-casted at 70 °C was employed as top gate electrode. The devices emitted light in proximity to the electron-injecting drain electrode when the drain-source voltage (V_{ds}) exceeded the energy gap of the polymer (ca 2.6 eV). No movement of the recombination region across the channel was observed.[216] The output characteristics showed well-defined linear and saturation behavior. The transfer characteristics showed a considerable hysteresis when the gate-source voltage (V_{gs}) was swept at 5 mV/s within the range of $-3 \leq V_{gs} \leq 1$. The onset voltage was ca -1.2 V and the ON/OFF ratio was 10^5.

An important concern in EG-OLETs is the effect of the proximity between the electrolyte and the light-emitting organic semiconductor. Understanding how this proximity affects the electroluminescence process is paramount to realize highly efficient EG-OLETs. Hodgkiss et al. made relevant observations employing time-resolved spectroscopy on conjugated polyelectrolytes with low-density ionic side chains derived from the conjugated polymer F8BT.[235] Time-resolved optical spectroscopy studies indicated that ions induce the formation of long-lived, weakly emissive and immobile charge states. In the electrochemical doping mode, the photoluminescence of the organic semiconductor is quenched in the bulk and the charge carrier injection at the drain and source electrodes is enhanced.[235,236]

Another open question is about the relationship between the quantum efficiency of the emitted light and the charge carrier density and charge carrier mobility. It has been observed experimentally that in planar light-emitting transistors it is difficult to simultaneously maximize the brightness, the quantum efficiency and the ON/OFF ratio.[224]

CHAPTER 9 CONCLUSION AND PERSPECTIVES

Organic semiconductor small molecules and polymers are interesting for printable electronics and for their properties tunable by chemical synthesis. Furthermore, they also exhibit mechanical flexibility and are compatible with simple deposition methods. Last but not least, organic semiconductors allow ionic and electronic coupling. In particular, exploiting ionic electronic coupling in EG transistors is an effective approach to lower the operation voltage in organic transistors.

First we demonstrated that the use of a suitable gate electrode in EG transistors is important to avoid undesirable electrochemical reactions at the electrolyte/gate interface and to overcome the need of a reference electrode to monitor the channel potential. This was demonstrated by using high surface area activated carbon as gate electrode in transistors employing MEH-PPV as the channel material and [EMIM][TFSI] as the gating medium. High surface area gate electrodes resulted in sub-1 V operation and charge carrier mobilities of $(1.0 \pm 0.5) \times 10^{-2}$ $cm^2V^{-1}s^{-1}$.

We observed a limited cation influence to establish the *p*-type doping in MEH-PPV films gated with various RTILs. The transistor response time depends on at least two processes, the redistribution of ions from the electrolyte into the transistor channel and the redistribution of charges (ionic and electronic) in the transistor channel, the latter process being the slowest.

The electrochemical doping process in MEH-PPV transistors based on activated carbon gate electrodes and RTIL gating medium enables energy storage in a device we named TransCap for its Transistor-superCapacitor features. The polymer/electrolyte/carbon vertical stack of the TransCap is analogue to the cell configuration of a hybrid supercapacitor. When the TransCap is ON the polymer and the carbon gate electrodes store charge (Q) at a given V_{gs}, hence the stored energy equals $Q \cdot V_{gs}$. When the TransCap is switched OFF the energy can be delivered back to power other electronic components. The energy and power normalized to the TransCap electrode geometric area (0.36 cm^2) are 0.02 $\mu Wh \cdot cm^{-2}$, 13 $\mu W \cdot cm^{-2}$. These values are of interest for energy autonomous electronic devices.

We introduced EG transistors based on PCBM thin films as channel material and [EMIM][TFSI] or [PYR_{14}][TFSI] as gating medium. Typical *n*-type transistor behavior was observed.

In perspective, we propose to investigate the evolution of the structural properties of PCBM films gated with various RTILs belonging to the same family, i.e. with different cations and a common anion. We propose to collect the XRD patterns of PCBM films before and after setting them in contact with a RTIL and applying an electrical bias.

Other interesting studies in EG transistors include the effect of the size of the electrolyte doping species, i.e. the anion in *p*-type channels or the cation in *n*-type channels, on the transistor doping process, and the stability (life cycle) of EG transistors.

BIBLIOGRAPHY

[1] H. Shirakawa, E.J. Louis, A.G. MacDiarmid, C.K. Chiang, and A.J. Heeger, J. Chem. Soc. Chem. Commun. 578 (1977).

[2] A. Tsumura, H. Koezuka, and T. Ando, Appl. Phys. Lett. **49**, 1210 (1986).

[3] C. d. Dimitrakopoulos and P. r. l. Malenfant, Adv. Mater. **14**, 99 (2002).

[4] G. Malliaras and R. Friend, Phys. Today **58**, 53 (2005).

[5] F. Cicoira and C. Santato, *Organic Electronics: Emerging Concepts and Technologies* (John Wiley & Sons, 2013).

[6] F. Cicoira and C. Santato, Adv. Funct. Mater. **17**, 3421 (2007).

[7] A. Dadvand, A.G. Moiseev, K. Sawabe, W.-H. Sun, B. Djukic, I. Chung, T. Takenobu, F. Rosei, and D.F. Perepichka, Angew Chem Int Ed **51**, 3837 (2012).

[8] D. Braga and G. Horowitz, Adv. Mater. **21**, 1473 (2009).

[9] C.R. Newman, C.D. Frisbie, D.A. da Silva Filho, J.-L. Brédas, P.C. Ewbank, and K.R. Mann, Chem. Mater. **16**, 4436 (2004).

[10] I.F. Perepichka and D.F. Perepichka, *Handbook of Thiophene-Based Materials: Applications in Organic Electronics and Photonics, 2 Volume Set* (John Wiley & Sons, 2009).

[11] L.-L. Chua, J. Zaumseil, J.-F. Chang, E.C.-W. Ou, P.K.-H. Ho, H. Sirringhaus, and R.H. Friend, Nature **434**, 194 (2005).

[12] D.M. de Leeuw, M.M.J. Simenon, A.R. Brown, and R.E.F. Einerhand, Synth. Met. **87**, 53 (1997).

[13] A. Facchetti, M.-H. Yoon, and T.J. Marks, Adv. Mater. **17**, 1705 (2005).

[14] R. Ponce Ortiz, A. Facchetti, and T.J. Marks, Chem. Rev. **110**, 205 (2010).

[15] D.K. Hwang, K. Lee, J.H. Kim, S. Im, C.S. Kim, H.K. Baik, J.H. Park, and E. Kim, Appl. Phys. Lett. **88**, 243513 (2006).

[16] S.H. Lee, S. Jeong, and J. Moon, Org. Electron. **10**, 982 (2009).

[17] W. Xu and S.-W. Rhee, J. Mater. Chem. **19**, 5250 (2009).

[18] K. Cousins, *Polymers for Electronic Components* (iSmithers Rapra Publishing, 2001).

[19] J. Bardeen, in *Nobel Lect.* (1956).

[20] H. Letaw and J. Bardeen, J. Appl. Phys. **25**, 600 (1954).

[21] D. Ofer, R.M. Crooks, and M.S. Wrighton, J. Am. Chem. Soc. **112**, 7869 (1990).

[22] C.F. Shu and M.S. Wrighton, J. Phys. Chem. **92**, 5221 (1988).

[23] M.J. Natan, D. Belanger, M.K. Carpenter, and M.S. Wrighton, J. Phys. Chem. **91**, 1834 (1987).

[24] M.J. Natan, T.E. Mallouk, and M.S. Wrighton, J. Phys. Chem. **91**, 648 (1987).

[25] H.S. White, G.P. Kittlesen, and M.S. Wrighton, J. Am. Chem. Soc. **106**, 5375 (1984).

[26] P. Bergveld, Sens. Actuators B Chem. **88**, 1 (2003).

[27] S.D. Moss, J. Janata, and C.C. Johnson, Anal. Chem. **47**, 2238 (1975).

[28] M.O. Schloh, N. Leventis, and M.S. Wrighton, J. Appl. Phys. **66**, 965 (1989).

[29] L. Mariucci, G. Fortunato, A. Pecora, A. Bearzotti, P. Carelli, and R. Leoni, Sens. Actuators B Chem. **6**, 29 (1992).

[30] J.T. Mabeck and G.G. Malliaras, Anal. Bioanal. Chem. **384**, 343 (2005).

[31] P.J.C. S. Sherry Zhu, J. Am. Chem. Soc. - J AM CHEM SOC **118**, (1996).

[32] M.J. Marsella, P.J. Carroll, and T.M. Swager, J. Am. Chem. Soc. **117**, 9832 (1995).

[33] S. Chao and M.S. Wrighton, J. Am. Chem. Soc. **109**, 6627 (1987).

[34] S. Chao and M.S. Wrighton, J. Am. Chem. Soc. **109**, 2197 (1987).

[35] J.W. Thackeray, H.S. White, and M.S. Wrighton, J. Phys. Chem. **89**, 5133 (1985).

[36] D. Ofer and M.S. Wrighton, J. Am. Chem. Soc. **110**, 4467 (1988).

[37] H.B. Tatistcheff, I. Fritsch-Faules, and M.S. Wrighton, J. Phys. Chem. **97**, 2732 (1993).

[38] S.H. Kim, K. Hong, W. Xie, K.H. Lee, S. Zhang, T.P. Lodge, and C.D. Frisbie, Adv. Mater. Weinheim **25**, 1822 (2013).

[39] M.J. Panzer and C.D. Frisbie, Adv. Mater. **20**, 3177 (2008).

[40] D. Braga, M. Ha, W. Xie, and C.D. Frisbie, APL Org. Electron. Photonics **3**, 245 (2010).

[41] A. Sandström, P. Matyba, O. Inganäs, and L. Edman, J. Am. Chem. Soc. **132**, 6646 (2010).

[42] J. Wuensche, Eumelanin Films for Organic Bioelectronics: Growth, Charge Transport, and Interaction with Metal Electrodes., PhD, École Polytechnique de Montréal, 2014.

[43] N. Ueno, in *Phys. Org. Semicond.*, edited by W. Brütting and C. Adachi (Wiley-VCH Verlag GmbH & Co. KGaA, 2012), pp. 65–89.

[44] I. Kymissis, in *Org. Field Eff. Transistors* (Springer US, 2009), pp. 1–11.

[45] W. Xie and C.D. Frisbie, J. Phys. Chem. C **115**, 14360 (2011).

[46] D. Knipp, R.A. Street, A. Völkel, and J. Ho, J. Appl. Phys. **93**, 347 (2003).

[47] A.B. Chwang and C.D. Frisbie, J. Appl. Phys. **90**, 1342 (2001).

[48] T. Kanbara, K. Shibata, S. Fujiki, Y. Kubozono, S. Kashino, T. Urisu, M. Sakai, A. Fujiwara, R. Kumashiro, and K. Tanigaki, Chem. Phys. Lett. **379**, 223 (2003).

[49] F. Cicoira, C.M. Aguirre, and R. Martel, ACS Nano **5**, 283 (2011).

[50] R.D. McCullough, R.D. Lowe, M. Jayaraman, and D.L. Anderson, J. Org. Chem. **58**, 904 (1993).

[51] T.-A. Chen, X. Wu, and R.D. Rieke, J. Am. Chem. Soc. **117**, 233 (1995).

[52] R.J. Kline, M.D. McGehee, E.N. Kadnikova, J. Liu, J.M.J. Fréchet, and M.F. Toney, Macromolecules **38**, 3312 (2005).

[53] I. Kymissis, *Organic Field Effect Transistors Theory, Fabrication and Characterization* (Springer, New York, 2009).

[54] J.-F. Chang, B. Sun, D.W. Breiby, M.M. Nielsen, T.I. Sölling, M. Giles, I. McCulloch, and H. Sirringhaus, Chem. Mater. **16**, 4772 (2004).

[55] M.L. Chabinyc, F. Endicott, B.D. Vogt, D.M. DeLongchamp, E.K. Lin, Y. Wu, P. Liu, and B.S. Ong, Appl. Phys. Lett. **88**, 113514 (2006).

[56] M.L. Chabinyc, R.A. Street, and J.E. Northrup, Appl. Phys. Lett. **90**, 123508 (2007).

[57] J.H. Burroughes, D.D.C. Bradley, A.R. Brown, R.N. Marks, K. Mackay, R.H. Friend, P.L. Burns, and A.B. Holmes, Nature **347**, 539 (1990).

[58] B.R. Hsieh, Y. Yu, E.W. Forsythe, G.M. Schaaf, and W.A. Feld, J. Am. Chem. Soc. **120**, 231 (1998).

[59] S. Hotta, editor , *Electronic and Optical Properties of Conjugated Molecular Systems in Condensed Phases: 2003* (Research Signport, Kerala, India, 2003).

[60] W. Osikowicz, M.P. de Jong, S. Braun, C. Tengstedt, M. Fahlman, and W.R. Salaneck, Appl. Phys. Lett. **88**, 193504 (2006).

[61] J. Mei and Z. Bao, Chem. Mater. **26**, 604 (2014).

[62] P. Prins, F.C. Grozema, F. Galbrecht, U. Scherf, and L.D.A. Siebbeles, J. Phys. Chem. C **111**, 11104 (2007).

[63] A. Salleo, R.J. Kline, D.M. DeLongchamp, and M.L. Chabinyc, Adv. Mater. **22**, 3812 (2010).

[64] C. Kloc, P.G. Simpkins, T. Siegrist, and R.A. Laudise, J. Cryst. Growth **182**, 416 (1997).

[65] R.A. Laudise, C. Kloc, P.G. Simpkins, and T. Siegrist, J. Cryst. Growth **187**, 449 (1998).

[66] X. Yang, J.K.J. van Duren, M.T. Rispens, J.C. Hummelen, R. a. J. Janssen, M. a. J. Michels, and J. Loos, Adv. Mater. **16**, 802 (2004).

[67] H. Minemawari, T. Yamada, H. Matsui, J. Tsutsumi, S. Haas, R. Chiba, R. Kumai, and T. Hasegawa, Nature **475**, 364 (2011).

[68] C. Liu, T. Minari, X. Lu, A. Kumatani, K. Takimiya, and K. Tsukagoshi, Adv. Mater. **23**, 523 (2011).

[69] J. Soeda, T. Uemura, T. Okamoto, C. Mitsui, M. Yamagishi, and J. Takeya, Appl. Phys. Express **6**, 076503 (2013).

[70] J. Peet, M.L. Senatore, A.J. Heeger, and G.C. Bazan, Adv. Mater. **21**, 1521 (2009).

[71] C. Reese, W.-J. Chung, M. Ling, M. Roberts, and Z. Bao, Appl. Phys. Lett. **89**, 202108 (2006).

[72] J. Liu, T.-F. Guo, and Y. Yang, J. Appl. Phys. **91**, 1595 (2002).

[73] Y. Shi, J. Liu, and Y. Yang, J. Appl. Phys. **87**, 4254 (2000).

[74] S. Walheim, M. Böltau, J. Mlynek, G. Krausch, and U. Steiner, Macromolecules **30**, 4995 (1997).

[75] H.N. Tsao, H.J. Räder, W. Pisula, A. Rouhanipour, and K. Müllen, Phys. Status Solidi A **205**, 421 (2008).

[76] A. Luzio, E.V. Canesi, C. Bertarelli, and M. Caironi, Materials **7**, 906 (2014).

[77] D.H. Reneker and A.L. Yarin, Polymer **49**, 2387 (2008).

[78] T. Tunç, İ. Uslu, İ. Dökme, Ş. Altındal, and H. Uslu, Int. J. Polym. Mater. Polym. Biomater. **59**, 739 (2010).

[79] S.-Y. Min, T.-S. Kim, B.J. Kim, H. Cho, Y.-Y. Noh, H. Yang, J.H. Cho, and T.-W. Lee, Nat. Commun. **4**, 1773 (2013).

[80] H. Bässler and A. Köhler, in *Unimolecular Supramol. Electron. I*, edited by R.M. Metzger (Springer Berlin Heidelberg, 2011), pp. 1–65.

[81] P. Stallinga, Adv. Mater. **23**, 3356 (2011).

[82] T. Toccoli, A. Pallaoro, N. Coppedè, S. Iannotta, F. De Angelis, L. Mariucci, and G. Fortunato, Appl. Phys. Lett. **88**, 132106 (2006).

[83] W. Brütting, *Physics of Organic Semiconductors* (Wiley, 2005).

[84] E.J. Meijer, M. Matters, P.T. Herwig, D.M. de Leeuw, and T.M. Klapwijk, Appl. Phys. Lett. **76**, 3433 (2000).

[85] G. Horowitz, M.E. Hajlaoui, and R. Hajlaoui, J. Appl. Phys. **87**, 4456 (2000).

[86] M.C.J.M. Vissenberg and M. Matters, Phys. Rev. B **57**, 12964 (1998).

[87] B.D. Paulsen and C.D. Frisbie, J Phys Chem C **116**, 3132 (2012).

[88] G. Horowitz, Adv. Mater. **10**, 365 (1998).

[89] I. Kymissis, in *Org. Field Eff. Transistors* (Springer US, 2009).

[90] A. Köhler and H. Bässler, *Electronic Processes in Organic Semiconductors: An Introduction* (John Wiley & Sons, 2015).

[91] K.F. Schuegraf and C. Hu, Semicond. Sci. Technol. **9**, 989 (1994).

[92] D. Braga, N.C. Erickson, M.J. Renn, R.J. Holmes, and C.D. Frisbie, Adv. Funct. Mater. **22**, 1623 (2012).

[93] M.J. Panzer and C.D. Frisbie, Adv Funct Mater **16**, 1051 (2006).

[94] J. Takeya, K. Yamada, K. Hara, K. Shigeto, K. Tsukagoshi, S. Ikehata, and Y. Aoyagi, Appl. Phys. Lett. **88**, 112102 (2006).

[95] J.O. Bockris and A.K. Reddy, *Modern Electrochemistry, Volumes 1 & 2* (Macdonald, 1970).

[96] X. Peng, L. Peng, C. Wu, and Y. Xie, Chem. Soc. Rev. **43**, 3303 (2014).

[97] P. Simon and Y. Gogotsi, Nat. Mater. **7**, 845 (2008).

[98] F. Beguin and E. Frackowiak, *Supercapacitors: Materials, Systems and Applications* (John Wiley & Sons, 2013).

[99] J. Lee, L.G. Kaake, J.H. Cho, X.-Y. Zhu, T.P. Lodge, and C.D. Frisbie, J. Phys. Chem. C **113**, 8972 (2009).

[100] A. Yu, V. Chabot, and J. Zhang, *Electrochemical Supercapacitors for Energy Storage and Delivery: Fundamentals and Applications* (CRC Press, Boca Raton, 2013).

[101] Y. Zhang, H. Feng, X. Wu, L. Wang, A. Zhang, T. Xia, H. Dong, X. Li, and L. Zhang, Int. J. Hydrog. Energy **34**, 4889 (2009).

[102] G. Tarabella, F.M. Mohammadi, N. Coppedè, F. Barbero, S. Iannotta, C. Santato, and F. Cicoira, Chem. Sci. **4**, 1395 (2013).

[103] A.J. Bard and L.R. Faulkner, *Electrochemical Methods: Fundamentals and Applications* (Wiley, 2000).

[104] J. Liu, I. Engquist, X. Crispin, and M. Berggren, J. Am. Chem. Soc. **134**, 901 (2012).

[105] S.Y. Yang, F. Cicoira, R. Byrne, F. Benito-Lopez, D. Diamond, R.M. Owens, and G.G. Malliaras, Chem. Commun. **46**, 7972 (2010).

[106] F. Cicoira, M. Sessolo, O. Yaghmazadeh, J.A. DeFranco, S.Y. Yang, and G.G. Malliaras, Adv. Mater. **22**, 1012 (2010).

[107] S.Y. Yang, F. Cicoira, N. Shim, and G. Malliaras, in *Iontronics Chapter Org. Electrochem. Transistors Sens. Appl.* (CRC Press, 2010), pp. 163–192.

[108] V.S. Bagotsky, in *Fundam. Electrochem.* (John Wiley & Sons, Inc., 2005), pp. 709–710.

[109] J.H. Cho, J. Lee, Y. He, B.S. Kim, T.P. Lodge, and C.D. Frisbie, Adv. Mater. **20**, 686 (2008).

[110] S. Zhang, K.H. Lee, C.D. Frisbie, and T.P. Lodge, Macromolecules **44**, 940 (2011).

[111] M. J. Panzer and C. D. Frisbie, J. Am. Chem. Soc. **129**, 6599 (2007).

[112] Lars Herlogsson, *Electrolyte-Gated Organic Thin-Film Transistors, PhD Dissertation* (Linköping University, 2011).

[113] J. Barthel, H. Krienke, and W. Kunz, *Physical Chemistry of Electrolyte Solutions: Modern Aspects* (Springer, 1998).

[114] H. Semat and C.P. Baumel, *Fundamentals of Physics* (Holt, Rinehart and Winston, 1974).

[115] L. Kergoat, L. Herlogsson, D. Braga, B. Piro, M.-C. Pham, X. Crispin, M. Berggren, and G. Horowitz, Adv. Mater. **22**, 2565 (2010).

[116] M.E. Roberts, S.C.B. Mannsfeld, N. Queraltó, C. Reese, J. Locklin, W. Knoll, and Z. Bao, Proc. Natl. Acad. Sci. **105**, 12134 (2008).

[117] P. Huang, D. Pech, R. Lin, J.K. McDonough, M. Brunet, P.-L. Taberna, Y. Gogotsi, and P. Simon, Electrochem. Commun. **36**, 53 (2013).

[118] B. Nasr, Z. Zhao-Karger, D. Wang, R. Kruk, H. Hahn, and S. Dasgupta, J. Mater. Chem. C **1**, 2534 (2013).

[119] R.-S. Kühnel, N. Böckenfeld, S. Passerini, M. Winter, and A. Balducci, Electrochimica Acta **56**, 4092 (2011).

[120] H. Ohno, *Electrochemical Aspects of Ionic Liquids* (John Wiley & Sons, 2011).

[121] M. Freemantle, *An Introduction to Ionic Liquids* (Royal Society of Chemistry, 2009).

[122] T. Welton, Chem. Rev. **99**, 2071 (1999).

[123] M. Galiński, A. Lewandowski, and I. Stępniak, Electrochim. Acta **51**, 5567 (2006).

[124] D.R. McFarlane, J. Sun, J. Golding, P. Meakin, and M. Forsyth, Electrochim Acta **45**, 1271 (2000).

[125] B. Kirchner, *Ionic Liquids* (Springer, 2009).

[126] J.-H. Choi, W. Xie, Y. Gu, C.D. Frisbie, and T.P. Lodge, ACS Appl. Mater. Interfaces **7**, 7294 (2015).

[127] M. J. Earle, J. M.S.S. Esperança, M. A. Gilea, J. N. Canongia, L. P.N. Rebelo, J. W. Magee, K. R. Seddon, and J. A. Widegren, Nature **439**, 831 (2006).

[128] R. Giles, J. Evett, and C. Liu, *Schaum's Outline of Fluid Mechanics and Hydraulics, 3ed* (McGraw Hill Professional, 2009).

[129] L. C., G. V.S.M., J. Aires-de-Sousa, I. Lopez, R. Frade, and C. A.M., in *Ion. Liq. Theory Prop. New Approaches Chapter Phys.-Chem. Prop. Task-Specif. Ion. Liq.*, edited by A. Kokorin (InTech, 2011).

[130] J.H. Seo, E.B. Namdas, A. Gutacker, A.J. Heeger, and G.C. Bazan, Adv. Funct. Mater. **21**, 3667 (2011).

[131] S.I. Fletcher, F.B. Sillars, N.E. Hudson, and P.J. Hall, J. Chem. Eng. Data **55**, 778 (2010).

[132] Data Measured and Provided by IoLiTec Ionic Liquids Technologies GmbH, Heilbronn/Germany (2012).

[133] J.-H. Shin, W.A. Henderson, and S. Passerini, Electrochem. Commun. **5**, 1016 (2003).

[134] Z. Gadjourova, Y.G. Andreev, D.P. Tunstall, and P.G. Bruce, Nature **412**, 520 (2001).

[135] W.H. Meyer, Adv. Mater. **10**, 439 (1998).

[136] O. Larsson, E. Said, M. Berggren, and X. Crispin, Adv. Funct. Mater. **19**, 3334 (2009).

[137] D.R. MacFarlane, M. Forsyth, E.I. Izgorodina, A.P. Abbott, G. Annat, and K. Fraser, Phys. Chem. Chem. Phys. **11**, 4962 (2009).

[138] N. Leventis, M.O. Schloh, M.J. Natan, J.J. Hickman, and M.S. Wrighton, Chem. Mater. **2**, 568 (1990).

[139] D. Ofer, L.Y. Park, R.R. Schrock, and M.S. Wrighton, Chem. Mater. **3**, 573 (1991).

[140] E.W. Paul, A.J. Ricco, and M.S. Wrighton, J. Phys. Chem. **89**, 1441 (1985).

[141] Y. Xia, J. Cho, B. Paulsen, C.D. Frisbie, and M.J. Renn, Appl. Phys. Lett. **94**, 013304 (2009).

[142] Y. Xia, W. Zhang, M. Ha, J.H. Cho, M.J. Renn, C.H. Kim, and C.D. Frisbie, Adv. Funct. Mater. **20**, 587 (2010).

[143] J.H. Cho, J. Lee, Y. Xia, B. Kim, Y. He, M.J. Renn, T.P. Lodge, and C. Daniel Frisbie, Nat. Mater. **7**, 900 (2008).

[144] J. Lee, M.J. Panzer, Y. He, T.P. Lodge, and C.D. Frisbie, J. Am. Chem. Soc. **129**, 4532 (2007).

[145] T.P. Lodge, Science **321**, 50 (2008).

[146] L. Herlogsson, X. Crispin, S. Tierney, and M. Berggren, Adv. Mater. **23**, 4684 (2011).

[147] S. Ono, N. Minder, Z. Chen, A. Facchetti, and A.F. Morpurgo, Appl. Phys. Lett. **97**, 143307 (2010).

[148] E. Menard, V. Podzorov, S.-H. Hur, A. Gaur, M.E. Gershenson, and J.A. Rogers, Adv. Mater. **16**, 2097 (2004).

[149] Y. Liang, C.D. Frisbie, H.-C. Chang, and P.P. Ruden, J. Appl. Phys. **105**, 024514 (2009).

[150] S. Ogawa, Y. Kimura, H. Ishii, and M. Niwano, Jpn. J. Appl. Phys. **42**, L1275 (2003).

[151] M.J. Panzer and C.D. Frisbie, Appl. Phys. Lett. **88**, 203504 (2006).

[152] M.J. Panzer and C.D. Frisbie, J. Am. Chem. Soc. **127**, 6960 (2005).

[153] M. Hamedi, L. Herlogsson, X. Crispin, R. Marcilla, M. Berggren, and O. Inganäs, Adv. Mater. **21**, 573 (2009).

[154] C. Müller, M. Hamedi, R. Karlsson, R. Jansson, R. Marcilla, M. Hedhammar, and O. Inganäs, Adv. Mater. **23**, 898 (2011).

[155] T. Fujimoto and K. Awaga, Phys. Chem. Chem. Phys. **15**, 8983 (2013).

[156] I. S. Martinez and S. Baldelli, *Ionic Liquids: From Knowledge to Application* (American Chemical Society, 2009).

[157] H. Klauk, *Organic Electronics II: More Materials and Applications* (John Wiley & Sons, 2012).

[158] H. Shimotani, H. Asanuma, J. Takeya, and Y. Iwasa, Appl. Phys. Lett. **89**, 203501 (2006).

[159] S.N. Bhat, R.D. Pietro, and H. Sirringhaus, Chem. Mater. **24**, 4060 (2012).

[160] H. Yuan, H. Shimotani, J. Ye, S. Yoon, H. Aliah, A. Tsukazaki, M. Kawasaki, and Y. Iwasa, J. Am. Chem. Soc. **132**, 18402 (2010).

[161] S. Thiemann, S. Sachnov, S. Porscha, P. Wasserscheid, and J. Zaumseil, J. Phys. Chem. C **116**, 13536 (2012).

[162] J. Jeong, N. Aetukuri, T. Graf, T.D. Schladt, M.G. Samant, and S.S.P. Parkin, Science **339**, 1402 (2013).

[163] D. Ruzmetov, G. Gopalakrishnan, C. Ko, V. Narayanamurti, and S. Ramanathan, J. Appl. Phys. **107**, 114516 (2010).

[164] H. Ji, J. Wei, and D. Natelson, Nano Lett. **12**, 2988 (2012).

[165] E. Alarcón-Lladó, M.A. Mayer, B.W. Boudouris, R.A. Segalman, N. Miller, T. Yamaguchi, K. Wang, Y. Nanishi, E.E. Haller, and J.W. Ager, Appl. Phys. Lett. **99**, 102106 (2011).

[166] M.S. Kang, A. Sahu, D.J. Norris, and C.D. Frisbie, Nano Lett. **10**, 3727 (2010).

[167] M.S. Kang, J. Lee, D.J. Norris, and C.D. Frisbie, Nano Lett. **9**, 3848 (2009).

[168] B.E. Conway, *Electrochemical Supercapacitors: Scientific Fundamentals and Technological Applications* (Springer, 1999).

[169] G. Tarabella, C. Santato, S.Y. Yang, S. Iannotta, G.G. Malliaras, and F. Cicoira, Appl. Phys. Lett. **97**, 123304 (2010).

[170] M. Lazzari, C. Arbizzani, F. Soavi, and M. Mastragostino, in *Supercapacitors*, edited by F. Béguin and E. Frąckowiak (Wiley-VCH Verlag GmbH & Co. KGaA, 2013), pp. 289–306.

[171] D. Weingarth, A. Foelske-Schmitz, A. Wokaun, and R. Kötz, Electrochem. Commun. **18**, 116 (2012).

[172] Y.-S. Ye, J. Rick, and B.-J. Hwang, J. Mater. Chem. A **1**, 2719 (2013).

[173] M. Lazzari, M. Mastragostino, and F. Soavi, Electrochem. Commun. **9**, 1567 (2007).

[174] Y. Xia, J. H. Cho, J. Lee, P. P. Ruden, and C. D. Frisbie, Adv. Mater. **21**, 2174 (2009).

[175] T. Sakanoue, E. Fujiwara, R. Yamada, and H. Tada, Appl. Phys. Lett. **84**, 3037 (2004).

[176] T. Fujimoto, M.M. Matsushita, and K. Awaga, J. Phys. Chem. C **116**, 5240 (2012).

[177] J. Sayago, S. Bayatpour, F. Cicoira, and C. Santato, *Toward Electrolyte-Gated Organic Light-Emitting Transistors: Advances and Challenges* (Wiley-VCH Verlag GmbH & Co. KGaA, 2013).

[178] A.H. Pakiari, S. Siahrostami, and T. Ziegler, J. Mol. Struct. THEOCHEM **955**, 47 (2010).

[179] P. Bonhôte, A.-P. Dias, N. Papageorgiou, K. Kalyanasundaram, and M. Grätzel, Inorg. Chem. **35**, 1168 (1996).

[180] D. De Tullio, M. Magliulo, G. Colafemmina, K. Manoli, L. Torsi, and G. Palazzo, Sci. Adv. Mater. **5**, 1922 (2013).

[181] S. Ono, K. Miwa, S. Seki, and J. Takeya, Appl. Phys. Lett. **94**, 063301 (2009).

[182] T. Uemura, R. Hirahara, Y. Tominari, S. Ono, S. Seki, and J. Takeya, Appl. Phys. Lett. **93**, 263305 (2008).

[183] J. Sayago, F. Soavi, Y. Sivalingam, F. Cicoira, and C. Santato, J. Mater. Chem. C **2**, 5690 (2014).

[184] C. Yang, Q. Sun, J. Qiao, and Y. Li, J Phys Chem B **107**, 12981 (2003).

[185] S. Panozzo, M. Armand, and O. Stéphan, Appl. Phys. Lett. **80**, 679 (2002).

[186] T.-Q. Nguyen, I.B. Martini, J. Liu, and B.J. Schwartz, J. Phys. Chem. B **104**, 237 (2000).

[187] R. Kumar, R.G. Pillai, N. Pekas, Y. Wu, and R.L. McCreery, J. Am. Chem. Soc. **134**, 14869 (2012).

[188] V. Ruiz, T. Huynh, S.R. Sivakkumar, and A.G. Pandolfo, RSC Adv. **2**, 5591 (2012).

[189] B.K. Bose, IEEE Ind. Electron. Mag. **4**, 6 (2010).

[190] M. Beidaghi and Y. Gogotsi, Energy Environ. Sci. **7**, 867 (2014).

[191] Z.L. Wang, Adv. Funct. Mater. **18**, 3553 (2008).

[192] P. Andersson Ersman, D. Nilsson, J. Kawahara, G. Gustafsson, and M. Berggren, Org. Electron. **14**, 1276 (2013).

[193] A. Campana, T. Cramer, D.T. Simon, M. Berggren, and F. Biscarini, Adv. Mater. **26**, 3874 (2014).

[194] M. J. Panzer and C. D. Frisbie, Appl. Phys. Lett. **88**, 203504 (2006).

[195] C. Arbizzani, M. Mastragostino, and F. Soavi, J. Power Sources **100**, 164 (2001).

[196] M. Mastragostino and F. Soavi, in *J Garche C Dyer P Moseley Z Ogumi Rand B Scrosati Eds Encycl. Electrochem. Power Sources* (Amsterdam: Elsevier, 2009), pp. 649–657.

[197] T. Uemura, M. Yamagishi, S. Ono, and J. Takeya, Appl. Phys. Lett. **95**, 103301 (2009).

[198] R. Mens, S. Chambon, S. Bertho, G. Reggers, B. Ruttens, J. D'Haen, J. Manca, R. Carleer, D. Vanderzande, and P. Adriaensens, Magn. Reson. Chem. **49**, 242 (2011).

[199] E.J. Meijer, D.M. de Leeuw, S. Setayesh, E. van Veenendaal, B.-H. Huisman, P.W.M. Blom, J.C. Hummelen, U. Scherf, and T.M. Klapwijk, Nat. Mater. **2**, 678 (2003).

[200] S. Thiemann, M. Gruber, I. Lokteva, J. Hirschmann, M. Halik, and J. Zaumseil, ACS Appl. Mater. Interfaces **5**, 1656 (2013).

[201] M.J. Panzer and C.D. Frisbie, J. Am. Chem. Soc. **129**, 6599 (2007).

[202] J. Liu, L. Herlogsson, A. Sawatdee, P. Favia, M. Sandberg, X. Crispin, I. Engquist, and M. Berggren, Appl. Phys. Lett. **97**, 103303 (2010).

[203] L. Kergoat, L. Herlogsson, B. Piro, M.C. Pham, G. Horowitz, X. Crispin, and M. Berggren, Proc. Natl. Acad. Sci. **109**, 8394 (2012).

[204] G.A. Snook, P. Kao, and A.S. Best, J. Power Sources **196**, 1 (2011).

[205] A. Hepp, H. Heil, W. Weise, M. Ahles, R. Schmechel, and H. von Seggern, Phys. Rev. Lett. **91**, 157406 (2003).

[206] M.C. Gwinner, D. Kabra, M. Roberts, T.J.K. Brenner, B.H. Wallikewitz, C.R. McNeill, R.H. Friend, and H. Sirringhaus, Adv. Mater. **24**, 2728 (2012).

[207] C. Santato, F. Cicoira, and R. Martel, Nat. Photonics **5**, 392 (2011).

[208] M.A. McCarthy, B. Liu, E.P. Donoghue, I. Kravchenko, D.Y. Kim, F. So, and A.G. Rinzler, Science **332**, 570 (2011).

[209] R. Capelli, S. Toffanin, G. Generali, H. Usta, A. Facchetti, and M. Muccini, Nat. Mater. **9**, 496 (2010).

[210] J. H. Seo, E. B. Namdas, A. Gutacker, A. J. Heeger, and G. C. Bazan, Appl. Phys. Lett. **97**, 043303 (2010).

[211] F. Cicoira, C. Santato, M. Melucci, L. Favaretto, M. Gazzano, M. Muccini, and G. Barbarella, Adv. Mater. **18**, 169 (2006).

[212] J. Zaumseil, C.L. Donley, J.-S. Kim, R.H. Friend, and H. Sirringhaus, Adv. Mater. **18**, 2708 (2006).

[213] C. Santato, R. Capelli, M.A. Loi, M. Murgia, F. Cicoira, V.A.L. Roy, P. Stallinga, R. Zamboni, C. Rost, S.F. Karg, and M. Muccini, Synt. Met. **146**, 329 (2004).

[214] J. Zaumseil, in *Org. Electron. II Chapter Light-Emit. Org. Transistors*, edited by H. Klauk (Wiley-VCH Verlag GmbH & Co., 2012), pp. 353–386.

[215] J. Liu, I. Engquist, and M. Berggren, J. Am. Chem. Soc. **135**, 12224 (2013).

[216] J. Zaumseil, R. H. Friend, and H. Sirringhaus, Nat. Mater. **5**, 69 (2006).

[217] S.Z. Bisri, T. Takenobu, Y. Yomogida, H. Shimotani, T. Yamao, S. Hotta, and Y. Iwasa, Adv. Funct. Mater. **19**, 1728 (2009).

[218] S.Z. Bisri, T. Takenobu, K. Sawabe, S. Tsuda, Y. Yomogida, T. Yamao, S. Hotta, C. Adachi, and Y. Iwasa, Adv. Mater. **23**, 2753 (2011).

[219] S.Z. Bisri, K. Sawabe, M. Imakawa, K. Maruyama, T. Yamao, S. Hotta, Y. Iwasa, and T. Takenobu, Sci. Rep. **2**, (2012).

[220] K. Sawabe, M. Imakawa, M. Nakano, T. Yamao, S. Hotta, Y. Iwasa, and T. Takenobu, Adv. Mater. **24**, 6141 (2012).

[221] K. Sawabe, T. Takenobu, S. Z. Bisri, T. Yamao, S. Hotta, and Y. Iwasa, Appl. Phys. Lett. **97**, 043307 (2010).

[222] T. Takenobu, S.Z. Bisri, T. Takahashi, M. Yahiro, C. Adachi, and Y. Iwasa, Phys. Rev. Lett. **100**, 066601 (2008).

[223] G.P. Crawford, *Flexible Flat Panel Displays* (John Wiley & Sons, 2005).

[224] M. Ullah, K. Tandy, S.D. Yambem, M. Aljada, P.L. Burn, P. Meredith, and E.B. Namdas, Adv. Mater. **25**, 6213 (2013).

[225] F. So, J. Kido, and P. Burrows, MRS Bull. **33**, 663 (2008).

[226] B.W. D'Andrade and S.R. Forrest, Adv. Mater. **16**, 1585 (2004).

[227] M.C. Gwinner, S. Khodabakhsh, H. Giessen, and H. Sirringhaus, Chem. Mater. **21**, 4425 (2009).

[228] M.A. Baldo, R.J. Holmes, and S.R. Forrest, Phys. Rev. B **66**, 035321 (2002).

[229] N. Tessler, D.J. Pinner, V. Cleave, P.K.H. Ho, R.H. Friend, G. Yahioglu, P. Le Barny, J. Gray, M. de Souza, and G. Rumbles, Synth. Met. **115**, 57 (2000).

[230] S.Z. Bisri, T. Takenobu, and Y. Iwasa, J. Mater. Chem. C **2**, 2827 (2014).

[231] Y. Matsuda, K. Ueno, H. Yamaguchi, Y. Egami, and T. Niimi, Sensors **12**, 13899 (2012).

[232] L. Edman, J. Swensen, D. Moses, and A.J. Heeger, Appl Phys Lett **84**, 3744 (2004).

[233] C. Yumusak and N. S. Sariciftci, Appl. Phys. Lett. **97**, 033302 (2010).

[234] C. Yumusak, M. Abbas, and N.S. Sariciftci, J. Lumin. **134**, 107 (2013).

[235] J.M. Hodgkiss, G. Tu, S. Albert-Seifried, W.T.S. Huck, and R.H. Friend, J. Am. Chem. Soc. **131**, 8913 (2009).

[236] Q. Sun, Y. Li, and Q. Pei, J. Disp. Technol. **3**, 211 (2007).

APPENDIX A – SUPPORTING INFORMATION FOR ARTICLE 1

Supporting Information

Low Voltage Electrolyte-Gated Organic Transistors Making Use of High Surface Area Activated Carbon Gate Electrodes

J. Sayago, F. Soavi, Y. Sivalingam, F. Cicoira and C. Santato

J. Mater. Chem. C, 2014, **2**, 5690–5694.

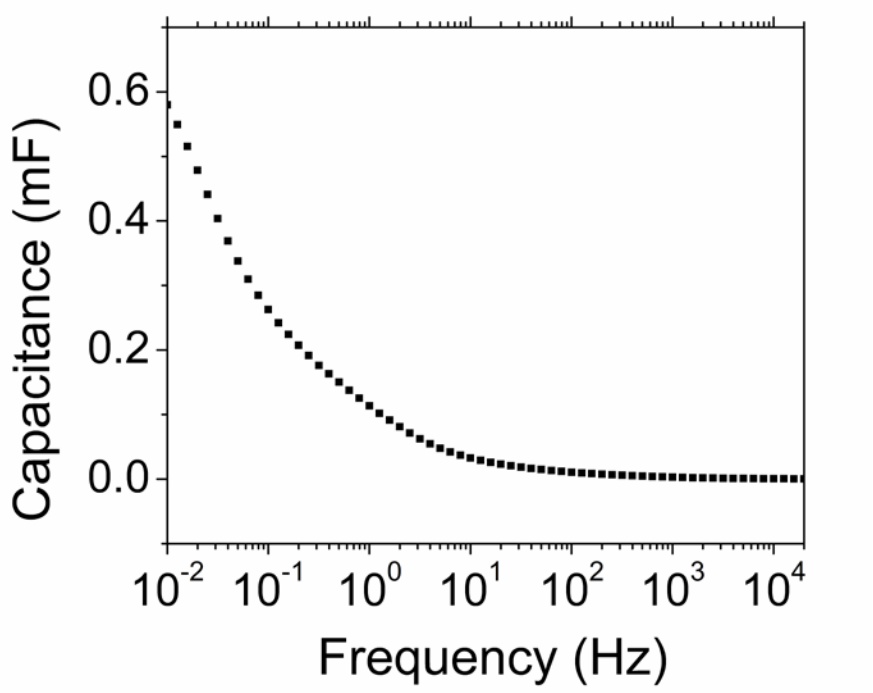

Fig. S1 Frequency dependence of the capacitance of the MEH-PPV working electrode at 0.8 V vs activated carbon (small sized) quasi reference electrode with activated carbon gate as the counter electrode.

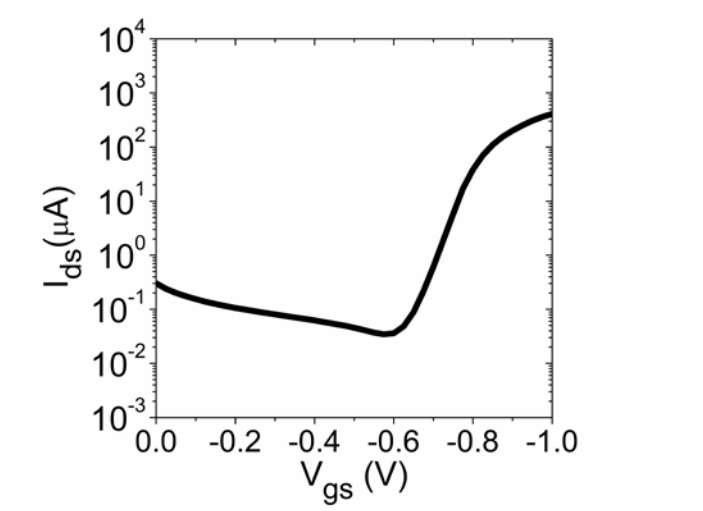

Fig. S2 Transfer characteristics in the saturation regime (V_{ds} = -0.3 V) for [EMIM][TFSI]-gated MEH-PPV transistors, sweep rate 50 mV·s^{-1}.

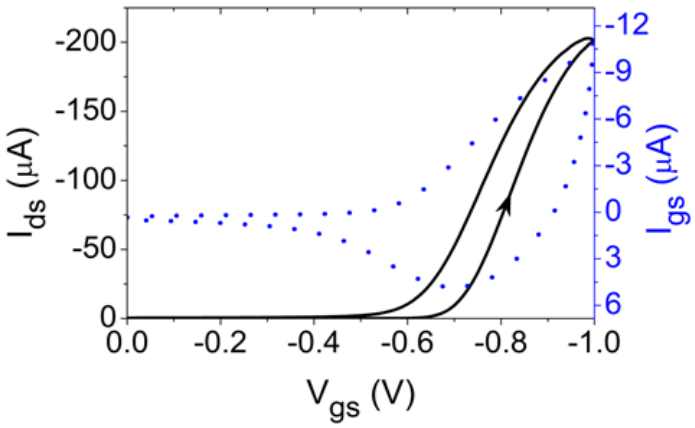

Fig. S3 [EMIM][TFSI]-gated MEH-PPV transistor transfer characteristics in the linear regime (V_{ds} = -0.1 V). I_{ds} (left axis, solid black line) and I_{gs} (right axis, dotted blue line) are plotted vs V_{gs}, sweep rate 10 mV·s^{-1}.

APPENDIX B – SUPPORTING INFORMATION FOR ARTICLE 2

Supporting Information

Electrolyte-gated polymer thin film transistors making use of ionic liquids and ionic liquid-solvent mixtures

Jonathan Sayago, Xiang Meng, Shuang Liang, Étienne Bourbeau, Francesca Soavi, Fabio Cicoira, and Clara Santato

J. of Appl. Phys, 2015, **117**, 112809.

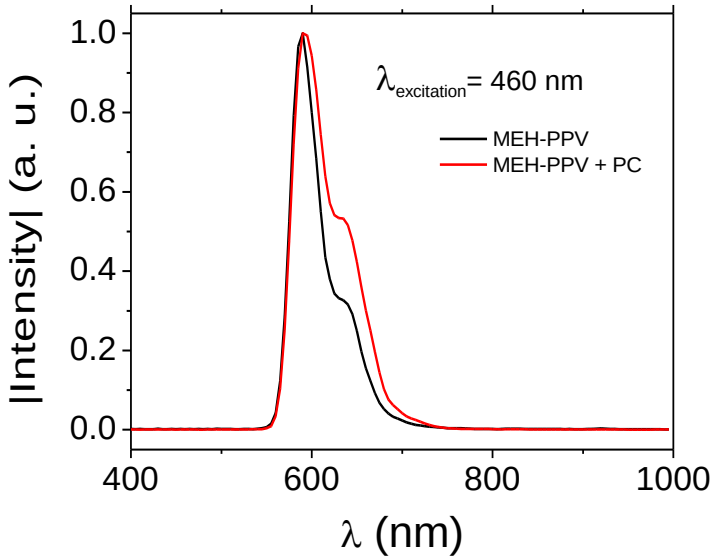

Fig. S1. Fluorescence spectra of MEH-PPV, black line, and MEH-PPV in contact with a drop of propylene carbonate (PC), red line.

Figs. S2a and S2b show the output and transfer characteristics of MEH-PPV transistors gated with 350:5 volume fraction of [PYR_{14}][TFSI] and deionized water. In the output curve (Fig. S2a) we observe an onset for the saturation region at around 0.2 V. The transfer curve displays a

similar behavior than transistors gated with pure [PYR_{14}][TFSI] showing I_{ds} hysteresis and a similar correlation with the I_{gs} sweeping speed. Despite the lower I_{ds} than [PYR_{14}][TFSI]-gated MEH-PPV transistors, the main performance parameters obtained by adding water remain similar. From the transfer curve at 10 mVs^{-1} we estimated an ON/OFF ratio of 1.4×10^3, doping charge (Q) of 9.7×10^{-5} C and mobility (μ) of 3.3×10^{-2} $cm^2V^{-1}s^{-1}$. The higher mobility can be explained from the effective operation at lower I_{gs}, thus lower Q as compared with [PYR_{14}][TFSI]-gated transistors.

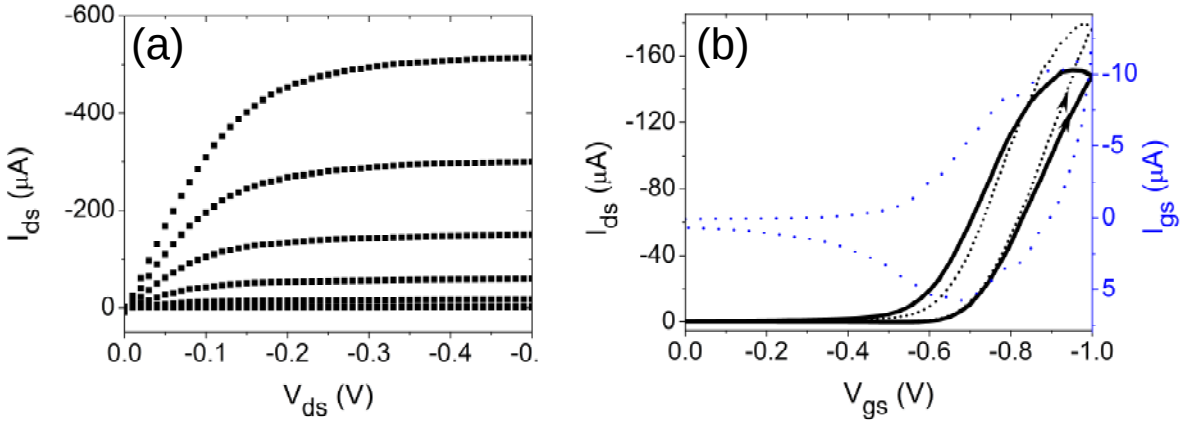

Fig. S2. Device characteristics of the MEH-PPV transistor gated with [PYR_{14}][TFSI] and H_2O with a volume ratio of 350:5 (a) output characteristics (I_{ds} *vs* $V_{ds,}$ for V_{gs} = 0, -0.6, -0.65, -0.7, -0.75 and -0.8 V) and (b) transfer characteristics in the linear regime, V_{ds}= -25 mV, for a V_{gs} sweeping rate of 50 mVs^{-1}, left axis black solid line, and sweeping rate of 10 mVs^{-1}, left axis black dotted line, and I_{gs} (gate-source current, right axis blue line) plotted *vs* V_{gs}.

APPENDIX C – SUPPORTING INFORMATION FOR ARTICLE 3

Supporting Information

TransCap: a monolithically integrated supercapacitor and electrolyte-gated transistor

J. Sayago, U. Shafique, F. Soavi, F. Cicoira, and C. Santato

J. Mater. Chem. C, 2014, **2**, 10273–10276.

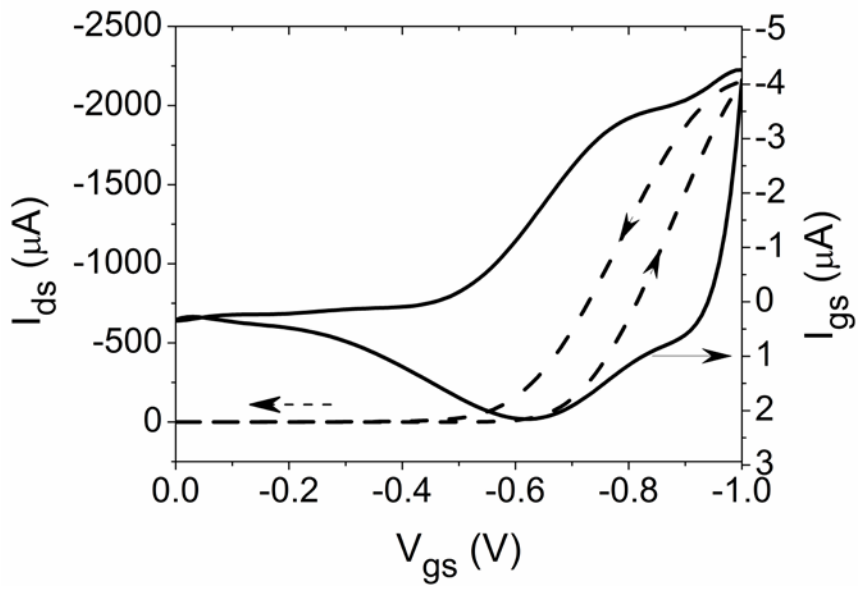

Fig. S1. Transfer characteristics of the $[N_{1113}][TFSI]$-gated MEH-PPV TransCap at saturation (V_{ds}= -300 mV) with V_{gs} at 10 mVs^{-1}. I_{ds} on the left axis, dashed line, I_{gs} on the right axis, solid line.

Materials: MEH-PPV Thin film deposition

Substrates were cleaned by sequential ultrasonic baths in isopropyl alcohol (IPA, J. T. Baker, microelectronic grade, 5 min), acetone (J. T. Baker, microelectronic grade, 10 min), and IPA (5 min), followed by a 5 min dehydration process at 120 °C in N_2 atmosphere consisting of 3 purging cycles of low pressure (20 Torr) and high pressure (500 Torr). Drain and source contacts of Ti/Au, 5/40 nm/nm, were photolithographically patterned on SiO_2 substrates (channel width, W, 4000 μm and length, L, 10 μm). 5 mg of MEH-PPV (Sigma Aldrich, 55 kDa) in 1 mL of toluene (anhydrous, Sigma Aldrich) were mixed and stirred overnight in a N_2 glove box (O_2, H_2O lower than 5 ppm) keeping the temperature at about 40 °C. MEH-PPV thin films were deposited by spin coating the solution at 1000 rpm. Afterwards, films were thermally treated at 70 °C for 3 hours. The final MEH-PPV thickness was 50 nm and the polymer mass loading was ca 5 $\mu g \cdot cm^{-2}$, considering a polymer density of ca 1 g/cm^3.[1]

1. H. Hoppe et al, *Thin Solid Films*, 511-512 (2006) 587-592

Materials: Ionic Liquid

$[N_{1113}][TFSI]$ (Solvionic, 99.5%) was used as received. At room temperature the ionic liquid features an electrochemical stability window of 5.7 V and an ionic conductivity of 3.3 $mS \cdot cm^{-1}$.[2]

2. M. Lazzari, C. Arbizzani, F. Soavi and M. Mastragostino, Ch. 9 in *Supercapacitors: Materials, Systems and Applications* (F. Béguin and E. Frackowiak Eds, Wiley-VCH, 2013), pp. 289–306.

Device fabrication

The device fabrication was carried out by sandwiching a Durapore® GVHP filter separator (9 mm × 4 mm × 125 μm) soaked in the ionic liquid between the MEH-PPV thin film and the activated carbon gate electrode. The gate electrode was prepared using carbon paper (Spectracarb 2050, 3 mm × 6 mm) coated with 6 μL of an ink of activated carbon (PICACTIF SUPERCAP BP10, Pica, BET specific surface area 1850 m^2g^{-1}, 28 $mg \cdot mL^{-1}$) and polyvinylidene fluoride (PVDF, KYNAR HSV900, 1.4 $mg \cdot mL^{-1}$) binder in N-methyl pyrrolidone (NMP, Fluka, >99.0%) solvent. The coating was followed by a thermal treatment at 60 °C for several hours to remove solvent and water traces. The activated carbon mass loading was ca. 0.9 $mg \cdot cm^{-2}$. The footprint of the TransCap corresponds to the geometric area of the separator (0.36 cm^2).

TransCap electrochemical and electrical characterization

The electrical and electrochemical characterizations of the TransCap were carried out in a N_2 glove box (H_2O, O_2 lower than 5 ppm). The electrochemical tests were performed using a PARSTAT 2273 (Princeton Applied Research) potentiostat. Transistor device characteristics were measured using a B1500A Agilent semiconductor parameter analyzer.

APPENDIX D – COMPLEMENTARY RESULTS ON PCBM ELECTROLYTE-GATED TRANSISTORS

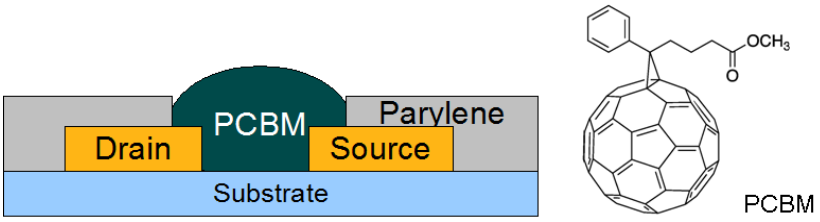

Figure S1. Setup to drop-cast PCBM solution onto Si/SiO_2 substrates patterned with Au drain and source electrodes and parylene C.

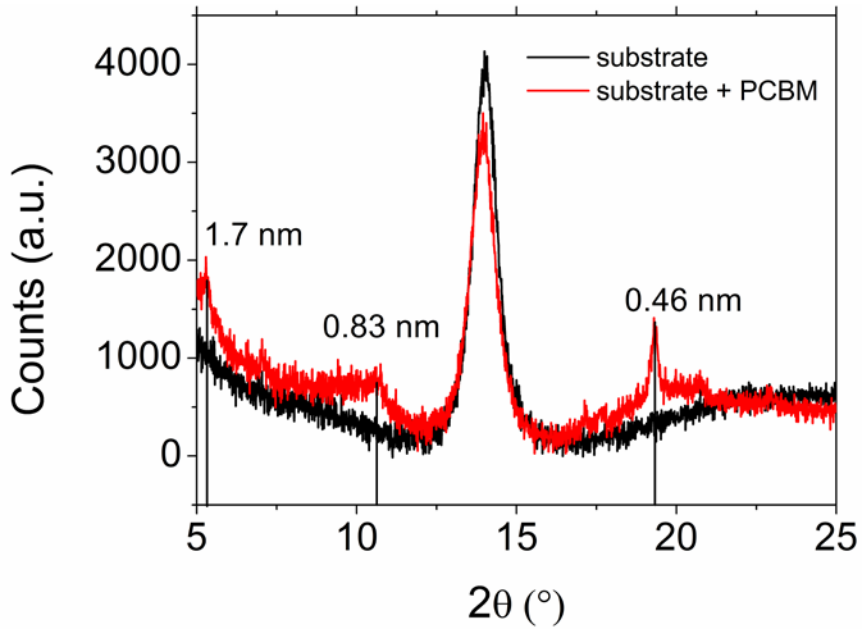

Fig. S2. XRD spectra of Si/SiO_2 substrates patterned with Au source and drain electrodes and patterned with parylene C wells (black line) and the same substrates with a thin film of PCBM. The corresponding d-spacings are indicated for each peak, estimated using Bragg's law, $2dsin\theta=\lambda$, where d is the spacing between planes of atoms, θ is the angle of incidence and λ is the radiation wavelength, 1.54 Å.

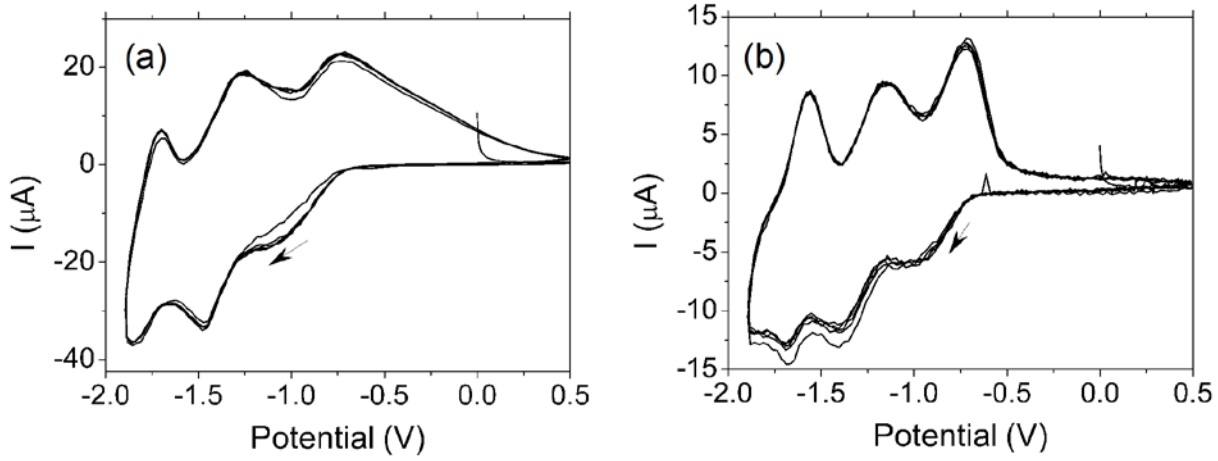

Fig. S3. Cyclic voltammetry of (a) [EMIM][TFSI]-gated and (b) [PYR_{14}][TFSI]-gated PCBM transistors. 5 cycles where obtained at 100 mVs^{-1}.

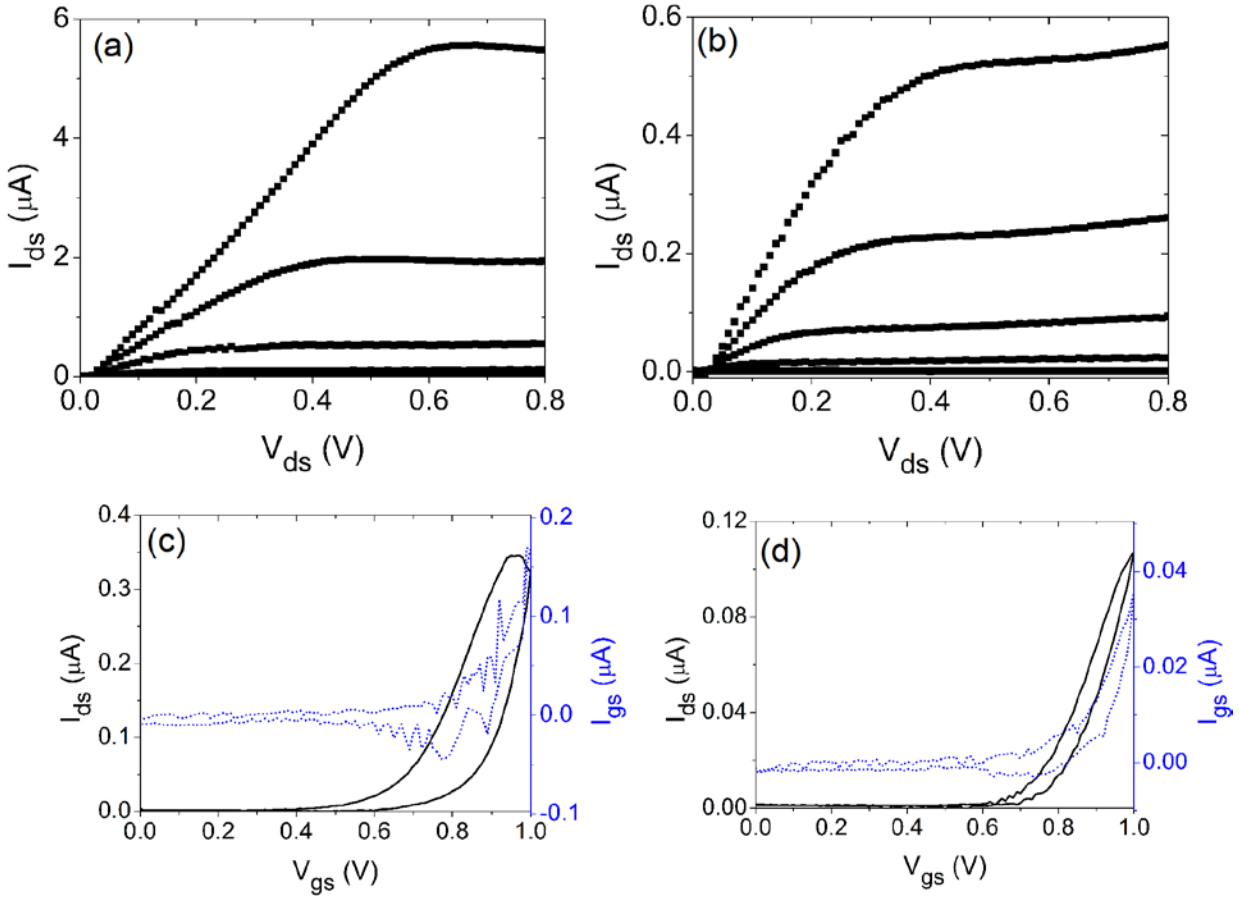

Fig. S4. Electrolyte-gated PCBM transistors making use of different ionic liquids as gating media. output characteristics (I_{ds} vs V_{ds} for V_{gs} = 0, 0.8, 0.9, 1 and 1.1 V) of (a) [EMIM][TFSI]- and (b) [PYR_{14}][TFSI]-gated PCBM transistors. Transfer characteristics in the linear regime (V_{ds}= 200 mV) (left axis, black solid line) together with I_{gs} vs V_{gs} (right axis blue line) for a V_{gs} sweeping rate of 10 mV·s^{-1}. In c and d the ionic liquid was [EMIM][TFSI] and [PYR_{14}][TFSI], respectively.

APPENDIX E – COMPLEMENTARY RESULTS ON PCBM ELECTROLYTE-GATED TRANSISTORS

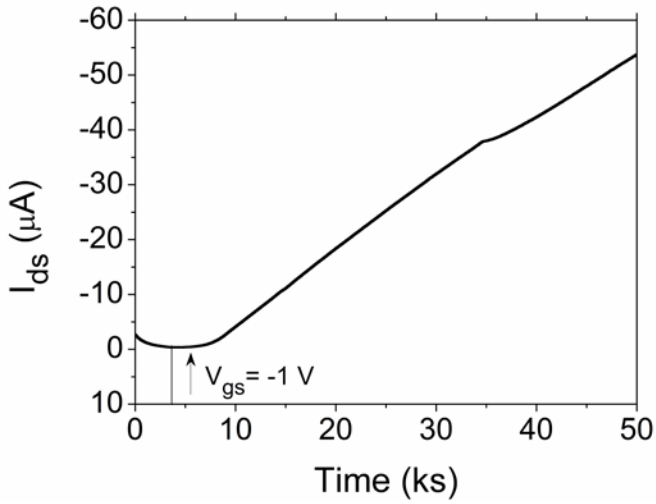

Fig. S1. Transient characteristics, I_{ds} vs Time, for V_{ds}=-1 V and V_{gs}= -1 V, for [BMIM][PF_6]-gated MEH-PPV transistors using Pt as gate electrode. Consistent behaviour was observed with transistors based on [EMIM][TFSI] and [BMIM][TFSI].

APPENDIX F – LIST OF PUBLICATIONS AT POLYTECHNIQUE MONTREAL NOT INCLUDED IN THE THESIS

Journal articles

J. Wünsche, Y. Deng, P. Kumar, E. Di Mauro, E. Josberger, J. Sayago, A. Pezzella, F. Soavi, F. Cicoira, M. Rolandi and C. Santato, Protonic and Electronic Transport in Hydrated Thin Films of the Pigment Eumelanin. *Chem. Mater.* 27, 436–442 (2015).

J. Sayago, F. Rosei, C. Santato, Organic photonics: Blending organic building blocks. *Nature Photonics* 6**,** 639–640 (2012).

Book chapter

J. Sayago, S. Bayatpour, F. Cicoira, C. Santato, Ch. 9 Toward Electrolyte-Gated Organic Light Emitting Transistors: Advances and Challenges in Organic Electronics: Emerging Concepts and Technologies (Eds. Cicoira, F. & Santato, C.) 215–232 (Wiley-VCH, 2013).

APPENDIX G – PARTICIPATION IN CONFERENCES AND MEETINGS

Materials and Technologies for Energy Conversion Saving and Storage, Querétaro, México, 2015

32nd International Conference on the Physics of Semiconductors, Austin Texas, USA, 2014

Materials Research Society, Fall Meeting, Boston, USA, 2014

European Materials Research Society, Lille, France, 2014

Materials Research Society, Spring Meeting, San Francisco, USA, 2013

Canadian Chemistry Conference and Exhibition, Quebec, Canada, 2013

Photonics North, Montreal, Canada, 2012

Next Generation Solar - Photovoltaics Canada, Montreal, Canada, 2012